POLITECNICO DI TORINO

**Corso di Laurea Magistrale
in Ingegneria Per l'Ambiente e il Territorio**

Tesi di Laurea Magistrale

**Radon deficit technique's variability in a DNAPL contaminated site:
a spatio-temporal approach**

Variabilità della "Radon deficit technique" in un sito contaminato da DNAPL:
un'analisi spazio-temporale

Progetto di tesi sviluppato presso l'Università Politecnica di Madrid

UNIVERSIDAD
POLITÉCNICA
DE MADRID

Relatori	**Candidato**
Prof.ssa Tiziana Anna Elisabetta Tosco	Elia Vasini
Prof. Fernando Barrio Parra	

Anno Accademico 2018/2019

Comunque vada,
è stato un successo!
(lo dice sempre Lauro)

ABSTRACT

Uncontrolled landfill sites are one of the main sources of underground and surface water contamination. The absence of appropriate monitoring and prevention measurements may often lead to the infiltration of leachates into the subsoil, thereby severely contaminating the aquifers of the area. That is what happened in Sardas landfill located close to Sabiñanigo (Huesca, Spain). It is an old uncontrolled landfill that has been dumping huge quantities of urban, agricultural and industrial wastes since the 70s.

Among all the waste residues in Sardas, the most toxic are the leachates of chloro-alkyl industry and the organochlorides generated by the pesticides industry. Inquinosa produced lindane from 1975 to 1988 and formulated lindane products until 1992. The disposal of waste generated a flooded area of DNAPL (Dense NonAqueous Phase Liquids) above the impermeable marl layer, composed by a mixture of HCHs (Hexachlorocyclohexane), Chlorobenzenes, BTEX (Benzene, Toluene, Ethylbenzene, Xylene) and other chlorinated compounds, which spread downstream the dump, imply a great threat for soil, surface water and groundwater quality, as for human health and ecosystems. As a persistent organic pollutant contaminated macro-site, Sardas became a very interesting heterogeneous area to study, and presents suitable conditions to assess whether non-invasive screening techniques such as the Radon Deficit Technique are applicable at sites contaminated by NAPL products.

The Radon deficit technique exploit the natural presence of Radon (Rn) in soil and its strong affinity to organic fluids relative to water. In correspondence of the contamination a decrease of the Rn signal on the surface would be seen. This technique was successfully tested in homogeneous contaminated sites by LNAPL and DNAPL. It was also assessed for the Inquinosa industrial site.

With the objective to find which conditions influence the measurement of Radon, and if it is possible to determine a relationship between the Rn deficit peaks and the contamination, the current work analyzes data from four different campaigns, lasting from 2016 to 2019. The results of an ANOVA test have showed that the only atmospheric condition that influence the measurement of Radon is the temperature. A spatial interpolation of data has been carried out for contaminants in water and HCHs in soil at different depths. A significative Pearson correlation between Rn signal and contaminants

was found. It was also possible to carry out a qualitative comparison between Rn signal and the contamination.

The results of Sardas site show that there is a relationship between the decrease of Rn signal and contaminants in water and HCHs in soil, but that correlation decrease with depth. Results also allow to say that Rn deficit technique is applicable, as long as many measurements take place at almost constant temperature, with a single type of equipment, and covering a sufficiently wide area compared to the assumed contamination

ABSTRACT

Le discariche incontrollate costituiscono una delle principali fonti di contaminazione delle acque sotterranee e superficiali. L'assenza di monitoraggio porta al rilascio di percolato, che può contaminare gravemente le falde acquifere della zona. Questo è quanto è accaduto nella discarica di Sardas, situata nei pressi di Sabiñanigo (Huesca, Spagna). Si tratta di una vecchia discarica incontrollata che raccoglie enormi quantità di rifiuti urbani, agricoli e industriali dagli anni '70.

Tra tutti i residui, i più tossici sono i percolati dell'industria dei cloro-alcali e degli organo-clorurati generati dalla produzione di pesticidi. L'industria Inquinosa ha prodotto Lindano dal 1975 al 1988 e ha formulato i suoi sottoprodotti fino al 1992. Lo smaltimento dei rifiuti ha generato un'area contaminata da DNAPL (Dense NonAqueous Phase Liquids) sopra lo strato impermeabile di marne, composta da una miscela di HCH, Clorobenzeni, BTEX e altri composti clorurati, che, diffusi sino a valle della discarica, implicano una grande minaccia per la qualità del suolo, delle acque superficiali e sotterranee, ma anche per la salute umana e gli ecosistemi. In quanto macro-sito contaminato da POP (Persistant Organic Pollutants), il sito di Sardas risulta essere molto interessante da studiare e presenta le condizioni adeguate all'applicazione di tecniche di screening non invasive come la "Radon deficit technique".

La "Radon deficit technique" sfrutta la presenza naturale del Radon (Rn) nel suolo e la sua forte affinità ai fluidi organici rispetto all'acqua. In corrispondenza della contaminazione si dovrebbe osservare sulla superficie una diminuzione del segnale di Radon. Questa tecnica è stata testata con successo in siti omogenei contaminati da LNAPL e DNAPL. Inoltre, è stata confermata la sua validità anche per il sito industriale di Inquinosa.

Con l'obiettivo di trovare quali condizioni influenzano la misurazione del Radon, e stabilire se è possibile determinare una relazione tra i picchi di deficit di Radon e la contaminazione, il presente lavoro analizza i dati di quattro diverse campagne, effettuate tra il 2016 e il 2019. I risultati del test ANOVA hanno dimostrato che l'unica condizione atmosferica che influenza la misura del Radon è la temperatura. È stata inoltre effettuata un'interpolazione spaziale dei dati, sia per i contaminanti in acqua sia per gli HCH in suolo a diverse profondità. I risultati mostrano una correlazione di Pearson significativa

tra segnale di Radon e contaminanti. Inoltre, è stato possibile anche sviluppare un confronto qualitativo tra il segnale di Radon e la contaminazione.

I risultati ottenuti a Sardas mostrano che esiste una relazione tra la diminuzione del segnale di Radon sia per i contaminanti in acqua, che per gli HCH in suolo. I risultati permettono di dire che la "Radon Deficit Technique" è applicabile, purché le misurazioni vengano effettuate ad una temperatura quasi costante, con un unico campionatore e che l'area di campionamento sia sufficientemente estesa in confronto all'ipotizzata contaminazione.

CONTENTS

LIST OF TABLES

LIST OF FIGURES

INTRODUCTION

Pollution of subsurface soil and groundwater by non-aqueous phase liquids (NAPL) from spills and leaks coming from industrial facilities or landfills has become a global concern as it poses a serious risk to human health and the environment (USEPA, 2003).

Uncontrolled landfill sites are one of the main sources of underground and surface water contamination. The absence of monitoring of large volumes of different types of wastes leads to the infiltration of leachates into the environment (Casado, et al., 2015), thereby severely contaminating the aquifers of the area.

One example is the Sardas's landfill located close to Sabiñanigo (Huesca, Spain). It is an old uncontrolled landfill that has been dumping huge quantities of urban, agriculture and industrial wastes since the 70s. The presence of leachates in waters below the landfill area has been observed since 2004, and the presence of a dense non-aqueous phase liquid (DNAPL) has been detected in 2009 (Dirección General de Calidad Ambiental, 2010).

While the consequences of dense non-aqueous phase liquid (DNAPL) releases on groundwater quality are easily observed, characterization and remediation of DNAPLs in groundwater remains problematic (Starr, 2007). Conventionally, these operations have been carried out by drilling and establishing a network of piezometers and wells in order to take samples of soil, groundwater, and NAPL. In the absence of preliminary site assessment studies, intrusive sampling campaigns are high-cost and, even worse, could be unsuccessful for the initial purpose (García-González, et al., 2008).

As a persistent organic pollutant contaminated macro-site, Sardas became a very interesting heterogeneous site to study, and presents suitable conditions to assess whether non-invasive screening techniques as the Radon deficit technique are applicable at the site.

The Radon deficit technique is based on the preferential distribution of Radon with the pollutant-free phases with respect to air or water. The presence of free phases retains the vertical Radon flow from the subsoil mineral matrix, allowing the detection of Rn emissions through the quantification of a decrease in the emission of it at the surface in relation to the local background value. The Radon Deficit Technique has been tested in sites with homogeneous lithologies and affected by light free phases in the vadose area (LNAPL) (Barbosa, et al., 2014) (Barrio Parra, et al., 2017). This technique was also

successfully tested in homogeneous contaminated sites by DNAPL and for the Inquinosa industrial site.

The main objective of this work is to determine whether the "Radon deficit technique" can be used as a method of detection in a DNAPL contaminated site, through a statistical analysis evaluate Radon's variability in time and identify conditions affecting Radon measurement. Then, with spatial interpolation, find a correlation between the contamination hotspots and the Radon deficit peaks. Concentrations of contaminants in water are evaluated, but mostly, HCHs contamination present as residual saturation in the vadose zone has been studied. This study also assesses up to what depth there is correlation between Radon signal and contaminants.

This thesis is developed as follows:

- Chapter 1: the chapter reports an overview of the theoretical background relevant to understand how DNAPLs are originated and how physical-chemical properties influence their propagation. Chapter 1 also includes a review on DNAPLs characterization techniques and how can the Radon Deficit Technique be a good non-invasive screening method of detection.

- Chapter 2: in this chapter an overview of Sardas site is provided, including a description of its peculiar hydrogeology, and the contamination history. Radon campaigns and the contamination collection of data are described.

- Chapter 3: statistical analysis. The analysis was carried out by using histograms, boxplots, Q-Q plots. The ANOVA test was performed to identify which atmospheric condition influences the Rn measurements.

- Chapter 4: spatial interpolation. IDW interpolation was chosen to compare Radon deficit peaks and contaminants hotspots. In Chapter 4 are described the results of the Pearson correlation obtained with R studio, and the qualitative comparison provided by ArcGIS.

- Chapter 5: Conclusions.

Chapter 1

1. THEORETICAL BACKGROUND

1.1. DNAPL ORIGIN

Many organic industrial chemicals and petroleum derivatives such as chlorinated solvents or polycyclic aromatic hydrocarbons are not soluble in water (Lemke, et al., 2004). In some cases, water resources are contaminated by these organic substances, not miscible with water. All these compounds are included in the generic term NAPL (NonAqueous phase liquids). They show behaviors and properties which are different from soluble contaminants (tracers), which are completely miscible with groundwater (Di Molfetta, et al., 2012).

Nonaqueous phase liquid (NAPL) is a term used to describe the hydrocarbon liquid that presents physical and chemical differences with water, which result in a physical interface between a mixture of the two liquids. The interface is a physical dividing surface between the bulk phases of the two liquids, but compounds found in the NAPL are not prevented from solubilizing into the ground water. Immiscibility is typically determined based on the visual observation of a physical interface in a water- hydrocarbon mixture (Lyman, et al., 1982).

NAPLs typically have been divided into two general categories, dense and light. These terms describe the specific gravity, or the weight of the nonaqueous phase liquid relative to water. Correspondingly:

- Dense NonAqueous Phase Liquids (DNAPLs) have a specific gravity greater than water;

- Light NonAqueous Phase Liquids (LNAPLs) have a specific gravity lower than water, and therefore tend to float on the water table (Huling, et al., 1991).

These substances have been found to persist in groundwater bodies for several decades due to their low solubility in water as well as elevated resistance against biodegradation (Pankow, et al., 1996). Several DNAPL compounds are carcinogenic and mutagenic,

posing significant risk to human health and other biota in the environment (European Commission, 2004). Besides being toxic themselves, DNAPL degradation often leads to the formation of daughter compounds such as vinyl chloride with even greater toxicological risks (Gandhi, et al., 2002).

1.2. DNAPL MIGRATION IN THE SUBSOIL

The mechanisms controlling the migration and fate of DNAPLs in the subsurface are complex and have been the subject of extensive research. The migration of DNAPLs in the subsurface is affected by numerous factors, including: the volume released, infiltration area, release duration, DNAPL properties, and the physical characteristics of the subsurface (Mercer, et al., 1990).

1.2.1. DNAPLs Physical properties

A number of physical properties influence DNAPL behavior in the environment and are therefore critical in optimizing site characterization and remediation. These properties are briefly summarized below.

Density

Fluid density is defined as the mass of fluid per unit volume, i.e. g/cm^3 and in general, density variates with temperature and pressure. The density of the DNAPL is critical in establishing the hydrostatic pressure that drives gravity flow. A greater density results in a greater hydrostatic driving force. Density is often described in terms of specific gravity (s.g.), which is the ratio of the mass of a volume of substance to the mass of an equivalent volume of water at a specific temperature (s.g. > 0 , NAPL penetrates in the water table).

Interfacial tension

Interfacial tension is defined as the free surface energy at the interface between two immiscible substances (Mercer, et al., 1990). This energy results from the difference between the mutual attraction of like molecules in a substance and the attraction of unlike molecules across the interface between the two substances. Figure 1.1 shows a three-phase system composed of a Liquid 1 (L1), Liquid 2 (L2), and Solid (S).
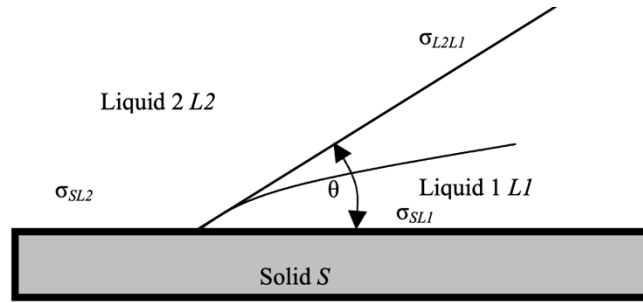
Figure 1.1 - Interfacial tension (Davis, et al., 2002)

In Figure 1.1 the relationship between the contact angle θ (measured through the denser fluid) and the interfacial tensions (σ) is given by:

$$cos\theta = \frac{\sigma_{SL2} - \sigma_{SL1}}{\sigma_{L2L1}}$$

When θ is less than 90°, Liquid L2 will wet the solid surface, while when θ is greater than 90°, Liquid L1 will wet the solid surface. Since water has a lower interfacial tension with solid surfaces than DNAPLs, it tends to wet the solid surfaces in saturated and unsaturated zones. The interfacial tension directly influences the wettability, that is, the preferential spreading of one liquid over a solid surface in a two-liquid system (U.S. EPA, 1990).

Viscosity

Viscosity is defined as a liquid's resistance to shear. As viscosity increases a DNAPL's resistance to shear increases, potentially decreasing its rate of penetration in the saturated zone. The lower the viscosity, the more readily a fluid will penetrate a porous media. The hydraulic conductivity of porous media is a function of both the density and viscosity of the fluid as indicated in equation:

$$K = \frac{k \, \rho \, g}{\mu}$$

Where K is hydraulic conductivity, k the intrinsic permeability, ρ is the fluid mass density, g the gravity and μ the dynamic (absolute) viscosity.

Capillary pressure (Pc)

Capillary pressure (Pc) defines the pore pressure of two liquids at the curved interface between those two liquids, as described by (Fetter, 1999).

$$P_c = \left(\frac{2\sigma}{r}\right)\cos\theta$$

Where r is the radius of curvature of the interface between the two liquids and σ is the interfacial tension between the two liquids. This property causes the porous media to attract the wetting liquid and repel the nonwetting liquid.

Relative permeability

Relative permeability (in reference to DNAPLs) refers to the reduction of the intrinsic permeability of a given medium in the presence of water and DNAPL. As DNAPL fills pores and displaces water, the relative permeability of the medium decreases for water and increases for DNAPL. Relative permeability is defined as the ratio of the permeability of a fluid at a given saturation to its permeability at 100% saturation. Thus, it can have a value between 0 and 1 .

Residual saturation

Residual saturation is defined as the volume of hydrocarbon trapped in the pores relative to the total volume of pores (Morrow, 1979). In Figure 1.2 is represented the relative permeability behavior of the wetting and non-wetting phases, for both is defined a value (residual saturation), below which the permeability is equal to zero. S_{wr} for a NAPL in the vadose zone variates from 0.1 and 0.2, from 0.1 to 0.5 in the saturated zone.
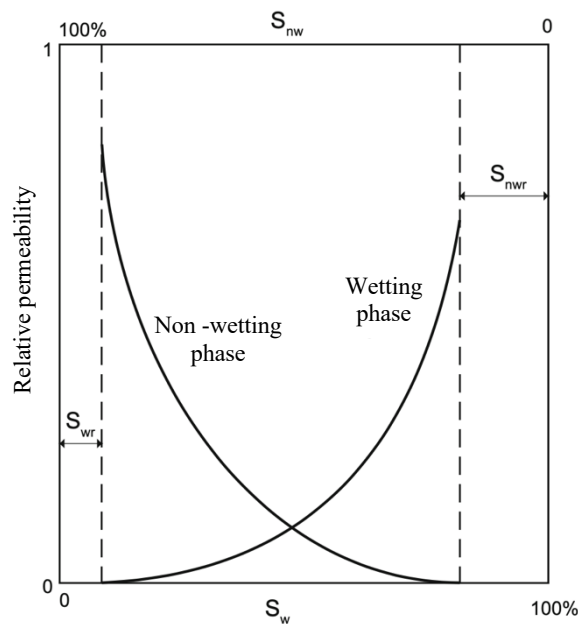
Figure 1.2 - Relative permeability behavior (Di Molfetta, et al., 2012)

1.2.2. DNAPLs behavior

DNAPLs are characterized by a higher density than water. Their movement in the non-saturated zone is characterized by a less lateral dispersion than the LNAPL, unless there are levels with reduced permeability. Once reached the water table, they tend to displace the water due to their higher density.

If the volume of DNAPL is limited and a continuous supply is missing, the product may not reach the base of the aquifer, but stop at a certain depth, once reached the residual saturation value. If instead the released volume is significant or if the feed is continuous, they may affect the full saturated thickness of the aquifer, accumulating on the waterproof substrate. Reached the base of the aquifer, they tend to move according to the topographic slope of the substrate, which may not coincide with the flow direction of the water. In the capillary fringe and in the aquifer, there is lateral dispersion until reaching residual saturation.

These areas with residual saturation, as in the case of LNAPL, however, represent a permanent source of contaminants dissolved in water.

The final configuration of a DNAPL contamination is strongly conditioned by the degree of heterogeneity of the aquifer, as well as by the release entity (Di Molfetta, et al., 2012).
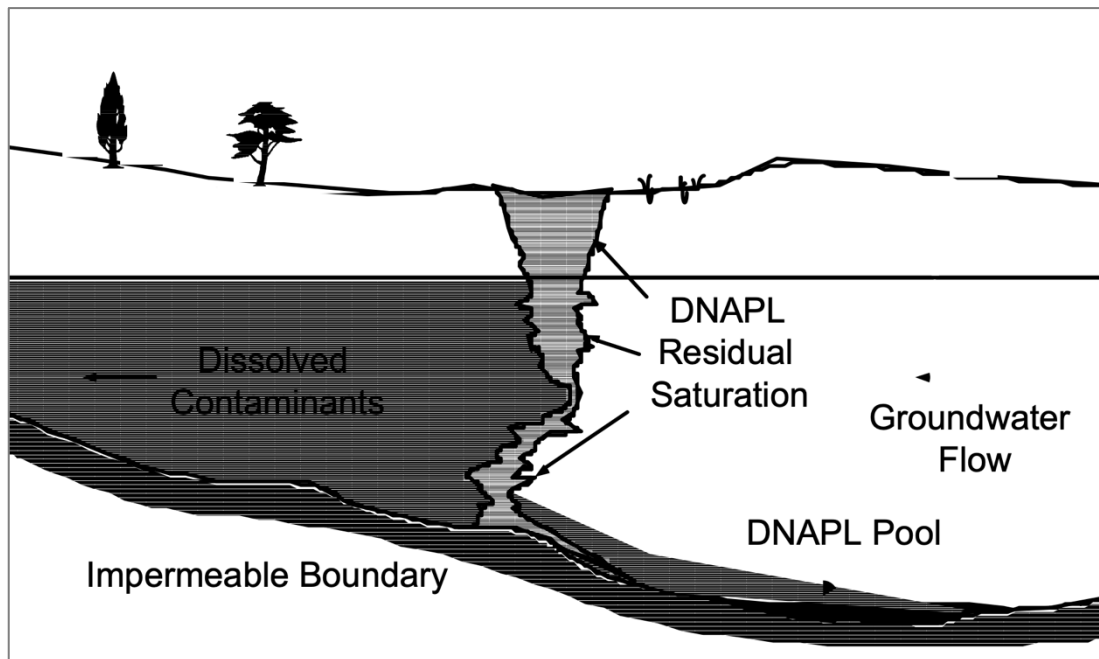
Figure 1.3 - DNAPL's fate in the subsoil (U.S. EPA, 1990)

Residual or pooled NAPL contamination provides a long-term source of contamination as it slowly dissolves into groundwater (Mercer, et al., 1990). And as dissolved contaminant plumes may reach extents up to several kilometers.

1.3. DNAPLs CARACHTERIZATION TECHNIQUES

Even when the lithology of the subsoil of a polluted site is well known, locating DNAPL source zones is difficult. Most methods for locating DNAPLs are either spatially limited, for example groundwater and soil sampling, or relatively expensive and time consuming as the Partitioning Interwell Tracer Tests (Zutphen, et al., 2000) (Goes, et al., 2004). Locating DNAPLs is often a bottleneck for the successful remediation and/or control of polluted sites.

The following methods are selected by (Kram, et al., 2001) because they have demonstrated potential for successful DNAPL source zone delineation at several sites. Some of the methods have been extensively tested (as geophysical surveys), while others are considered relatively new techniques.

1.3.1. Geophysical surveys

Electrical prospecting methods are based on the existence of variations in electrical properties, in particular the resistivity of the various subsoil formations, with the aim of determining the depth distribution (resistivity and thicknesses) of the geoelectric levels present. In particular, the electric tomography allows to obtain lateral and in-depth information by determining the resistivity values of the different cells in which the underlying soil can be divided under a given profile.

DNAPLs have a very high electrical resistivity, this attribute has been used successfully to monitor and to locate DNAPLs with Electrical Resistivity Tomography (ERT) (Newmark, et al., 1998). For the development of this method, the passage of a direct current through the subsoil is analyzed. The relationship between the difference in potential measured at certain points on the surface and the current intensity of the circuit will result in an apparent resistivity. This value depends initially on the arrangement of the emission and potential electrodes (measuring device).

By analyzing the apparent resistivity values for different devices, it is possible to determine the distribution of the real resistivity of the medium, depending on the characteristics it presents.

1.3.2. Non-geophysical surveys

Assessed technologies:

- **Baseline Methods**: typically consists of sample collection during drilling operations (usually at each 1.5 m), to characterize the soil matrix contamination analyzing undisturbed soil samples. Samples are typically collected using conventional drilling equipment and are immediately analyzed for identifying volatile organic compounds (VOCs).

- **Soil-Gas Surveys**: consist of insertion of soil-vapor collection devices into the subsurface, most commonly using a direct-push approach, application of a slight vacuum to the soil, collection of a vapor sample, and on-site measurement of VOCs using a gas chromatograph. This technique can be used only in the vadose zone.

- **Partitioning Interwell Tracer Tests (PITT):** is based on transport properties of several tracers, each with different partitioning characteristics (Jin, et al., 1995). A forced flow field is established to transport tracers through a specific volume of aquifer investigated. A suite of tracer is introduced in the subsoil using injection and recovery wells, at least one of the tracers is nonreactive with respect to the DNAPL organic liquid, while the other tracers partition, to various levels, into the organic liquid. The organic liquids retain the partitioning tracers and retard their migration, thereby leading to differential recovery times corresponding to the strength of partitioning and amount of DNAPL encountered (Nelson, et al., 1999).

- **Radon Flux Rates:** As for the traces used in the PITT approach, Rn-222 has a strong preferential affinity to organic fluids relative to water. By observing a relative deficit in the aqueous Rn-222 concentration, one can surmise that partitioning into a NAPL phase has occurred (Semprini, et al., 2006).

- **Backtracking dissolved VOC Concentrations in Wells**: Monitoring dissolved VOCs concentrations in wells, (Anderson, et al., 1992) describes the use of

downgradient solute concentrations to locate DNAPL source zones through the application of physical and analytical models.

Here is in Table 1.1 a resume of main advantages and disadvantages of these techniques.

Table 1.1 - Advantages and disadvantages of the main DNAPL characterization techniques.

METHOD	ADVANTAGES	DISADVANTAGES
Geophysical surveys (Electrical Tomography)	- Indirect evidence based on potential migration pathways.	- Anomalies may not be indicative of contrasts between source area and background.
Baseline Methods	- Can be both direct and indirect evidence.	- Best guess approach for sampling location/depth. - Volume not easily quantifiable.
Soil-Gas surveys	- Indirect evidence based on VOC detection in the vadose zone.	- DNAPL may not be easily volatized. - Preferential pathways can lead to misinterpretation.
Partitioning Interwell Tracing Test (PITT)	- Indirect evidence. - Can be used for volume estimates and evaluation of remediation method efficiency.	- Tracer migration may follow different pathways than DNAPL. - In organic rich soils, may have partitioning into organics other than DNAPL.
Radon Flux Rates	- Indirect evidence based on aqueous Rn concentration deficits. - Rapid equilibration of Rn. - Passive sampling (as opposite to injection).	- Lack of reliable sampling methodology. - Specialized sampling and analytical procedures required. - Site-specific partition coefficients difficult to obtain.

Backtracking dissolved VOC Concentrations in Wells	- Indirect evidence provided conditions are ideal. - Spatial distribution of dissolved material can provide information about spatial distribution of DNAPL.	- Concentrations may not be indicative of how close to source sample was collected. - Lower than 1% of effective aqueous solubility concentrations do not preclude the presence of NAPL.
Modified from (Kram, et al., 2001)		

1.4. RADON DEFICIT TECHNIQUE

DNAPLs migration in groundwater tends to follow preferential pathways in favor of gravity which are very difficult to delineate. Thus, the more complex the geology, the more difficult it is to characterize plume migration.

At regional or local scales, small changes in the hydrogeological characteristics of the subsoil can lead to very complex migration patterns which, if there is not much prior information, sampling using traditional intrusive techniques may be unproductive and costly, with the location of boreholes or piezometers producing information of little use or difficult interpretation, making it difficult to delimit the DNAPL plume and monitor the decontamination process (García-González, et al., 2008).

The aim is to validate the Radon Deficit Technique as a screening method to detect DNAPLs. Screening is term used to describe a test procedure that is designed to provide semiquantitative or range-finding results. A screening procedure will typically employ a single-point calibration. The calibration point is related to a specific decision (e.g., is the sample result above or below a given concentration?). On the other hand, quantitative assessments are more sophisticated procedures involving analytical data and quantitative data (Harris, et al., 1994).

1.4.1. Radon Deficit Technique applicability

The Radon Deficit Technique (or Emanometry) is a non-intrusive method, which may be a low-cost alternative to detect DNAPL on the surface and to monitor and control site remediation, even in the presence of low-volatility mixtures (Barrio Parra, et al., 2017). Emanometry has been validated as an exploration technique where there is a homogeneous geospatial subsurface structure ((Barbosa, et al., 2014); (Yoon, et al., 2013)), taking advantage of the existence of natural tracers as Radon.

In the subsurface, Radon-222 (Radon) is produced by the decay of naturally occurring Radium-226 contained in the mineral fraction of aquifer solids. In the saturated zone radon occurs as a dissolved gas, with a half-life of 3.83 days. In the absence of NAPL, radon concentrations in groundwater quickly reach a site-specific equilibrium (maximum) value that is determined by the mineral composition of the aquifer solids, which controls the rate of Radon emanation.

In the presence of NAPL, however, radon concentrations in groundwater can be substantially reduced due to the preferential partitioning of radon into the organic NAPL phase (Semprini, et al., 1998) (Semprini, et al., 1993). As a result, the spatial characterization of radon activity is useful to define areas affected by hydrocarbon spills. A reduced Rn concentration in soil air with respect to the local background values may be associated with the presence of regions highly saturated with NAPL (De Miguel, et al., 2018).

Due to its relatively low half-life 222Rn is expected to have a low mobility in the vadose zone through diffusion processes. However, co-advective transport processes with carrier gases (mainly CO_2) may be responsible of the ascent of 222Rn from deeper formations (Martinelli, 1998), making the Radon Deficit Technique suitable for the detection of NAPL in the vadose and saturated zones, as it is stated in (Semprini, et al., 2000) (Etiope, et al., 2002) (Yoon, et al., 2013) (Barbosa, et al., 2014) (De Simone, et al., 2017).

In addition to the applications found for sites contaminated by LNAPL, the technique has also been validated for contamination by DNAPL under the main industrial site of Inquinosa (De Miguel, et al., 2018).

1.4.2. Application in Sardas - methodology

Soil-gas sampling has been carried out to collect information on Sardas site contamination. The equipment used in Sardas are Radon detector by pulse ionization chamber RM-2 and RM-3 with a detection volume of 250 cm^3. The measurement is based on the difference in potential generated between the metallic exterior of the positively charged chamber and the electrode located along the longitudinal axis (0 V).

Figure 1.4 - Chambers, syringe, and Radon detector (Arco, 2017)

Alpha particles generated in the decomposition process of the two major isotopes of radon (222Rn and 220Rn), introduced into the chamber with the gas sample, create a measurable current that can be transformed to Radon concentration in Bq/m3.

The sampling execution protocol shall be as follows:

- Vacuum is applied to the 250 ml chambers prior to sampling.

- A steel bar is placed on the ground up to a depth of 80 -170 cm to minimize the influence of atmospheric factors (Thomas, et al., 1992).

- Sampling is performed by inserting a 150 ml syringe into the bar. Between the bar and the syringe is attached a drierite container tube to avoid the influence of moisture and contamination in the chamber.

- Three pumping are made with the syringe to remove the air inside the bar. The fourth suction is introduced inside the chamber. Are allowed 100 ml of atmospheric air (it does not affect the final result).
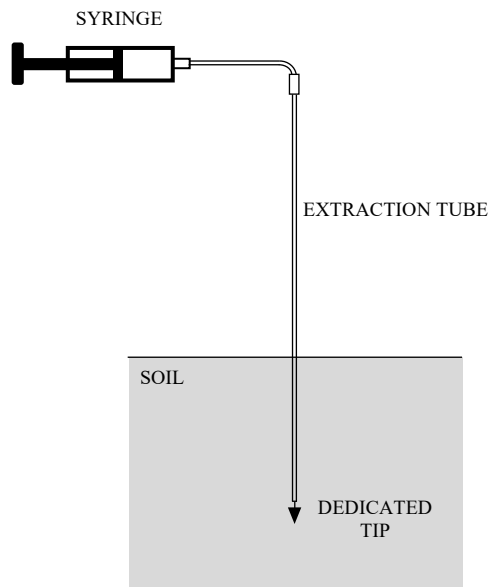
Figure 1.5 - Radon extraction scheme

- The sample must stay 15 minutes in the chamber since it is introduced to ensure that the measurement corresponds to that of 222Rn (after this time the activity of the 220Rn is negligible since its half-life is 51.5 s).

Chapter 2

2. STUDY CASE: SABIÑANIGO – SARDAS

2.1. SITE HISTORY

The site is located at the foot of the N-260 road that surrounds the city of Sabiñanigo in the province of Huesca, Aragón (Spain). To the West it is limited by the Sabiñanigo reservoir, filled by the river Gallego, and to the East the N-260 road separates it from the landfill of Sardas (source of pollution).

Figure 2.1 - Sardas site location

The pollution affecting this site comes from a historically uncoated landfill of about 240,000 m^3 (Casado, et al., 2015) in which large quantities of urban and industrial waste were deposited. The results of these discharges are two types of leachate: part is originated from the chlor-alkali industrial waste, part is and others formed by organochlorine compounds resulting from the manufacture of pesticides by the company INQUINOSA that is possible to see in Figure 2.1 (Fernandez, et al., 2012).

2.2. PAST ACTIVITIES AND CONTAMINANTS

Inquinosa produced lindane from 1975 to 1988 and formulated lindane products until 1992. Waste generation data differ depending on the information source used: about 6,800 MT/year of solid waste (1,500 MT/year according other sources) and 300-500 MT/year of liquid waste were estimated.

Lindane is the γ isomer of 1,2,3,4,5,6-hexachlorocyclohexane (HCH). γ - HCH and its hexachlorocyclohexane isomers (HCH-isomers) are classified as organochlorine pesticides (OCPs).
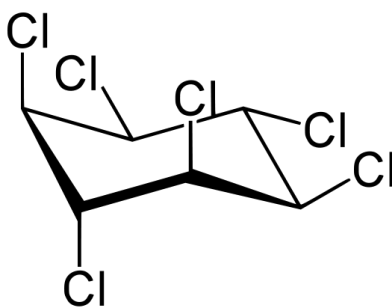
Figure 2.2 - Lindande chemical structure (Santos, et al., 2018)

The liquid residue resulted from the mixing of failed production head reactions and distillation tails for gamma isomer enrichment. This residue was initially sent to a lindane plant in France for treatment by thermal cracking. Later on, due to a lack of market for the sub-products of this cracking process, it was eliminated in drums dumped directly on the ground (Fernandez, et al., 2012).

In 2009, dense non-aqueous phase liquid (DNAPL) was detected in the surface in the Sardas site. Containment works and studies of the hydro-geological behavior of the site were initiated immediately, as a previous work to check the viability of confinement and treatment alternatives.

The disposal of waste generated a flooded area of DNAPL above the impermeable marl layer, composed by a mixture of HCH, Chlorobenzenes, BTEX and others chlorinated compounds, which spread downstream the dump, imply a great threat for soil, surface water and groundwater quality, as for human health and ecosystems (Barrio Parra, et al., 2017).

2.2.1. HCH

1, 2, 3, 4, 5, 6-Hexachlorocyclohexane (HCH) is a cyclic saturated chlorinated compound that persists in the environment (Vijgen, et al., 2019). There are eight geometric isomers of HCHs, which differ in the axial and equatorial positions of the chlorine atoms (Walker, et al., 1999).
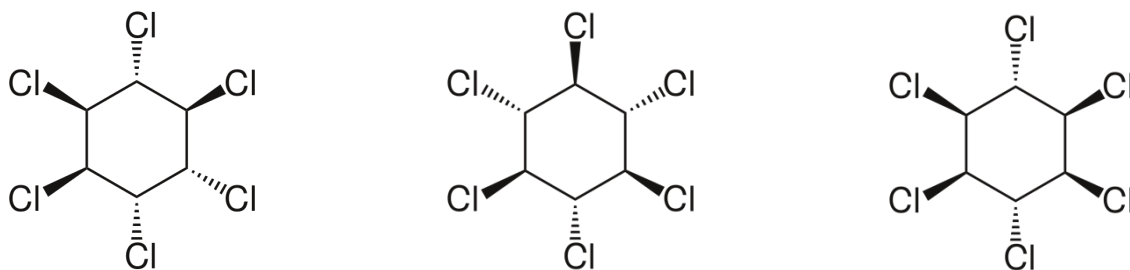
Figure 2.3 - HCH isomers (α-, β-, and γ-HCH)

HCH isomers (α-, β-, and γ-HCH) were recently added to the list of persistent organic pollutants (POPs) at the Stockholm Convention (Vijgen, et al., 2011). HCHs are available in two formulations: technical HCH and lindane. The isomers of α-HCH and γ-HCH are the main ingredients for the commercial product of technical HCHs (containing 60–70% α-HCH and 10–15% γ-HCH), and γ-HCH is the absolute ingredient of insecticide "lindane" (containing more than 99% γ-HCH). The ratio of α-/γ-HCH is frequently used as the indicator to identify the source of the HCHs.

Despite being a banned toxic substance in the vast majority of countries, HCH is regularly detected in the aquatic environment. Among the isomers of HCHs, α-HCH can cause human neurological disorders and gastrointestinal discomfort, resulting in liver and kidney damage, human endocrine system disorders and immune system abnormalities. In addition, as the only isomer with specific insecticidal properties γ-HCH was found to be a tumor promoter (Crawford, et al., 2017) (Kong, et al., 2014).

2.2.2. Chlorobenzenes

Chlorobenzenes are chlorinated aromatic hydrocarbons derived directly from benzene with replaced one or more hydrogen atoms (up to a maximum of six) with as many chlorine atoms; are thus obtained from monochlorobenzene to hexachlorobenzene (Di Molfetta, et al., 2012).
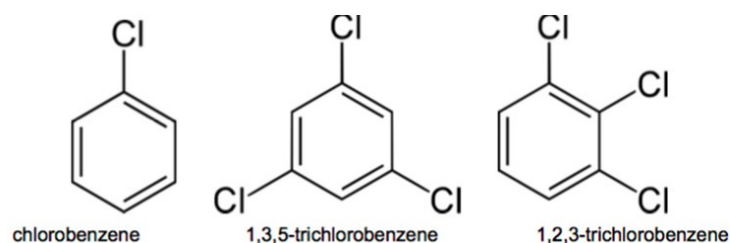

Figure 2.4 - Chlorobenzenes chemical structure

They are used as intermediates in several chemical processes and as solvents for degreasing operations. Their properties cover a wide range of behaviors:
- Volatilization is relevant only for mono- and bi-substituted compounds; same for solubility.
- Compounds with higher degree of chlorination (Penta- and esa- CB) are more hydrophobic, less mobile, more persistent.
- In general, susceptible to oxidation and biological degradation.

Some chlorobenzenes can be very toxic to aquatic organisms at certain concentrations and may cause long-term adverse effects in the aquatic environment above certain exposure levels. Long-term exposure to some chlorobenzenes may result in the development of particular cancers. Above certain exposure levels, some chlorobenzenes are toxic by inhalation or skin contact.

2.2.3. BTEX

Benzene is, of course, the base compound of the series, together with Toluene, Ethyl benzene and the three isomers of Xylene constitutes BTEX, among the most important components of gasolines.

Occur naturally in crude oil, can be found in sea water in the vicinity of natural gas and petroleum deposits (Di Molfetta, et al., 2012).
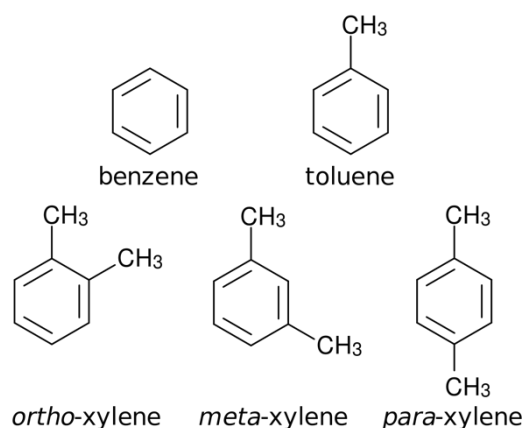
Figure 2.5 - BTEX Chemical structure

BTEX are created and used during the processing of petroleum products and during the production of consumer goods such as paints and lacquers, thinners, rubber products, adhesives, inks, cosmetics and pharmaceutical products. They are mainly found close to refineries. Relatively low solubility, high volatility.

2.3. GEOLOGY AND CONTAMINATION

The Sardas landfill is located a few meters from the Sabiñanigo hydroelectric reservoir. Geologically, it is situated within the southern area of the Pyrenees range, specifically in the central-eastern area of the Anticline Basin. The local geology (represented in Figure 2.6) is composed of sands and marlstones from the Larres marls Formation, Sabiñanigo sandstone and Pamplona marls that are locally covered by quaternary sediments (gravels, sands and shales). These sediments form glacis or via alluvial terraces that cover the landfill site (Casado, et al., 2015).

From the geological point of view, the site can be separated into two vertical sections (Figure 2.7 is a profile obtained from a section corresponding to the dashed lines in Figure 2.6), a porous dendritic one formed mostly by anthropic filling, in which the landfill was situated, on the top of the marl layer, and a second one which includes gravel corresponding to alluvial deposits of the Gallego river, and silt. The marls are not totally impermeable because they have an altered surface horizon of several meters, they are quite fractured because of regional tectonics they were subjected. In areas where they are neither altered nor fractured, marls can be considered impermeable.
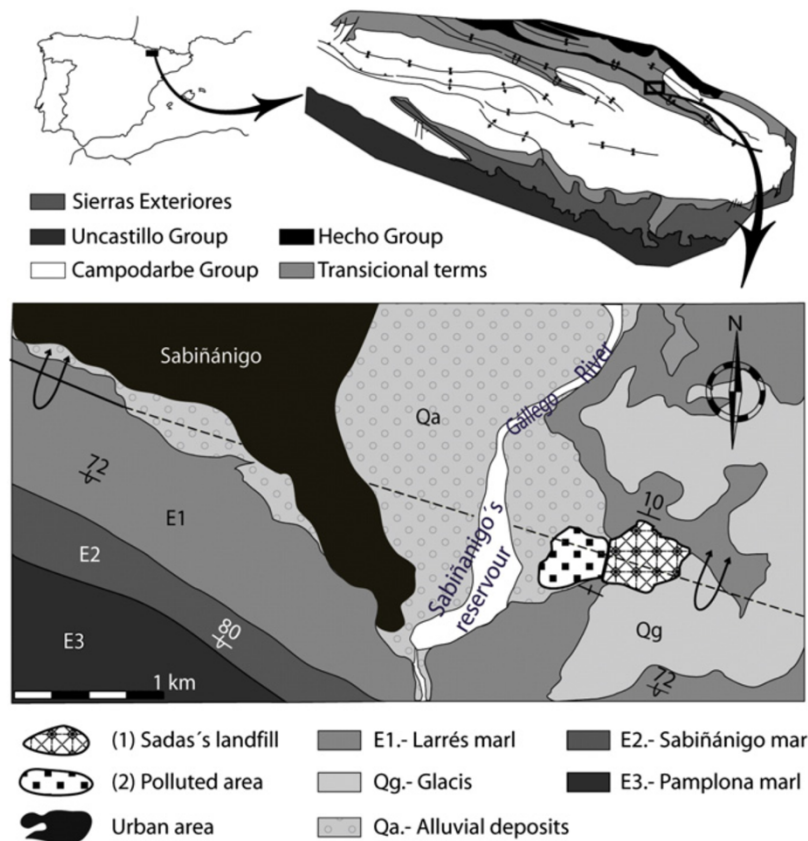
*Figure 2.6 - Sardas location and geology (Teixell, et al., 1994)*
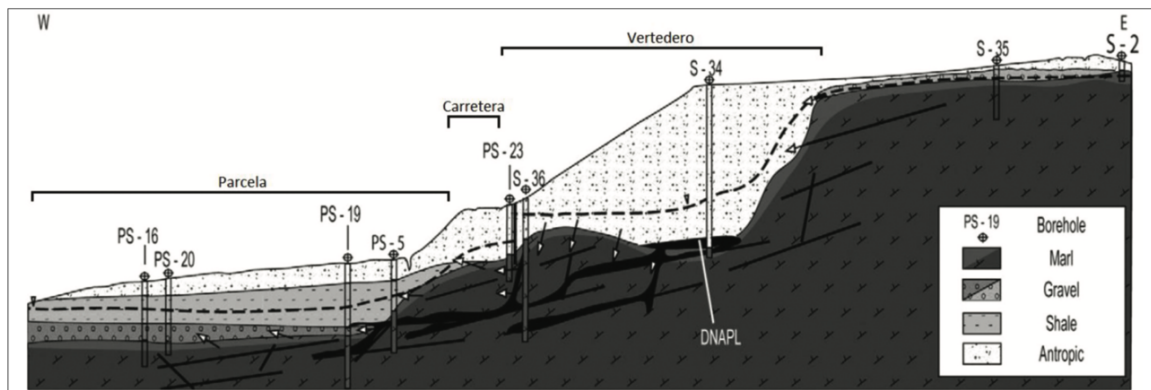
Figure 2.7 - E-W profile of the site's geology (Casado, et al., 2015)

The water table (dashed line in Figure 2.7) is between 5 and 10 m below the surface and the flow of groundwater occurs mainly in the upper debris layer and in the altered horizon of the marls in the direction of the reserve located south-west of the location.

The landfill leachate penetrated through the anthropic layer. As a case of a prolonged emission, the amount of material discharged into the soil allowed the DNAPL to penetrate through the aquifer and due to its higher density of water, to reach the basal layer of marls. Being the marls potentially impermeable, the DNAPL has accumulated taking the typical

conformation of "pool". However, the fractured horizon of the marls layer has facilitated the migration of DNAPL, according to gravity mechanisms, towards the road and the parcel of land near the river (Artalejo Lopez, et al., 2017).

In 1995, the Environmental Department of the "Diputación General de Aragón" decided to seal the landfill using sand and installing a high-density polyethylene (or HDPE) geotextile in addition, an impermeable layer was constructed at the foot of the landfill slope. (Casado, et al., 2015) also showed, thanks to the detection of two channels inside the marls, that these channels, formed by old streaming, serve as preferential routes for the DNAPL from the landfill vessel to the impermeable layer.

What is important in Sardas site it is also the contamination of the vadose zone. From the landfill was also found a stream of runoff water which dragged contaminants superficially to the lower limit of the anthropic layer which was subsequently filled. After that, there has been a percolation to the silt layer.

After sealing the landfill, a monitoring network consisting of 51 piezometers was installed, 7 of which are connected to a DNAPL pumping station. The mixture extracted from these seven wells is decanted and the resulting solid waste is sent to an incinerator. The aqueous phase is subjected to several physic-chemical procedures and an activated carbons treatment to decontaminate it (De Miguel, et al., 2018).

2.4. DATA SET

The current work analyzes Radon's data from four different campaigns, lasting from 2016 to 2019, to compare with collected data of the contamination in water and soil.

2.4.1. Radon samplings

The characterization of the Radon concentration in the subsoil was carried out by the team of the Laboratory of Research and Engineering Geochemical Environmental (LI2GA) of the UPM. Appendix A contains the entire database created and used for the analysis of this work, In Table 2.1 and Table 2.2 are summarized campaigns informations.

The methodology described in paragraph 1.4.2 has been used in all the Radon campaigns. In Figure from 2.8 to 2.11 is represented the location of the soil-gas Radon sampling points for each campaign, for which a regular grid sampling has been chosen.

Table 2.1 - Radon sampling campaigns

CAMPAIGN	DATA	EQUIPMENT	DEPTH [m]	COLLECTED SAMPLES
1	27-29/09/2016	RM2	0.8	65
2	14-15/03/2017	RM3	0.8 – 1.7	100
3	28/04/2017	RM3	1.7	15
4	04/06/2019	RM3	1.7	20
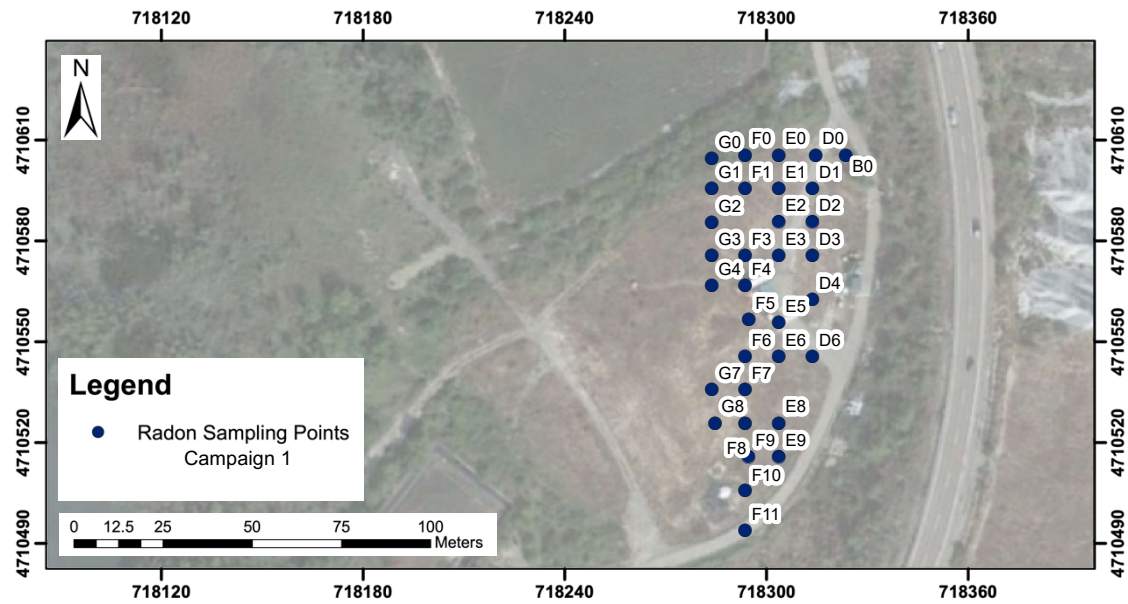
Figure 2.8 - Radon sampling campaign 1 - September 2016
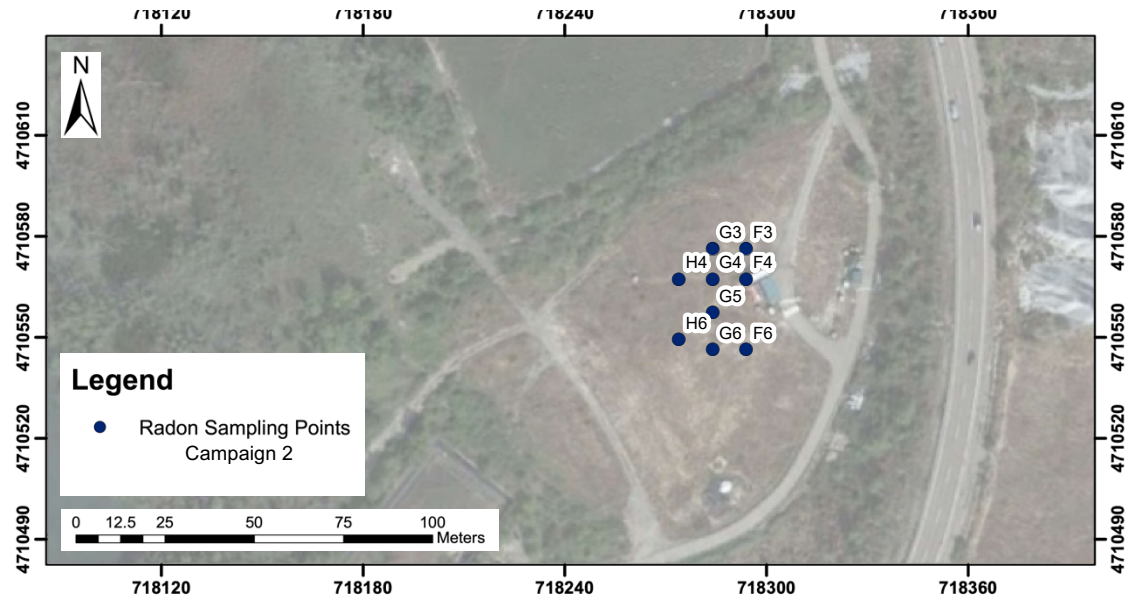
Figure 2.9 - Radon sampling campaign 2 - March 2017
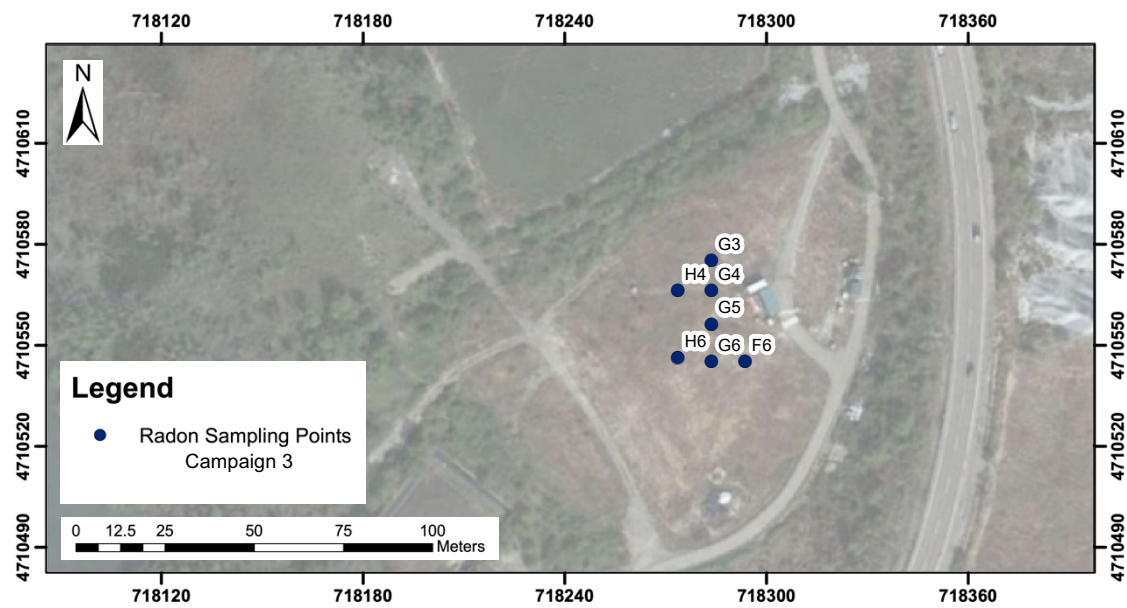
Figure 2.10 - Radon sampling campaign 3 - April 2017
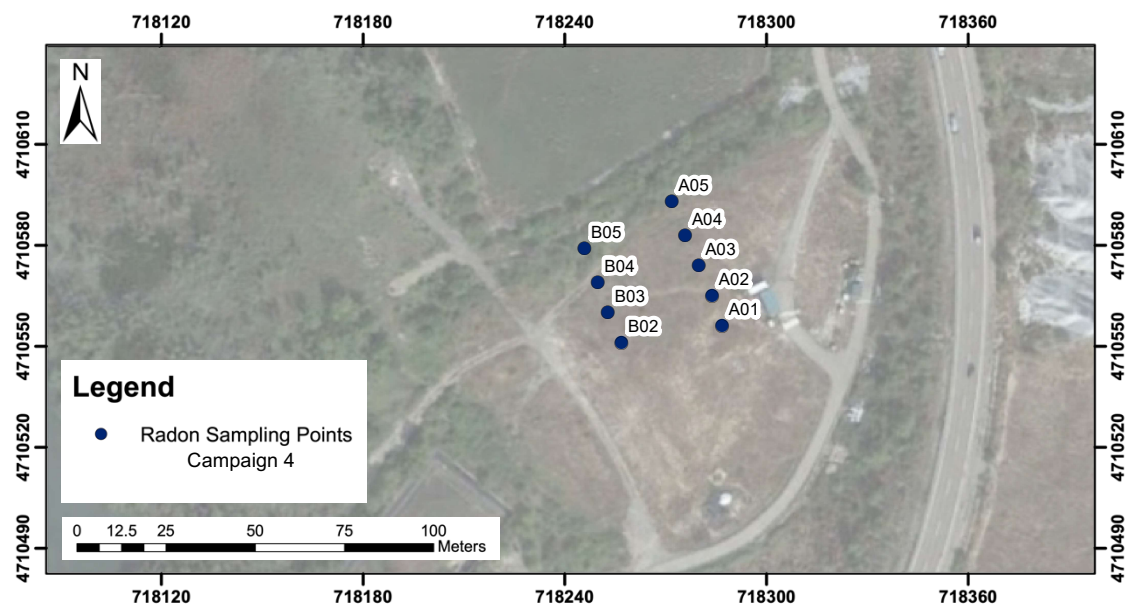
Figure 2.11 - Radon sampling campaign 4 - June 2019

Table 2.2 - Average parameters of the four Radon sampling campaigns

Campaign	Average Radon [Bq/m³]	Average Pressure [mbar]	Average Temp. [°C]	Average Wind Speed [m/s]
1	28635,11	939,59	21,97	2,11
2	18945,12	936,58	16,68	1,83
3	27861,54	927,58	14,04	/
4	42725,00	915,50	28,20	0,00

As it is possible to see in Appendix A, among the variables that characterized Radon measurement, it was also included if were found problems during the sampling phase. Problems that occurred are mainly:

- Difficulties in penetrating the soil with the equipment.

- Flow problems: may be referred to the presence of water in pores, the vacuum inside the syringe is not properly done, or simply there is no flux.

This distinction between measurements with problems or with not is important first of all to improve the sampling phase, secondly because Rn concentration values obtained are not representative if a problem occurred in its sampling.

The present work considered for the analysis only Radon measurements without problems, so instead of 200 samples, only 158 are representative.

2.4.2. Water sampling

The Company for the Management of Industrial Waste S.A (EMGRISA), commissioned by the Department of Environment of the Government of Aragon of the site remediation, facilitated independent analyses and data recordings of the piezometer network, from which the various maps of water chemical parameters were obtained. The control network of the landfill has 51 piezometers, seven of which are connected to a pumping station for DNAPL extraction. In Figure 2.12, the location of piezometers is reported.
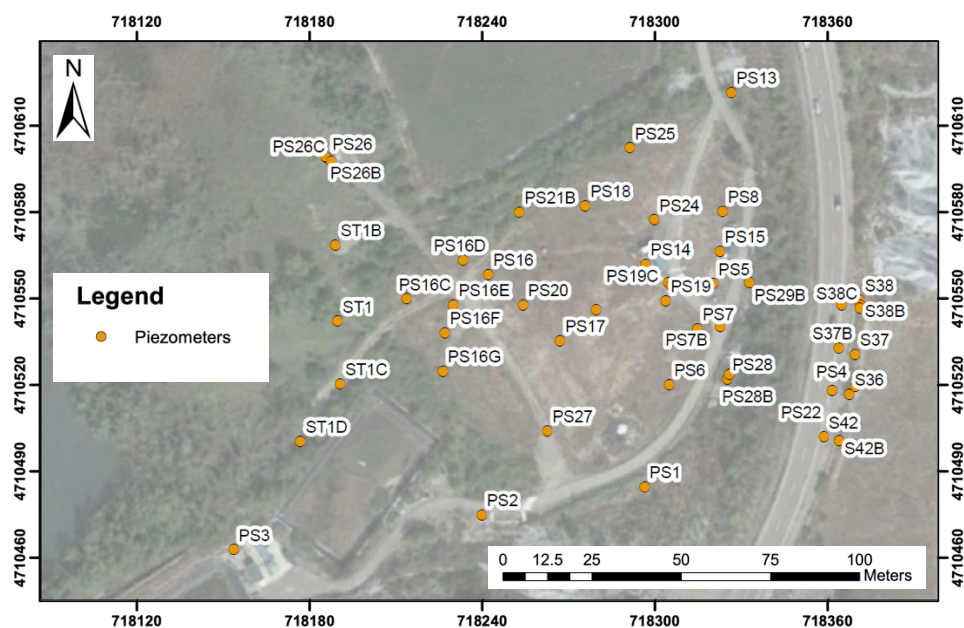
Figure 2.12 - EMGRISA installed piezometers

With the control network was possible to characterize the contamination, individuating the DNAPL plume extension and its chemical composition. In Chapter 4, it can be seen how HCHs, BTEX, and Chlorobenzenes are distributed in Sardas site.

2.4.3. Soil sampling

As the Radon deficit technique works in the vadose zone, it was very important to have information on the contamination in the vadose zone and not only the concentrations of contaminants in water. EMGRISA provided results of a detailed sampling campaign done in 2010, which contain measurements of HCHs concentration in soil at different sampling depth. Each depth is related to the variation of geological layers in Sardas site, starting from the anthropic one at the top, through the silt, the gravel, till the basal layer of marls. Therefore, this work divided all the measurements in 4 different levels:

- Level 1: up to a depth of 2-3 meters (corresponding to the anthropic layer).
- Level 2: up to a depth of 4-6 meters (corresponding to the silt layer).
- Level 3: up to a depth of 9 meters (corresponding to the gravel layer).
- Level 4: up to a depth of 18 meters (corresponding to the marl layer).

It was also necessary to convert the sampling points coordinates system from ETRS89 Zona 30N to UTM ED50 Zona 30N in which were set all the coordinates of the Radon's campaigns and the piezometers (OGP, 2009). The soil gas monitoring points installed by EMGRISA are located in Sardas site as it follows in Figure 2.13.
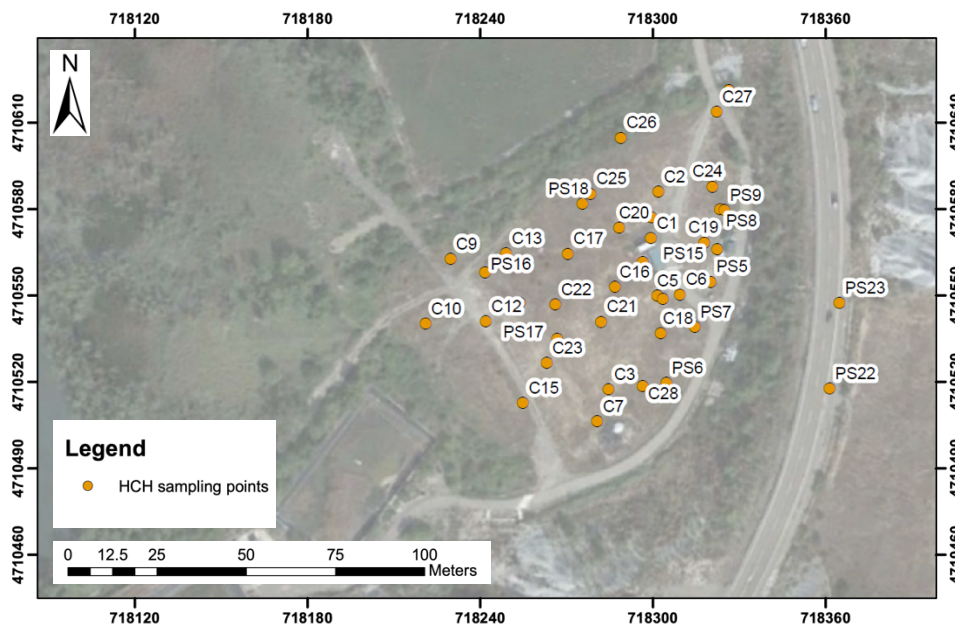
Figure 2.13 - Soil-gas sampling points

2.5. DATA ANALYSIS PROCEDURE

The main objective of this work is to determine whether the "Radon deficit technique" can be used as a method of detection in a DNAPL contaminated site, to identify conditions affecting Radon measurement as atmospheric conditions, and through spatial interpolation, find a correlation between the contamination hotspots and the Radon deficit peaks. In Chapter 3 and Chapter 4 the two parts of the dataset analysis are described:

- The first part is the statistical analysis, including the representations of the dataset and its subsets, using the software R studio. The analysis is carried out by using histograms, boxplots, Q-Q plots. The Tukey Test will be done in order to know the differences between means of the campaigns, and the ANOVA test will be performed to identify which atmospheric condition influence the Rn measurements.

- Chapter 4 will report the results of the Pearson correlation, done with the software R studio, between the IDW interpolation of Rn signal and contaminants, both in water and soil. Then, this work will involve a qualitative comparison between Rn and contamination IDW interpolation provided by ArcGIS.

Chapter 3

3. STATISTICAL ANALYSIS

3.1. DESCRIPTIVE STATISTICS

Before starting with graphical representations, in Table 3.1 it is possible to see a summary of the main statistics, for the entire dataset and each subset of data taken into account in the following paragraphs.

As mentioned before, for the statistical analysis and the spatial interpolation, only the measurements with no errors in the sampling will be considered, so the analysis is done on the basis of 154 observations and not 200.

Table 3.1 - Summary of the main statistics

	N° of samples	Min [Bq/m^3]	1st Quartile [Bq/m^3]	Median [Bq/m^3]	Mean [Bq/m^3]	3rd Quartile [Bq/m^3]	Max [Bq/m^3]
Dataset	154	200	10750	24750	25038	34100	112000
Campaign 1	44	9000	22275	27600	29175	34200	68500
Campaign 2	81	200	5100	16400	18843	28900	50500
Campaign 3	13	7300	24300	27800	27862	32600	40500
Campaign 4	16	500	25475	35150	42725	57975	112000
Depth 0,8 m	49	7400	22200	26000	28657	34100	68500
Depth 1,7 m	105	200	6000	21300	23349	34100	112000

With the database prepared and described in the previous paragraph it was possible to extract some statistical representations.

In statistics, the mode in a list of numbers refers to the integers that occur most frequently. Unlike the median and mean, the mode is about the frequency of occurrence. Sometimes

the average value of a variable is the one that occurs most often. For this reason, it is important to see if a data set is bimodal. Instead of a single mode, it has two (Figure 3.1).
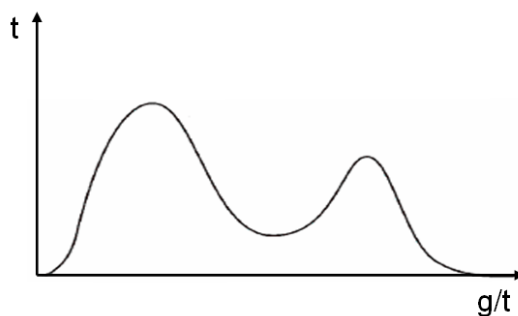
Figure 3.1 - Example of bimodal distribution

One major implication of a bimodal data set is that it can reveal that there are two different populations of data represented. For example, a histogram of a bimodal data set will exhibit two peaks or humps. These peaks will correspond to where the highest frequency of concentration value scored. If there are two modes, then this could show that there are two group of Radon concentration: the one who represent the Rn signal and the one who indicates the contamination, so a lower value of Radon concentration.

Histograms are excellent for showing the mode, the spread and the symmetry of a data set (Crawley, 2013). In Figure 3.2, the Rn distribution of the entire dataset is plotted including information of all items in all campaigns.
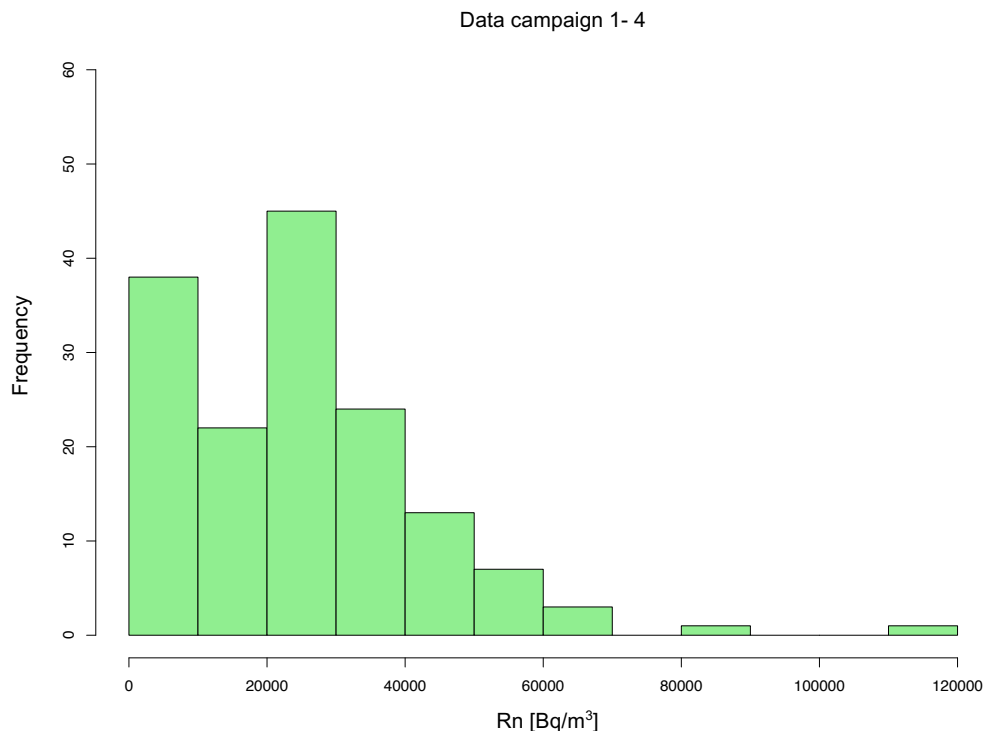
Figure 3.2 - Histogram of all the Rn concentration data

As it is possible to see, the Rn distribution may follow a bimodal distribution and two different populations of data could be recognized: the first with a low mean of values and the second ones with intermediate values. Thus, the two populations may come from two datasets grouped by spatial (position, depth) or temporal characteristics.

However, the dataset includes four different campaigns, at two different depths, so it is important to explicit the variation between each one of these. In Figure 3.3 are represented histograms of Rn concentration measured at 0.8 m and 1.7 m, while in Figure 3.4 are represented histograms considering each campaign separately.

Considering different depths brings to the attention that the two populations recognized in Figure 3.2 could be represented only if the sampling depth is 1,7 m, with the exception of campaign 4, probably because it contains a low number of data.

As these histograms show different distributions, and campaign 1 does not allow to find two populations of data, it is important to proceed with other analysis in order to understand more on this dataset.

Depth 0.8 m

Depth 1.7 m
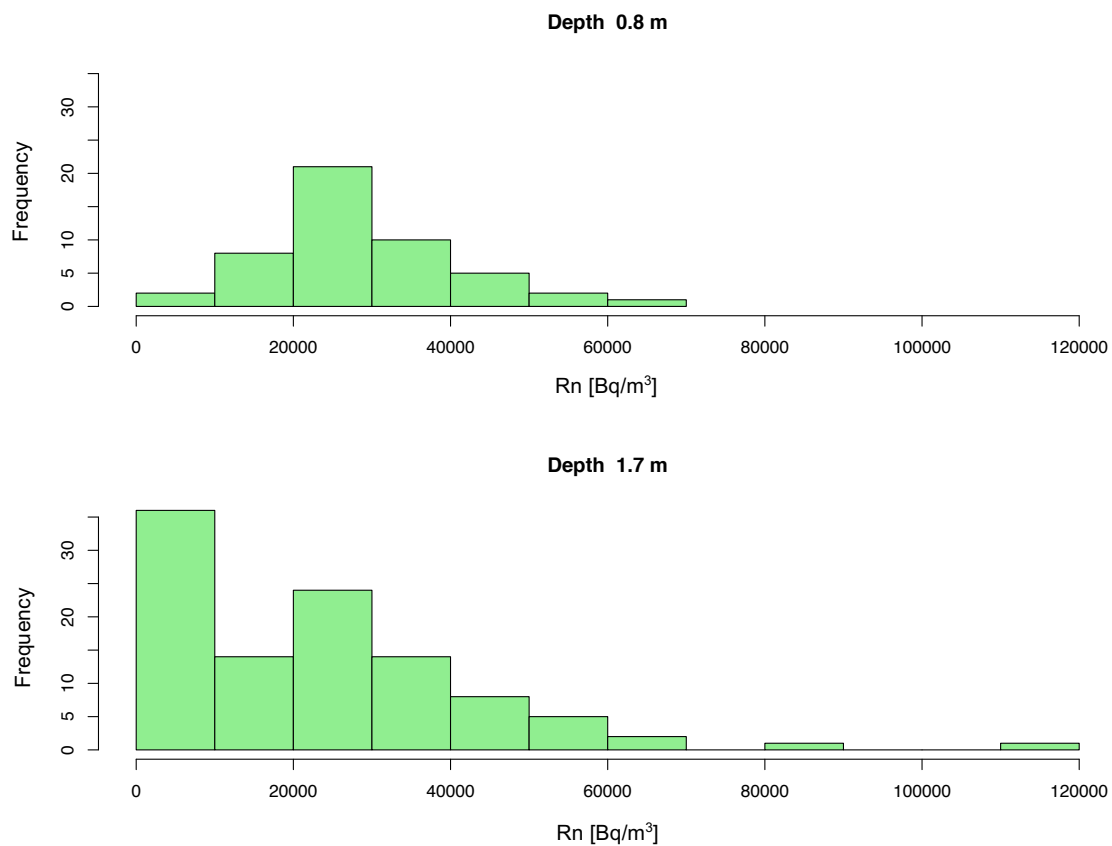
Figure 3.3 - Histograms of Rn concentration divided by sampling depth
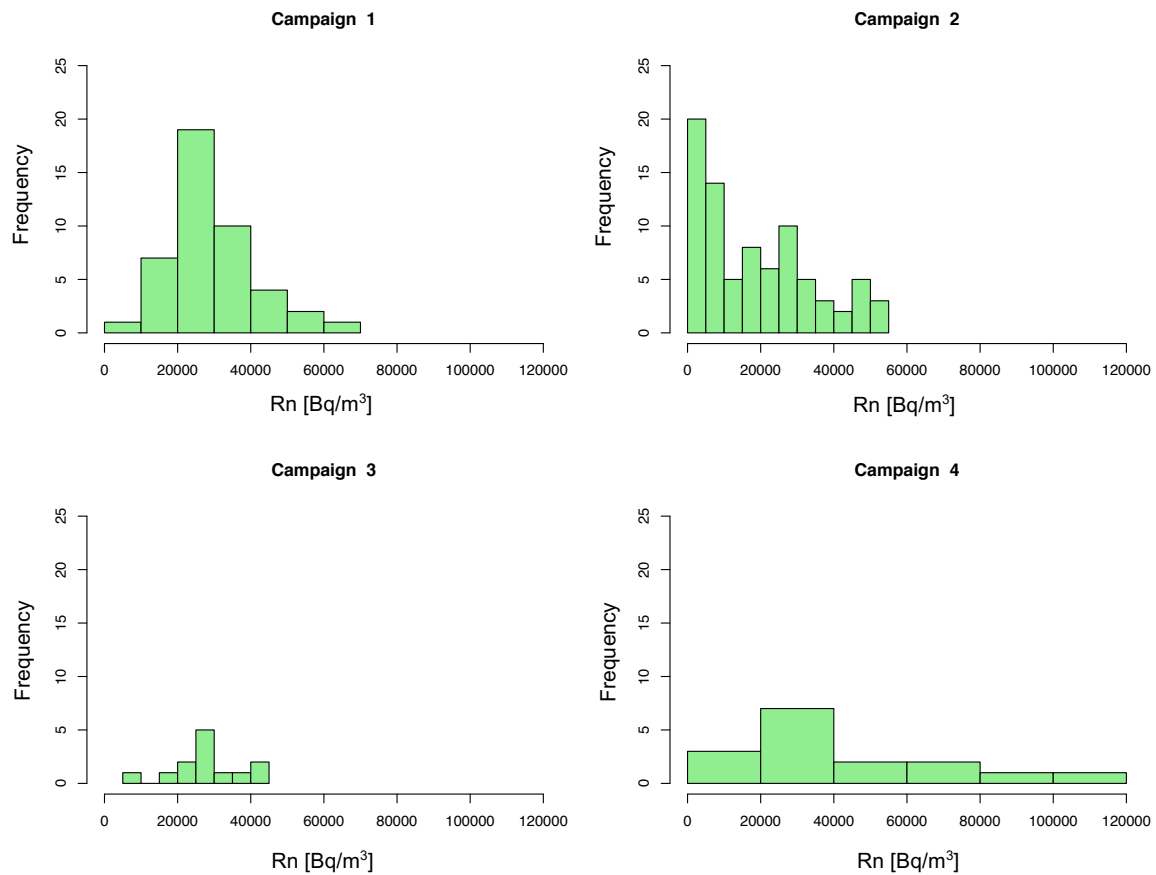
Figure 3.4 - Histograms of Rn concentration divided by campaign

From histograms it is also possible to see that the data distribution could be not normal. In order to verify this hypothesis two statistics tests on the four campaigns were performed:

- **Shapiro – Wilk normality test;**
- **Kolmogorov – Smirnov test.**

The first test is performed on campaigns 1, 3 and 4, the second one for campaign 2 because it contains more than 50 measurements. The four tests results (Appendix B) confirmed the hypothesis that the distribution of Rn concentration is not normal (that is reinforced with the Q-Q plots results in the next paragraph).

3.1.1. Plots for testing normality

The "quantile-quantile (q-q) plot" is a graphical technique for determining if two data sets come from populations with a common distribution. This plots the ranked samples from the distribution that is tested against a similar number of ranked quantiles taken from a normal distribution. If the sample is normally distributed, the line will be straight. Departures from normality show up as various sorts of non-linearity.
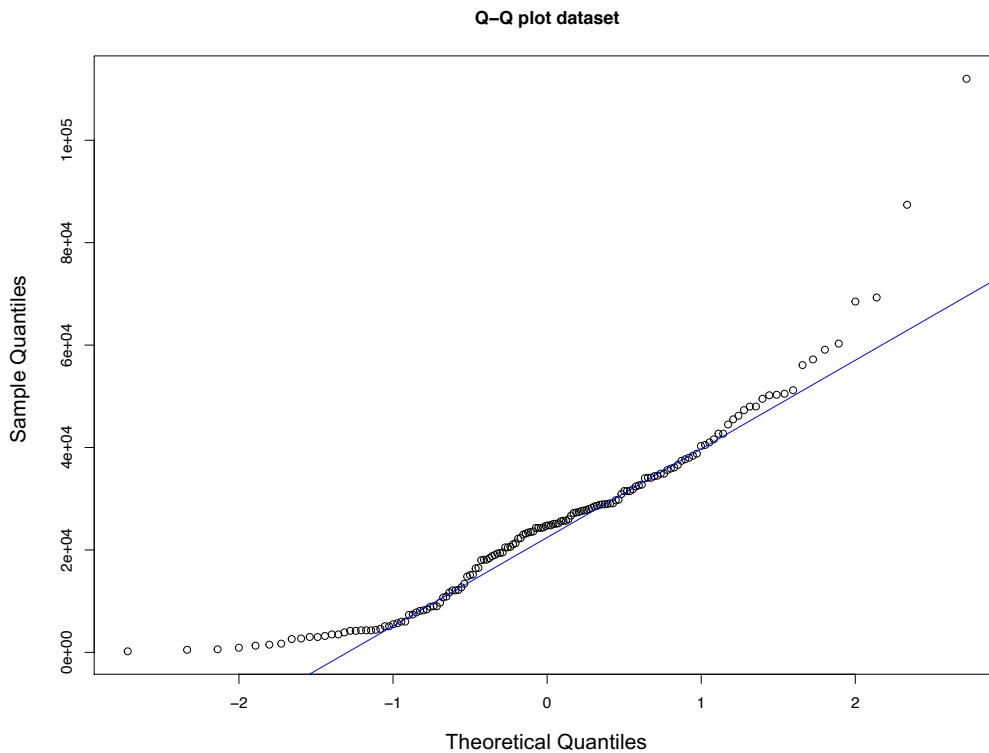
Figure 3.5 - Q-Q plot of Rn concentration of the dataset

In Figure 3.5 it is represented the Q-Q plot of the entire dataset, considering all the measurements without errors. In Figure 3.6 the result is plotted for each campaign separately. Except for campaign 3, whose different behavior could be explained by observing that it is the one containing the lowest number of data, Q-Q plots for dataset, campaigns 1, 2, and 4 show that the upper and the lower sections of the distribution are not following the straight line. This S-shape means that there are at least two populations of data, due to a different behavior of the Radon signal.
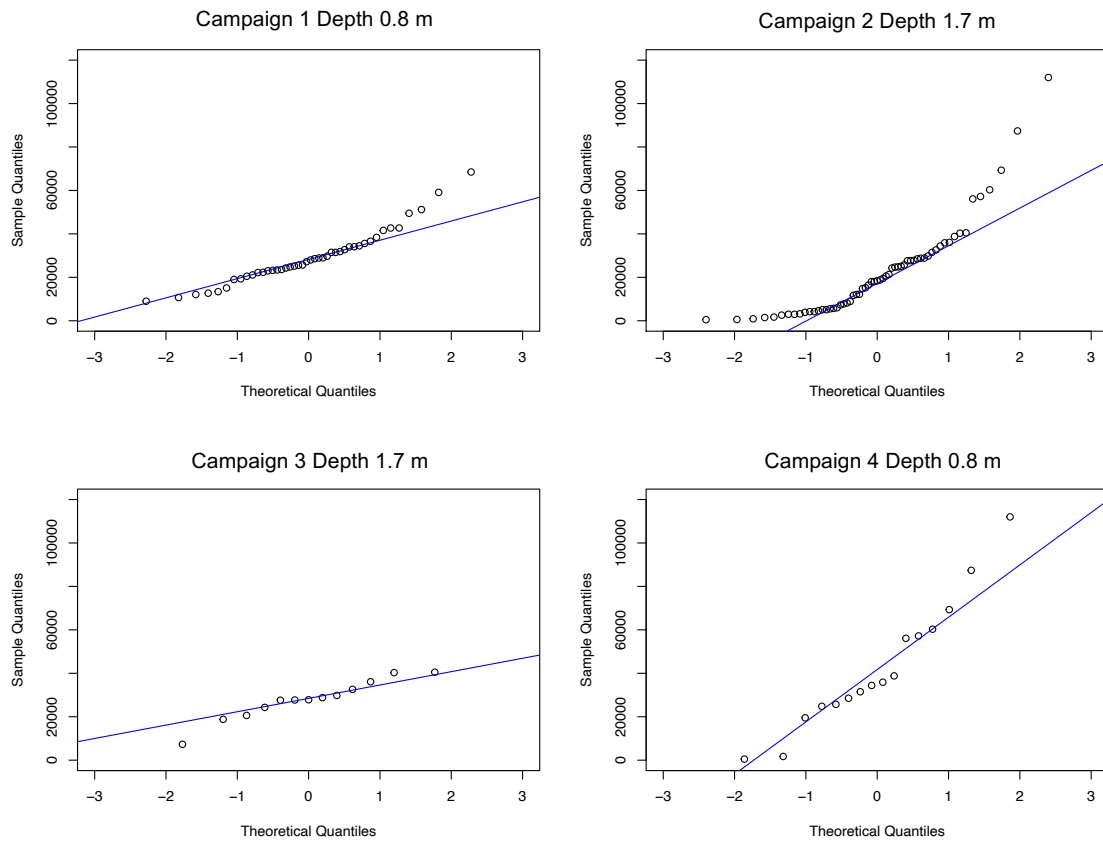
Figure 3.6 - Q-Q plot of Rn concentration divided by campaign

Results from Shapiro – Wilk and Kolmogorov – Smirnov test, with Q-Q plots of Rn concentration, indicate that Rn concentration's data need a change from Rn to ln(Rn) to have most similar distribution between points, this because to apply the average test Tukey HSD (Honestly Significant Difference) in the following paragraph data have to be approximated to a normal distribution.

In Figure 3.7 histograms of the four campaigns are represented; the data are reported after applying the logarithm to each Rn concentration value. Since they show a more normal distribution shape compared to Figure 3.4, it is possible to say that the original Rn distribution follows a lognormal one.

Lognormal distributions often arise when there is a low mean with large variance, and when values cannot be less than zero. They are very common in environmental phenomena, as they can describe random phenomena (Wayne, 1990).
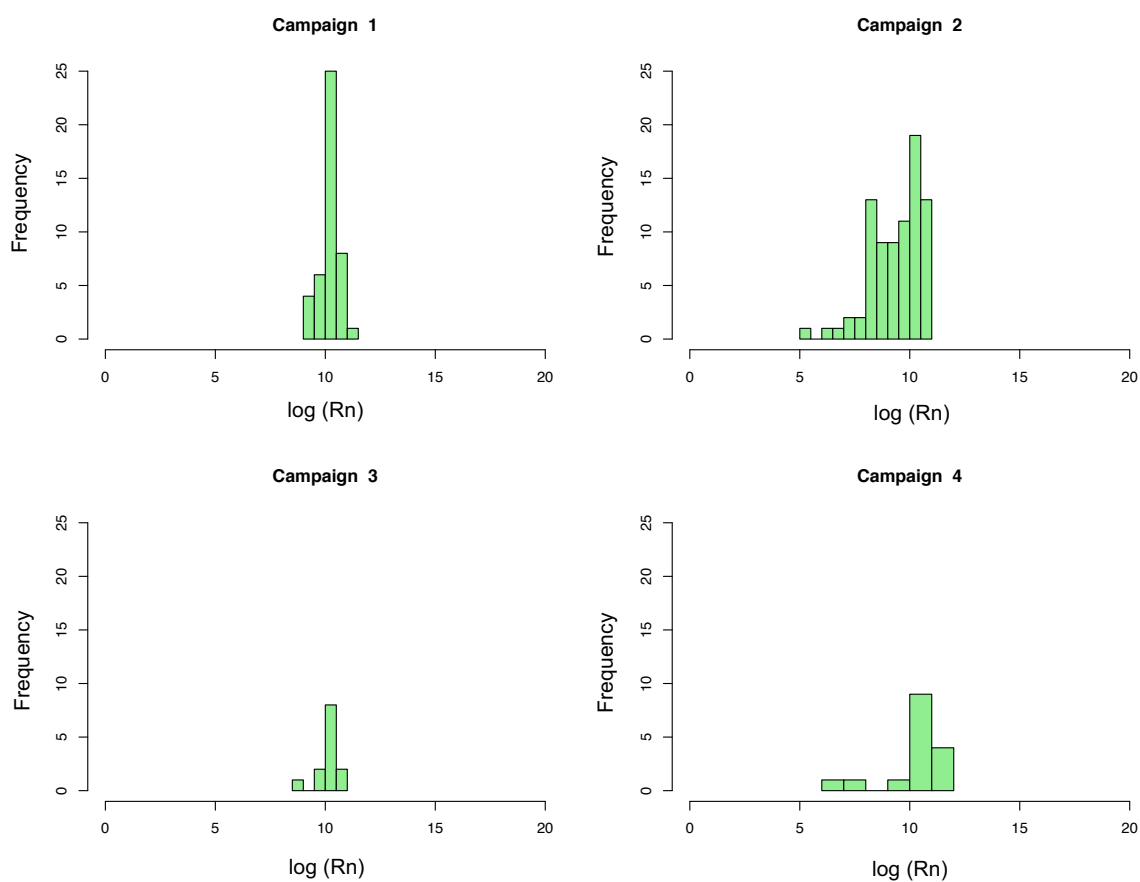
Figure 3.7 - Histograms of ln(Rn concentration) divided by campaign

These considerations bring to the necessity of a deep study of factors that may add uncertainty in data analysis as the sampling depth and the atmospheric conditions.

3.2. RADON VARIABILITY

Boxplots summarize a great deal of information very clearly. They are a standardized way of displaying the distribution of data based on a five-number summary ("minimum", first quartile (Q1), median, third quartile (Q3), and "maximum") (Galarnyk, 2018).
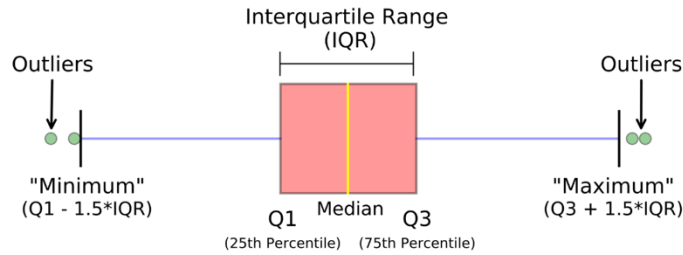
Figure 3.8 - Boxplot interpretation (Galarnyk, 2018)

Boxplots not only show the location and spread of data but also indicate skewness, which, as it can be seen in Figure 3.9, shows up as asymmetry in the sizes of the upper and lower parts of the box.
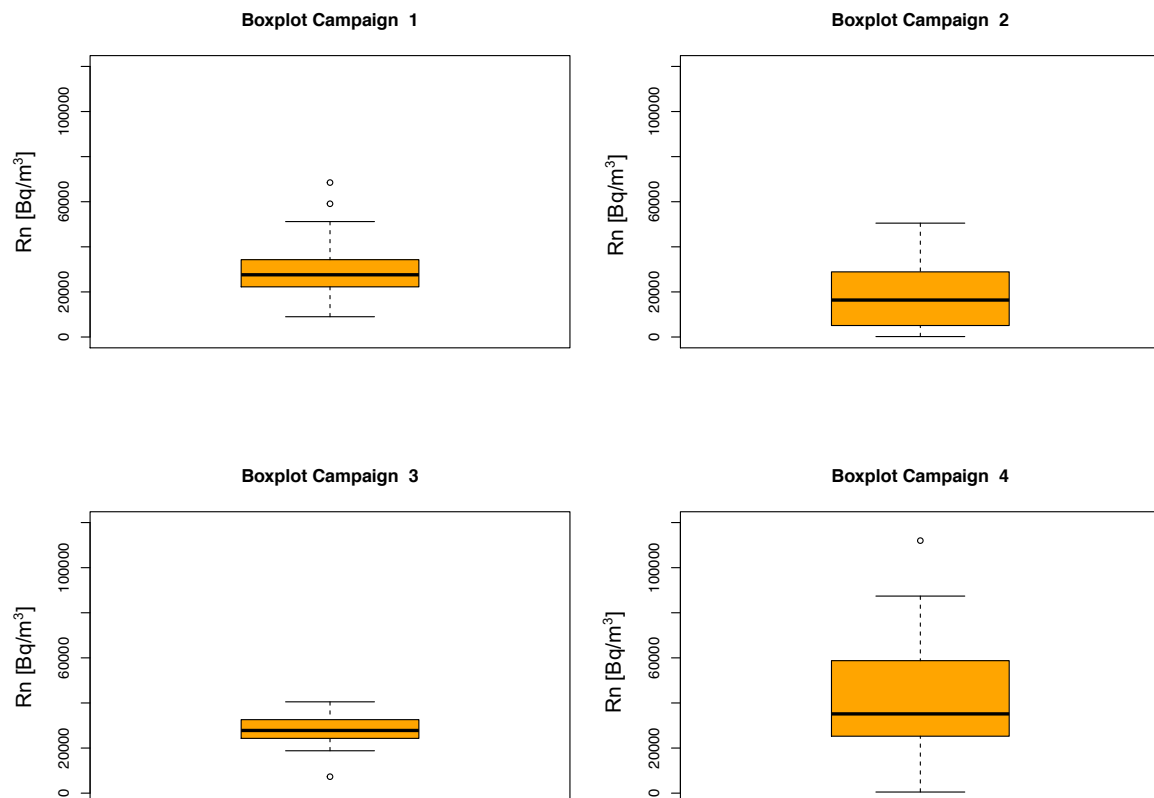
Figure 3.9 - Boxplots of Rn concentration divided by campaign

Besides being a less sensitive measure of the spread of a data set, the interquartile range has another important use. Due to its resistance to outliers, the interquartile range is useful in identifying when a value is an outlier. The quantity "$1,5 * IQR$" is roughly 2 standard deviations, and IQR the interquartile range $IQR = Q_3 - Q_1$. Points more than $1,5 * IQR$ above the third quartile and points more than $1,5 * IQR$ below the first quartile are defined as outliers and plotted individually (Crawley, 2013).

The horizontal line shows the median of Radon concentration for each campaign (Figure 3.9), and point divided by campaign (Figure 3.10).
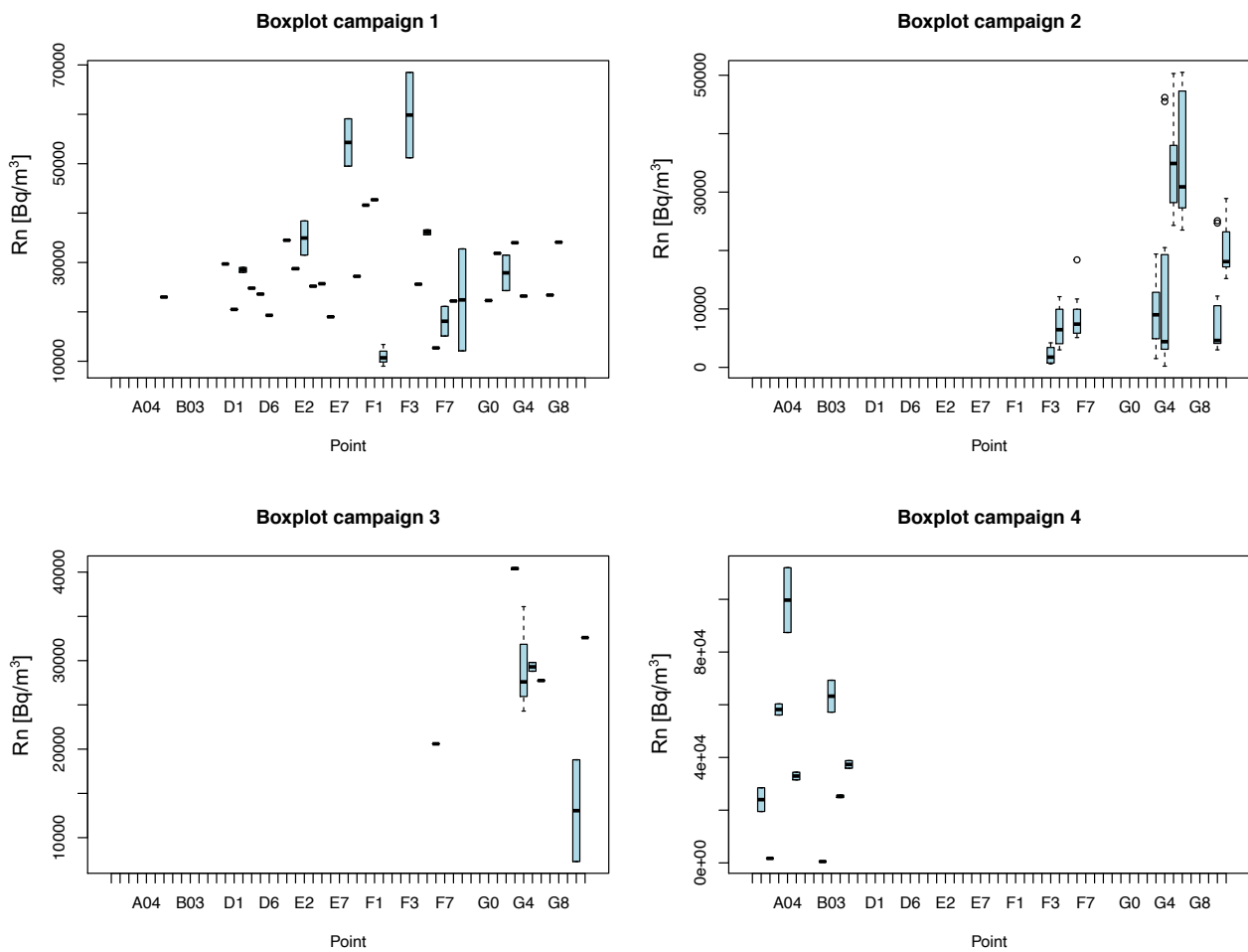
Figure 3.10 - Boxplots of Rn concentration for each sampling point divided by campaign

In Figure 3.9 it is shown that variabilities of campaigns 2 and 4 are wider than 1 and 3. The variability of campaign 2 could be explained with the multitude of collected samples, and the ones of campaign 4 by the effect of temperature on the Rn concentration (explained with the ANOVA test) which imply a wider range of values. Also, in Figure

3.10 it is represented that the sampling of each point is affected by a significative variability of Rn concentration.

The Tukey test was also performed on the four campaigns (Figure 3.11). It is a single-step multiple comparison procedure and statistical test. It can be used to find means that are significantly different from each other (Bretz, et al., 2011).

It has among the assumptions that the groups associated with each mean in the test have to be normally distributed, so for this test it has been used the logarithm value of Rn concentration.
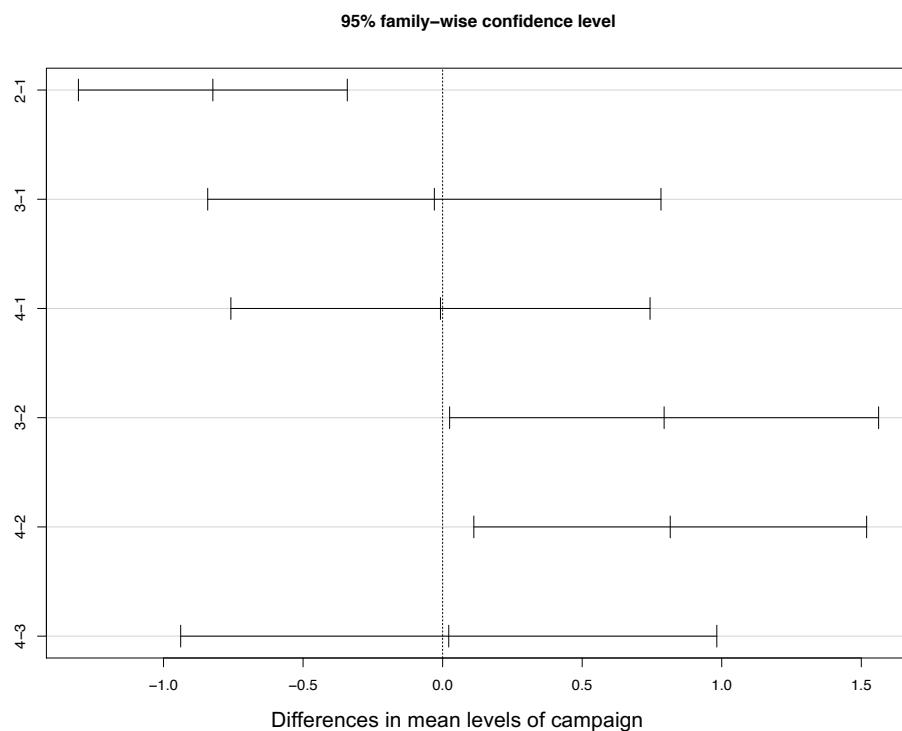
Figure 3.11 - Tukey Test performed on the four campaigns

Comparisons having intervals that do not overlap the vertical dashed line are significantly different. The vertical dashed line indicates no difference between the mean values for the factor-level comparisons indicated on the y axis.

It is possible to say that the contrast between campaigns (2 - 1), (3 - 2) and (4 – 2) fall just short of significance, but the interval is wide, so the means are quite different.

(Barrio Parra, et al., 2017) demonstrates that the use of different equipment could lead to a variation in the Rn concentration value. The difference between 2 – 1 could be explained by the use of equipment RM2 for the first campaign and equipment RM3 for the other, but also by the different average temperature. Differences between campaign 2 with

46

campaign 3 and 4 could be explained by the number of collected samples but also by the influence of atmospheric conditions (Paragraph 3.2.1).

3.2.1. ANOVA - Influence of atmospheric conditions

In order to understand if it is possible to characterize a site contaminated by a DNAPL with the Radon Deficit Technique, it is important to separate the dependence of each factor.

Analysis of Variance (ANOVA) is a statistical method that allows a comparison between two or more means, and it was implemented to understand whether the variance of each factor was influenced by the others.

The result of the ANOVA formula, the F statistic (also called the F-ratio), allows, for the analysis of multiple groups of data, to determine the variability between samples and within samples.

If no real difference exists between the tested groups, which is called the null hypothesis, the result of the ANOVA test, the F - ratio statistic, will be close to 1, instead, if exist a dependence, it will be higher. The higher the F-ratio value, the higher the dependency (Girden, 1992).

In Figure 12 are shown all the model generated with the software R:

- MODEL 1: it evaluates the influence of the depth and the campaign on the Radon measurement.
- MODEL 2: the depth is removed from the analysis, but the point of sampling and the atmospheric conditions are considered.
- MODEL 3: to eliminate the effect of the presence of four different campaigns, the variable campaign is removed from the analysis.
- MODEL 4: it is evaluated how the Rn measurement is affected by the atmospheric conditions.

The results of the ANOVA test are shown from Table 3.2 to 3.5.

Table 3.2 - ANOVA test results - MODEL 1

VARIABLES CONSIDERED	F VALUE	SIGNIFICANCE
Depth	3.597	NO
Campaign	10.411	YES
P-value: 3.807e-6		

Table 3.3 - ANOVA test results - MODEL 2

VARIABLES CONSIDERED	F VALUE	SIGNIFICANCE
Point	7.847	YES
Campaign	32.991	YES
Pressure	1.164	NO
Temperature	0.660	NO
Wind Speed	0.088	NO
P-value: < 2.2e-16		

Table 3.4 - ANOVA test results - MODEL 3

VARIABLES CONSIDERED	F VALUE	SIGNIFICANCE
Point	6.865	YES
Pressure	0.025	NO
Temperature	17.647	YES
Wind Speed	0.348	NO
P-value: < 2.2e-16		

Table 3.5 - ANOVA test results - MODEL 4

VARIABLES CONSIDERED	F VALUE	SIGNIFICANCE
Pressure	0.586	NO
Temperature	17.143	YES
Wind Speed	2.023	NO
P-value: 7.817e-06		

3.2.2. ANOVA interpretation

Summarizing the model's analysis of variance, it is very easy to interpret the results. As said before, when the F-ratio results much higher than 1, it is possible to consider that the Radon concentration is affected by that variable.

Results obtained from Table 3.2 to 3.5 it is possible say that:

- Rn measurements depend more on the campaign rather than on depth, that is because campaign 1 is at 0.8 m, in campaigns 2, 3 and 4 the sampling was done at 1.7 m.

- Campaign still remains significant over the atmospheric conditions; this could be related with the Radon's variability in time, in fact atmospheric conditions changes within the period of the campaign.

- Radon concentration depends on the superficial location from which it is observed; this result allows to relate the Rn measurement with the different lithology, or in case of a uniform lithology, with the presence of NAPL.

- The only atmospheric condition that affect the Rn concentration is Temperature. The explanation to this result will be provided in the following paragraph.

3.2.3. Radon affected by Temperature

The result obtained in Table 3.5 is crucial for this study and the applicability of the Radon Deficit Technique in a D-NAPL contaminated site.

It confirms that the sampling is done at a sufficient depth for which there is no influence of atmospheric conditions, wind speed and pressure as considered in paragraph 1.4.2 for (Thomas, et al., 1992) studies.

As already demonstrated in (Minkin, 2002) the Radon flow is not determined by pressure-driven mechanisms, but by thermo-diffusive mechanisms. Advective migration requires a sufficient concentration of gas for gravitational forces to act on it. Radon is present in concentrations too low to react to pressure gradients, that can be produced near the surface by atmospheric pressure (Etiope, et al., 2002), and flow autonomously due to advection. This result could also explain the high variability o Rn in the campaign "4" in the boxplots, which is the campaign with the highest temperatures, and the contrast between

campaign 4 and 2 in the Tukey test, as the campaign 2 is the one with the lowest temperatures.

Once completed the statistical analysis it is possible to proceed with the spatial interpolation of Rn concentrations, compared with the concentrations of contaminants. This is necessary to understand how the founded populations of data are distributed in the study area.

Chapter 4

4. SPATIAL INTERPOLATION

4.1. OBJECTIVES

The Radon deficit technique is based on the preferential distribution of Radon with the pollutant-free phases that retains the vertical Radon flow from the subsoil mineral matrix, allowing the detection of Rn emissions through the quantification of a decrease in the emission of it at the surface in relation to the local background value. In this chapter is described if it's possible to relate the decrease of Radon with the contamination hotspots both in water and soil, providing spatial interpolations of them. Through the calculation of Pearson correlation, it is also evaluated if the correlation between Rn concentration and contaminants change with depth.

4.2. IDW INTERPOLATION

Spatial interpolation is the process of estimating the values of properties at unknown points within an area covered by existing observed points. Spatial interpolation is a very important feature in many software, and it is also used for prediction and representation in many fields. There are several different ways to classify spatial interpolation procedures, such as point interpolation/area interpolation, global/local interpolation, and exact/approximate interpolation (Huang, et al., 2011).

As can be seen in paragraph 4.4 it was observed that the experimental variograms (points) fell inside the envelope of all variograms generated by random permutation of the observations (dashed lines). For a statistically significant spatial relationship, the actual semivariance should lie outside these random bounds at a specific distance (range). The absence of a significant semivariance at any distance indicates a spatially random process, with no spatial correlation between the different concentrations of Radon in soil air (Bivand et al. 2008). This lack of significant variograms precludes the construction of surface and iso values maps employing geostatistical models (i.e., Kriging). Consequently, an IDW interpolation was chosen for a 2-D representation of Rn concentration (De Miguel, et al., 2018).

The inverse distance weighted (IDW) spatial interpolation algorithm is a typical local interpolation algorithm. In the IDW interpolation method, the sample points are weighted during interpolation such that the influence of one point relative to another declines with distance from the unknown point is wanted to be created.
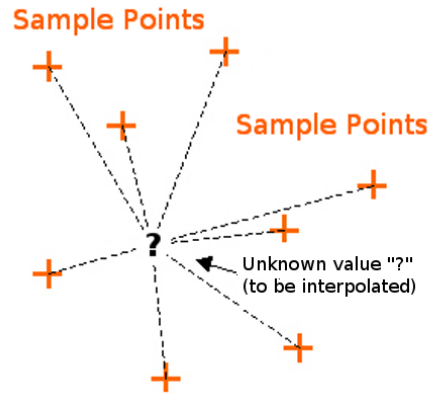
Figure 4.1 - IDW Interpolation (QGIS Training Manual, 2019)

Weighting is assigned to sample points through the use of a weighting coefficient that controls how the weighting influence will drop off as the distance from the new point increases. The greater the weighting coefficient, the less the effect points will have if they are far from the unknown point during the interpolation process. As the coefficient increases, the value of the unknown point approaches the value of the nearest observational point (QGIS Training Manual, 2019).

4.3. CONSIDERATIONS

The spatial interpolation has been developed in two parts, the first one will be described in paragraph 4.3 and it has been carried out with the use of the software RStudio (by RStudio Inc.), the second one, paragraph 4.4, reports some representations obtained using ArcGIS (by ESRI). IDW interpolation has been done for:

- Campaign 1, 2, 3 and 4.

- All the Rn concentration measurements from the four campaigns, by taking an average of the concentration's values in the common sampling points.

- Concentrations of BTEX, Chlorobenzenes and HCHs in water.

- Concentrations of HCHs in soil for each level described.

Since not all the data subsets are useful for a spatial representation, both parts of the analysis excluded:

- Campaign 2 and 3 individually represented, since they contain a small number of samples, compared to the others, and points are and close to each other, thus not allowing a meaningful representation.

- Also, the third level of the HCHs sampling in soil has been excluded from the comparison; the number of collected samples does not allow a representative interpolation.

In order to give a proper representation of the comparison between the Rn signal with contaminants it is important to eliminate the Rn dependence on temperature. To do that, in Figure 4.2 the linear dependence between the mean for each campaign of the two variables, Rn concentration and temperature, is plotted. As the dependence is linear it is only necessary to divide the Rn concentration value of each point for the average concentration of the correspondent campaign.
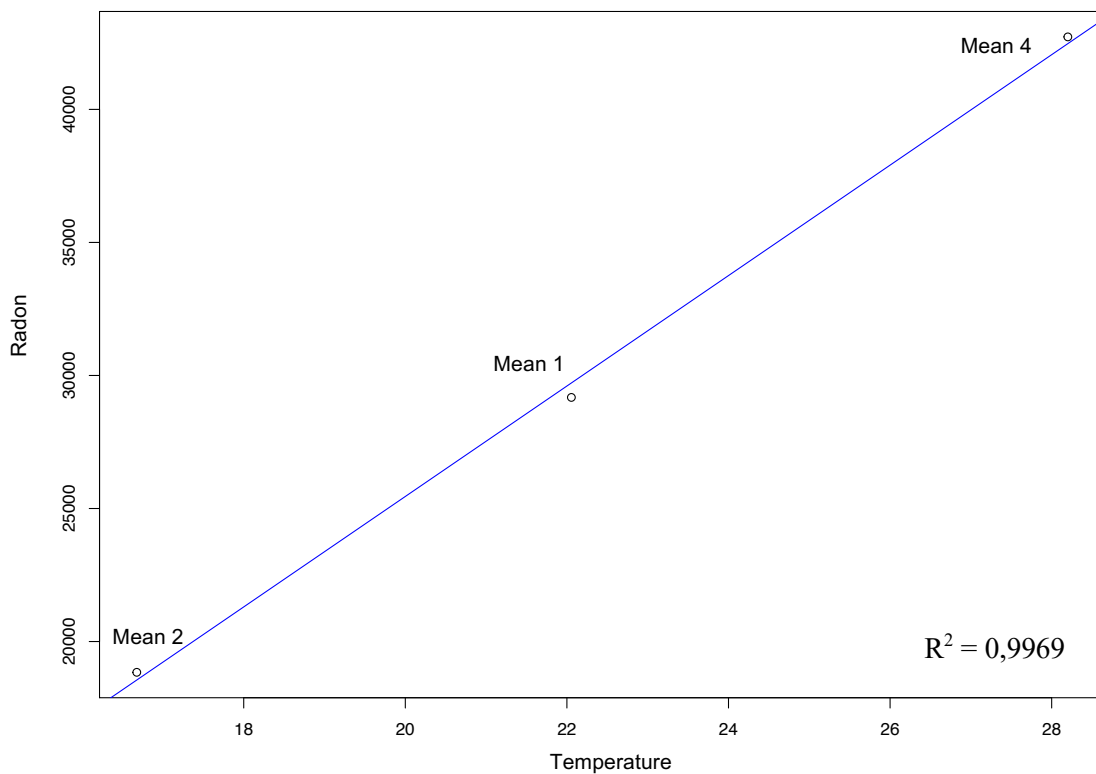
Figure 4.2 - Linear dependence between means of Rn concentration and Temperature

4.4.PEARSON CORRELATION

For the first part of the analysis and for the representation of Pearson correlation the RStudio software has been used, in particular its libraries: "geoR", "sp", "gstat", "raster", "tmap" and "rgdal". It has been used to plot in particularly:

- IDW Interpolation of the Radon concentration for campaigns 1, 4, and for all the campaigns joined.
- Variogram of the Rn concentration data.
- IDW Interpolation of the contaminants in water (BTEX, Chlorobenzenes, HCH).
- IDW Interpolation of the HCH in soil divided for depth levels.
- Pearson correlation between the Rn concentration and the contaminants.

All the plots are created by selecting a common area of interest. The area has the same coordinates for each interpolation as it is possible to see in Figure 4.3, and it is selected by considering all the Radon sampling points and the majority of the polluted area. This operation excludes some of the piezometers but is necessary to calculate the Pearson correlation.

4.4.1. Pearson correlation coefficient

Pearson's correlation coefficient is a statistical measure of the strength of a linear relationship between paired data. In a sample is denoted by r and is by design constrained as follows:

$$-1 \leq r \leq 1$$

Furthermore:
- Positive values denote positive linear correlation;
- Negative values denote negative linear correlation;
- A value of 0 denotes no linear correlation;
- The closer the value is to 1 or –1, the stronger the linear correlation.

According to this explanation, and considering that theoretically areas with hotspots of contaminant correspond to peaks of deficit of Radon, and vice versa, the result of the Pearson correlation should be a map representing most negative Pearson coefficient values, obviously this is ideal, it would be sufficient to obtain in the representation quite extended negative correlation areas.
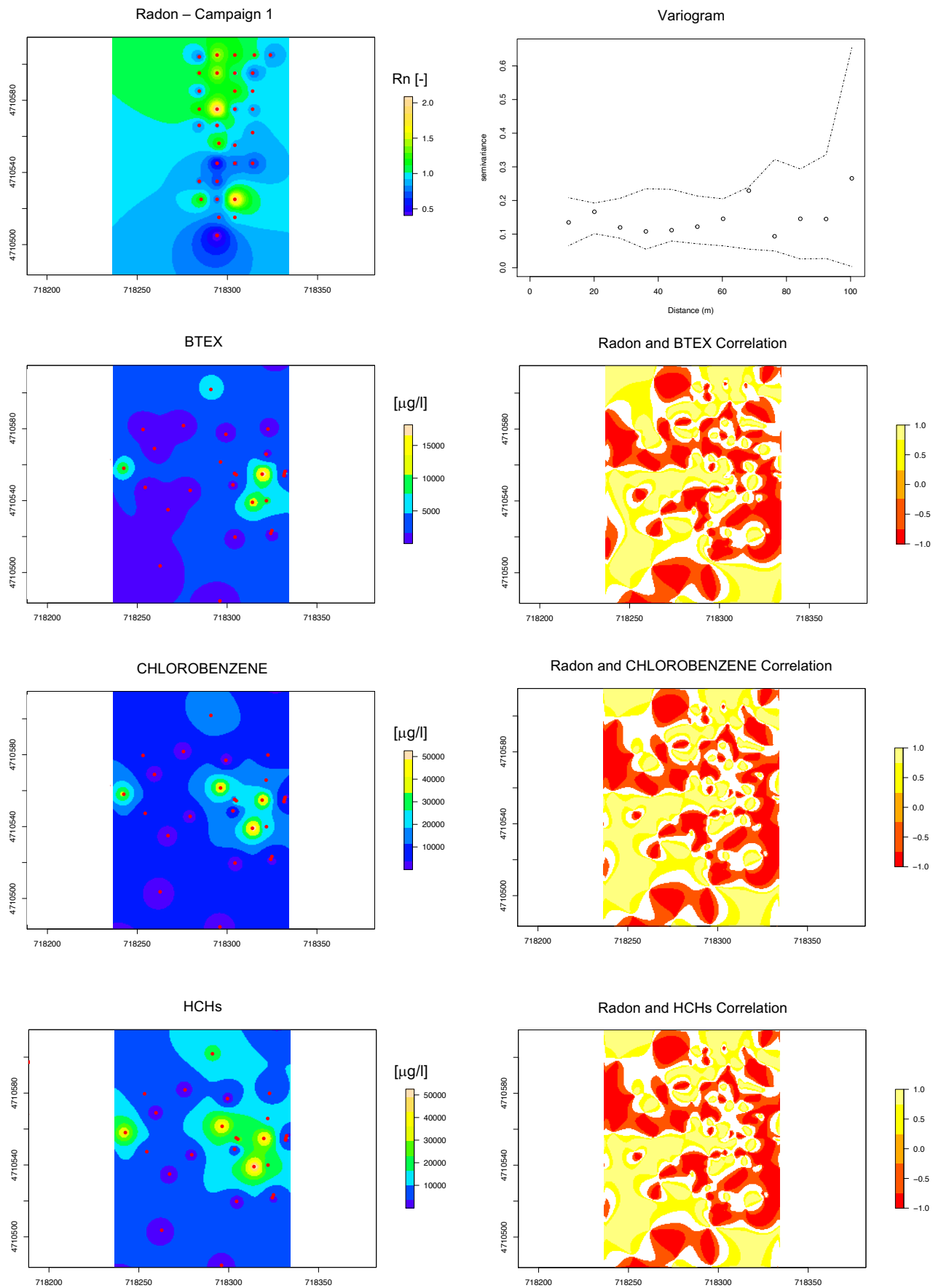
Figure 4.3 - Pearson correlation - Radon (Campaign 1) and contaminants in water

4.4.2. Contaminants in water

As can be seen in Figure 4.3 which represent Pearson correlation, between the Radon concentration of campaign 1 and contaminants in water there is a strong alternation of values very close to 1 or -1, but no area of such an extent to find a correlation between the represented interpolations. Campaign 1 it is just an example, but the same result was found with campaign 4 and with the interpolation of all the campaigns. The problem with this correlation will be better explained also in paragraph 4.5.

4.4.3. HCHs in soil

Different are the results of the Pearson correlation between Rn concentration and the soil-gas concentration measurements. The results of Figure 4.4 and 4.5 are the most useful to explain the relevance of this correlation, both qualitative and quantitative.
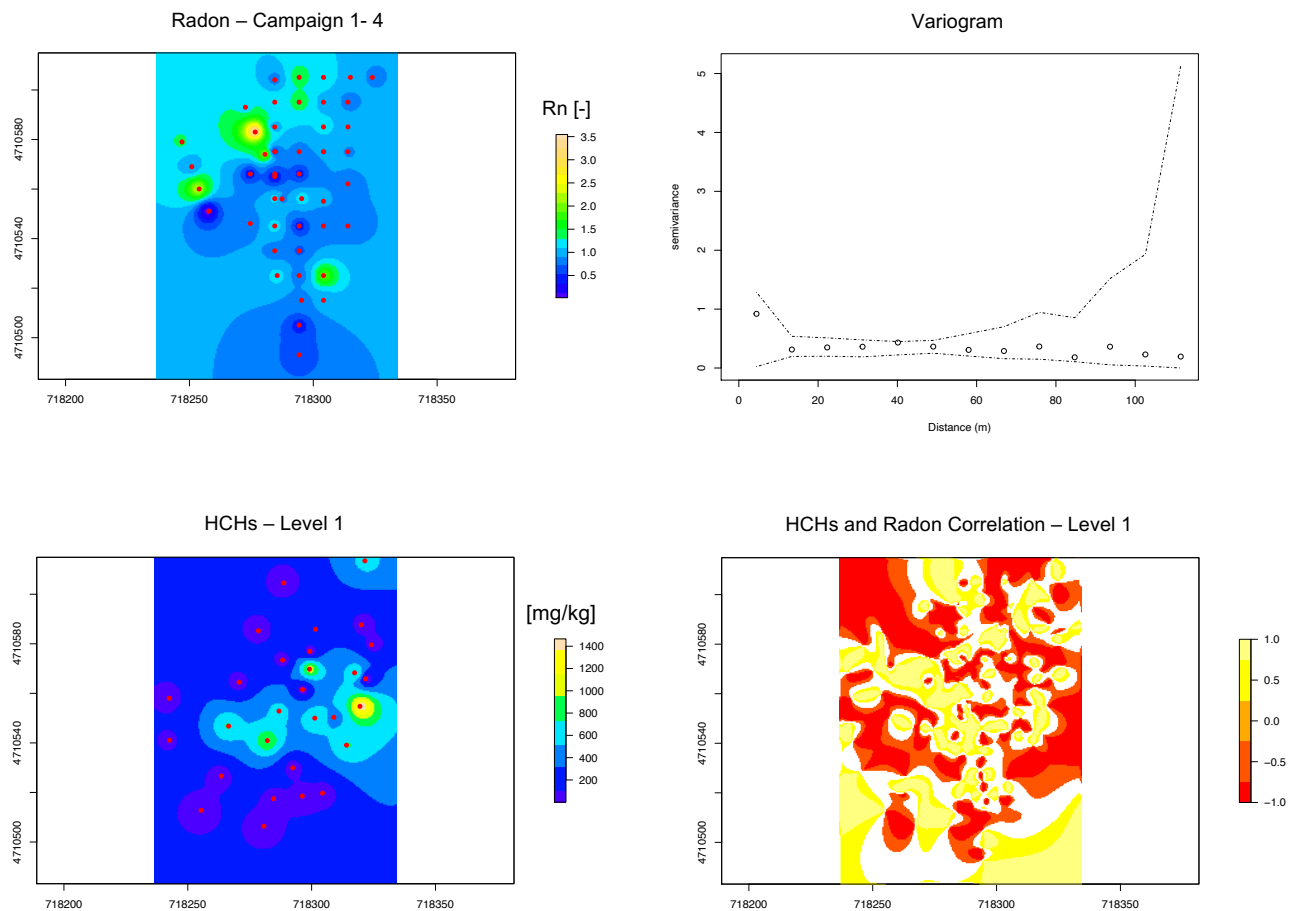
Figure 4.4 - Pearson correlation - Radon (campaigns 1-4) and HCHs in soil (level 1)
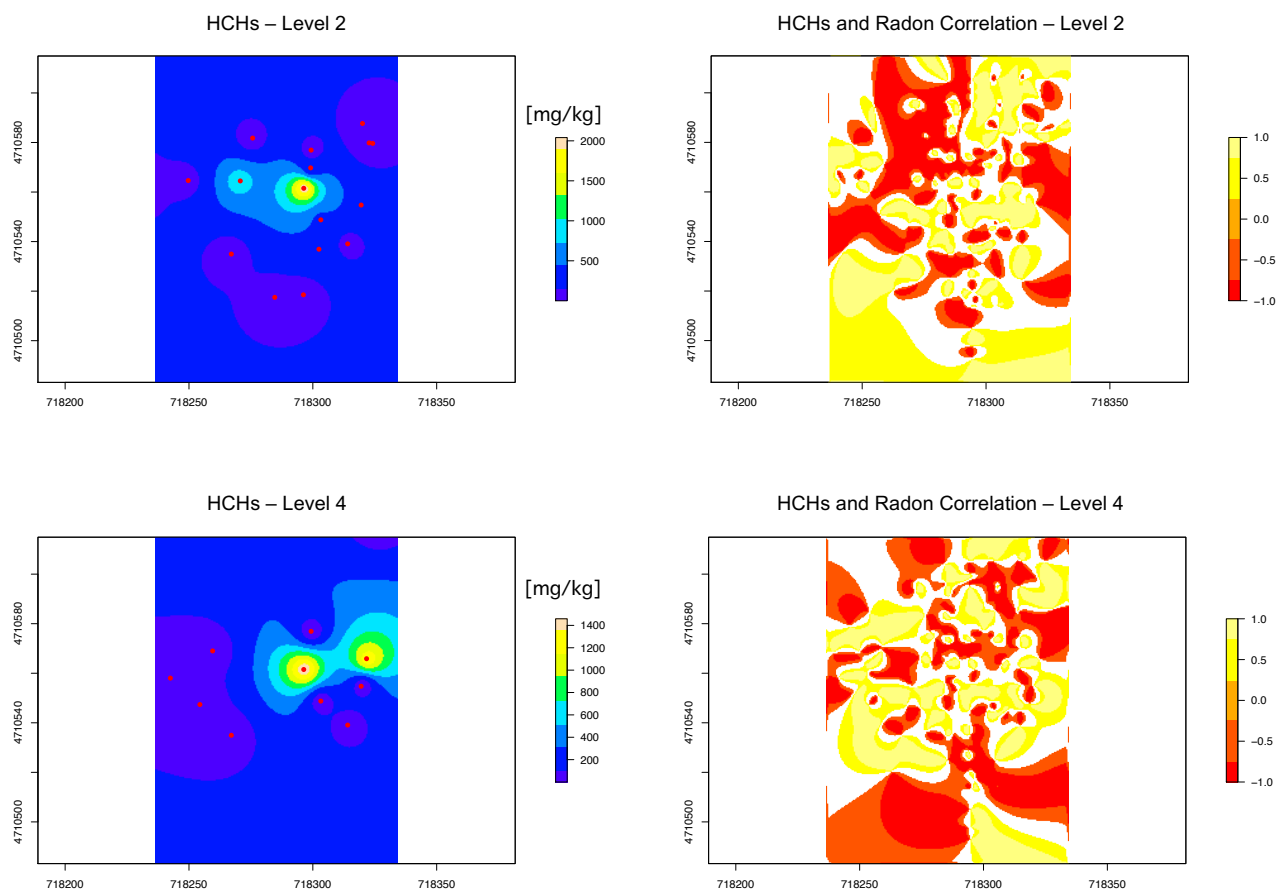
Figure 4.5 - Pearson correlation - Radon (campaigns 1-4) and HCHs in soil (level 2 and 4)
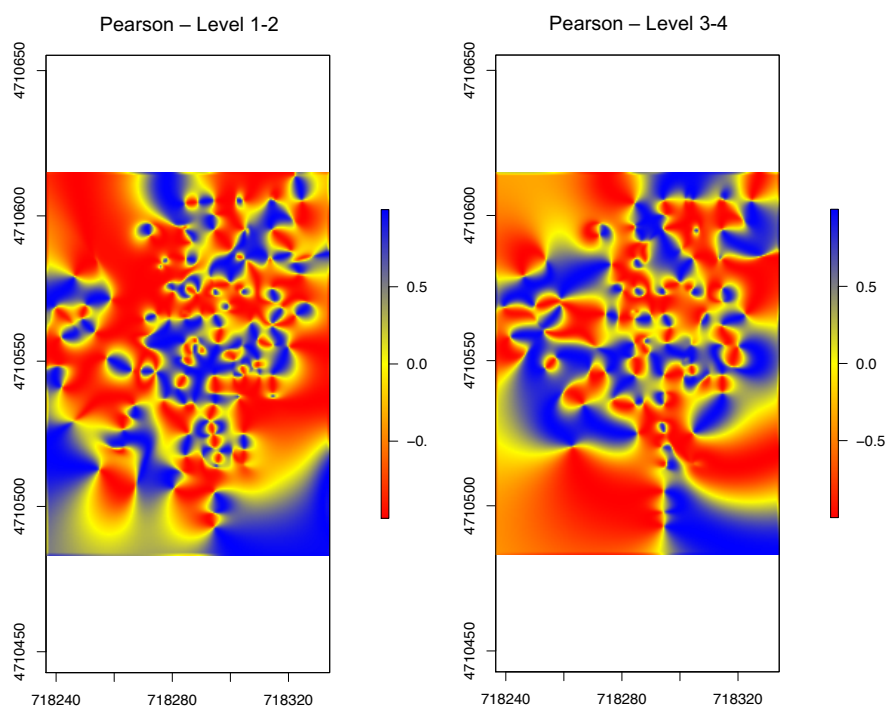
Figure 4.6 - Pearson correlation – campaigns 1-4 and HCHs in soil

The results show that with the increasing of depth, correlation decreases, and also, if level 1 and 2 (the anthropic fill and silt) are gathered, it is possible to obtain a better correlation. In Figure 4.6 are represented values of the Pearson coefficient, correlating the Rn signal with the upper layer (anthropic and silt) and with the lower (gravel and marls).

In this way it can be concluded that Radon allows to detect DNAPL up to the first two layers depth. Correlation decreases under the gravel layer, including correlation with contaminants in water. This behavior can be related with the limited Radon's migration capacity, and with the fact that it is not retained by a dissolved phase as it is by the residual saturation in soil.

The same results are found with the Pearson correlation of campaign 4 (Figure 4.7 and Figure 4.8).
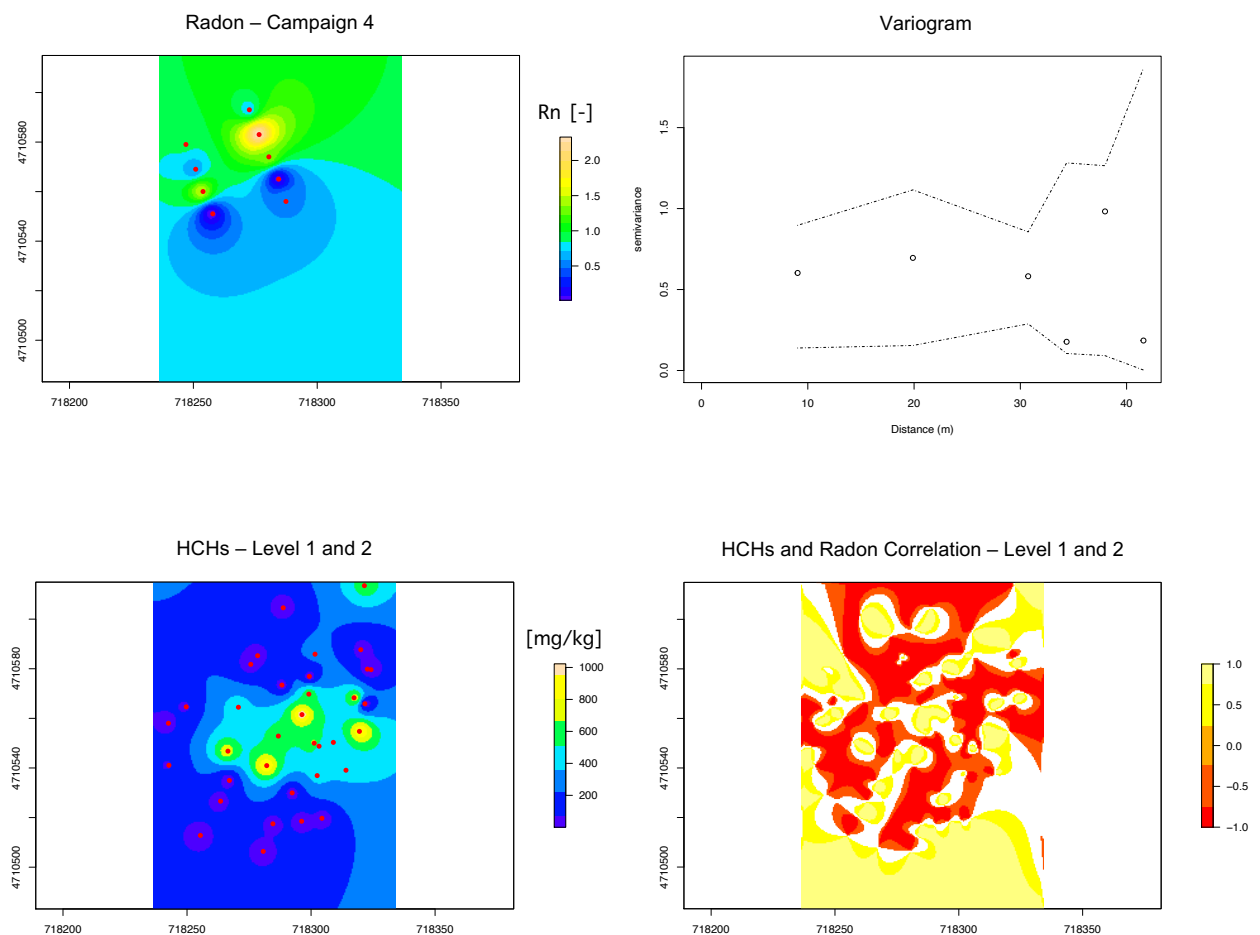
Figure 4.7 - Pearson correlation - Radon (campaign 4) and HCHs in soil

58
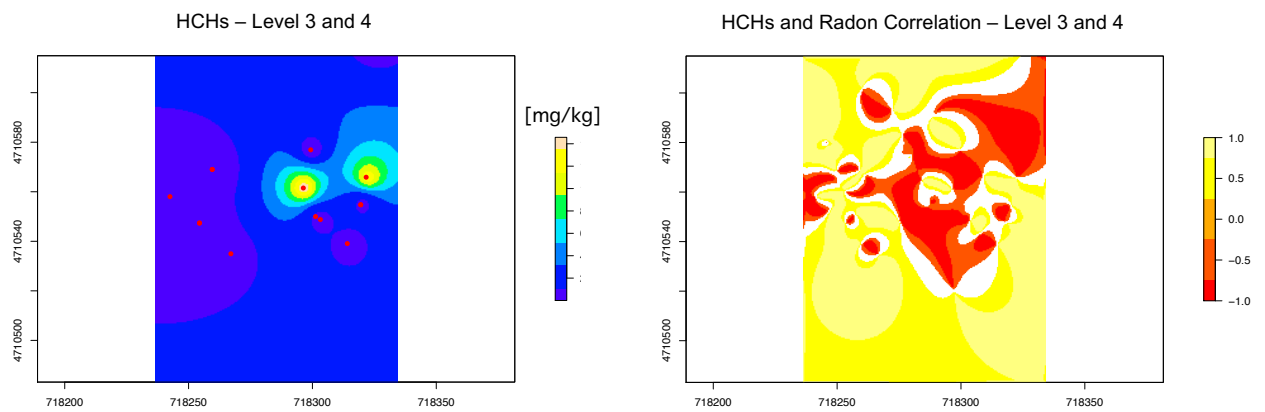
Figure 4.8 - Pearson correlation - Radon (campaign 4) and HCHs in soil
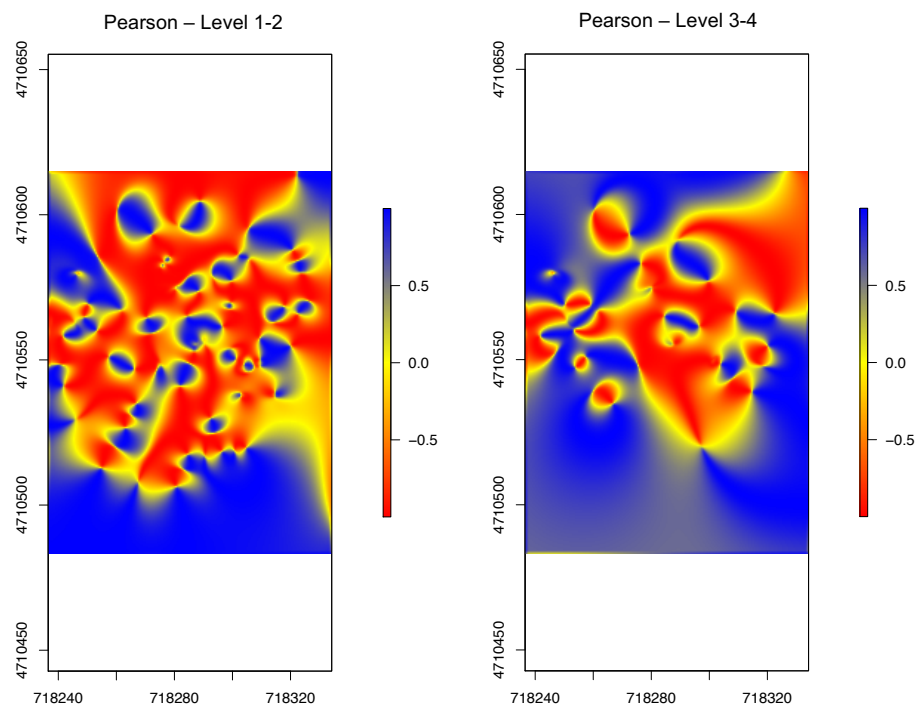
Figure 4.9 - Pearson correlation - Radon (campaign 4) and HCHs in soil

4.5.QUALITATIVE COMPARISON

In this paragraph it is shown if it's possible to find a qualitative correspondence between the contamination's hotspots and the Radon deficit peaks. The way to process data is the same as for the paragraph before (IDW Interpolation), the difference is that with ArcGIS a more detailed representation is obtainable, so instead of calculating a correlation, some correspondences between peaks are found visually. These representations also allow to verify some hypothesis on why it wasn't found a significative Pearson correlation between Rn concentration and contaminants in water.

4.5.1. Contaminants in water

First of all, Figure 4.10 shows the trend of the piezometric head, useful for the interpretation of data.
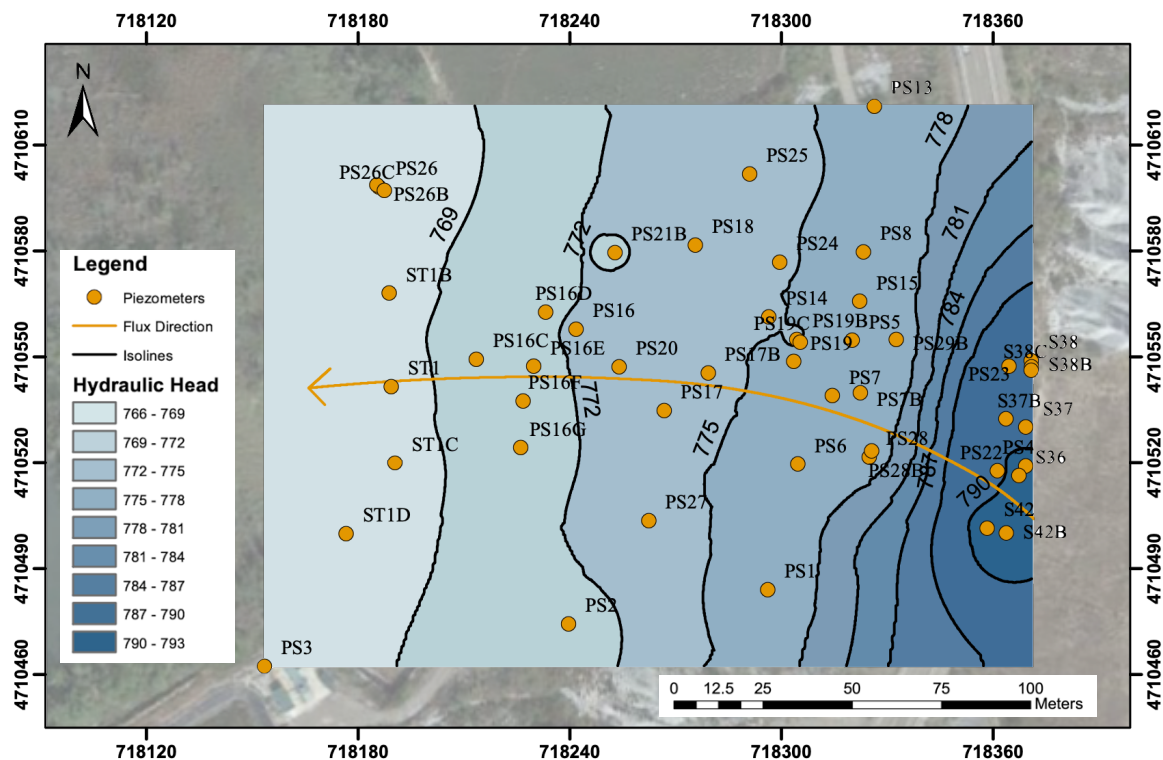
Figure 4.10 - Hydraulic head in Sardas site

As for the previous paragraph, each case of comparison (Radon sampling campaign – contamination) has been considered. From Figure 4.11 to 4.13 is reported, as a representative result, the IDW interpolation of Radon concentration, considering the sampling points of the first campaign, which has been overlapped with the IDW

60

interpolation of BTEX. For a more intuitive representation it was decided to identify Radon's deficit peaks with the color red.
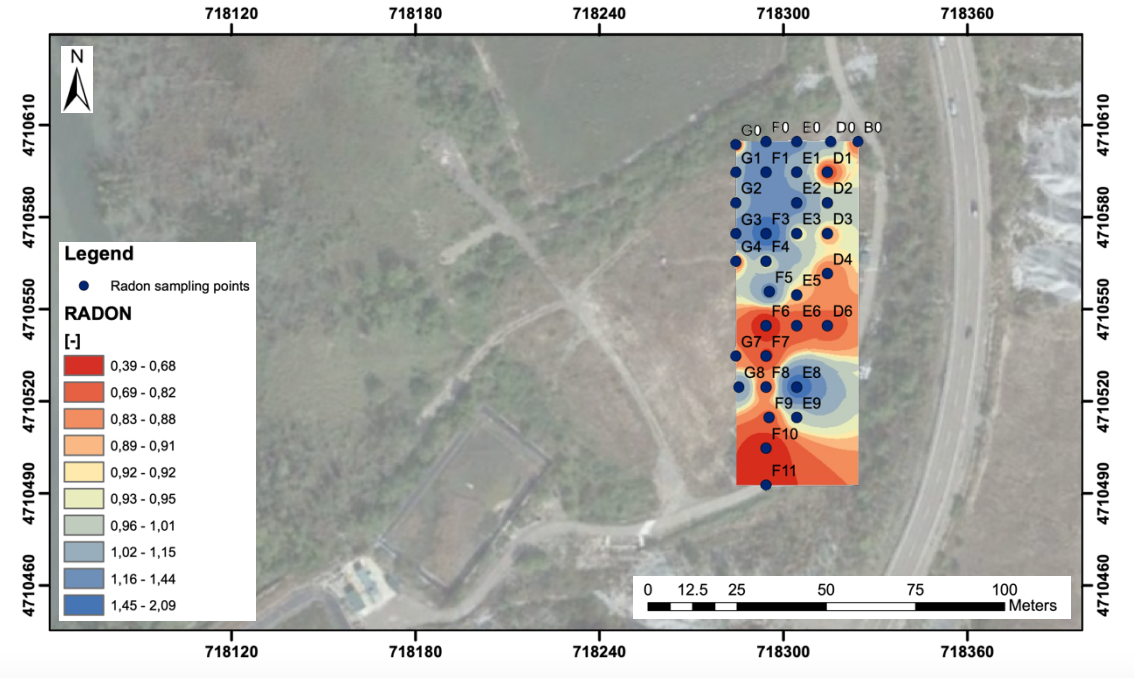
Figure 4.11 - IDW Interpolation of Radon concentration (campaign 1)
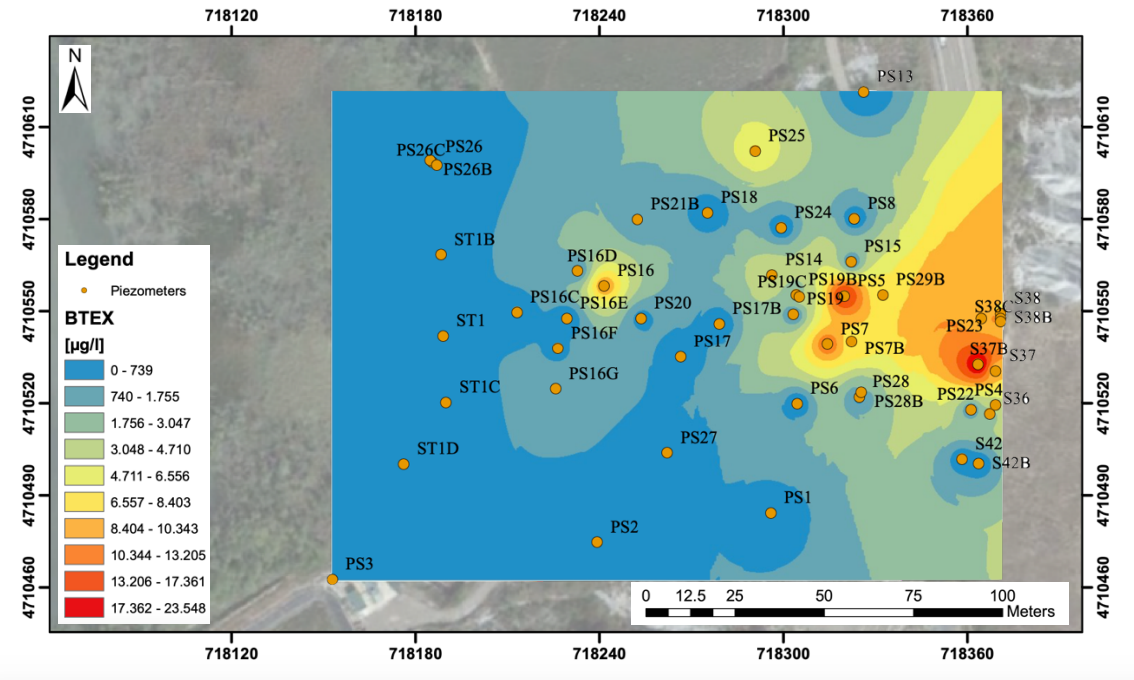
Figure 4.12 - IDW Interpolation of BTEX in water
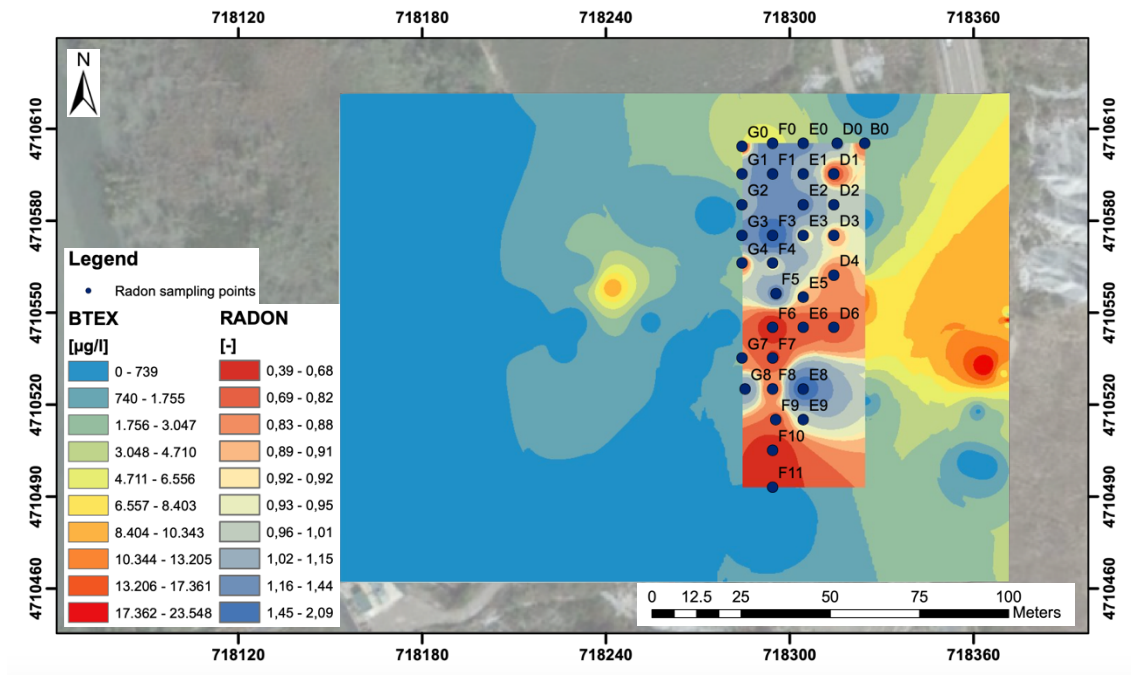
Figure 4.13 - Comparison between Radon (campaign 1) and BTEX
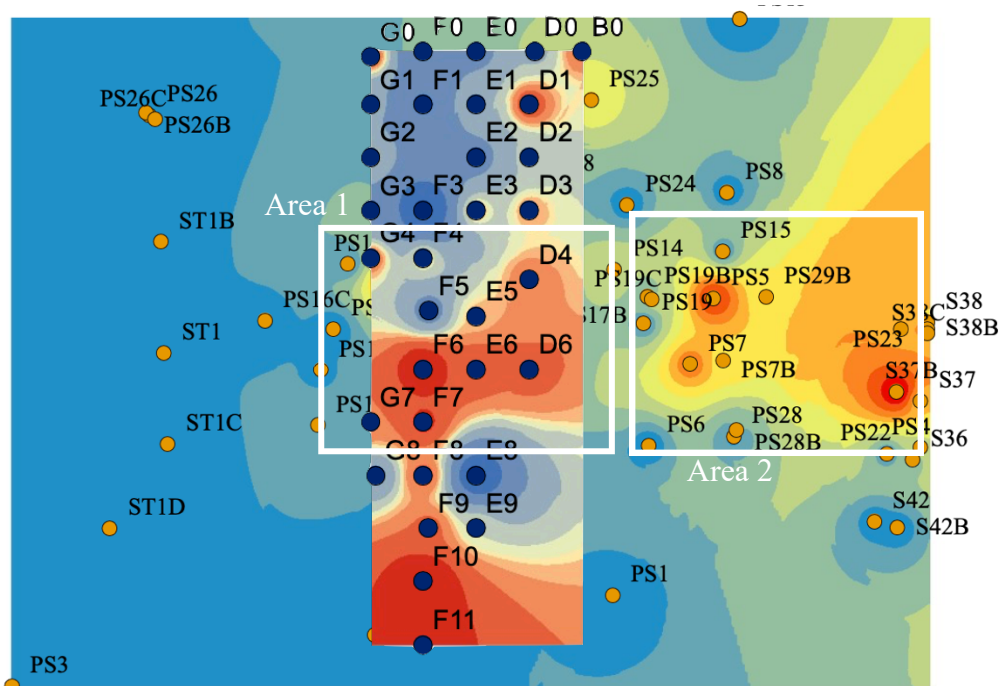
Figure 4.14 - Correspondence between Rn deficit peaks and BTEX hotspots

The hypothesis is that the area with a decrease in the Radon signal (identified as Area 1 in Figure 4.14 by sampling points F6, F7, E5, E6, D4, D6) is shifted according to the movement of the aquifer towards the river, and correspond to the contaminated area (identified as Area 2 by piezometers PS7, PS5, PS7B, PS29B, S37B).

This could be verified with the fact that the layers of gravel and marl are contaminated following the water regime and the high piezometric head variation could lead to a displacement. It also has to be considered the inaccuracy of the method and the effect of halo (Garcia-Gonzalez, et al., 2008).

4.5.2. The halo effects

In geochemical prospecting for petroleum deposits, the presence of hydrocarbons in the subsurface produces a reducing environment around the area where they accumulate. This reducing environment causes the uranyl ion (UO_2^{2+}) dissolved in groundwater to reduce from a +6 to a +4-oxidation state and to precipitate as UO_2 around the pool of hydrocarbons. A halo of precipitated U will form around the hydrocarbon pool where it will start disintegrating and become a source of Radon gas. Radon migrates upwards to the ground surface where it can be registered as higher-than-background signals that mark the contour of the subsurface NAPL accumulation (Mazadiego, 1994).

4.5.3. HCHs in soil

In Figure 4.15 is represented the IDW interpolation of the Rn concentration considering all the campaigns and the means in the common points.
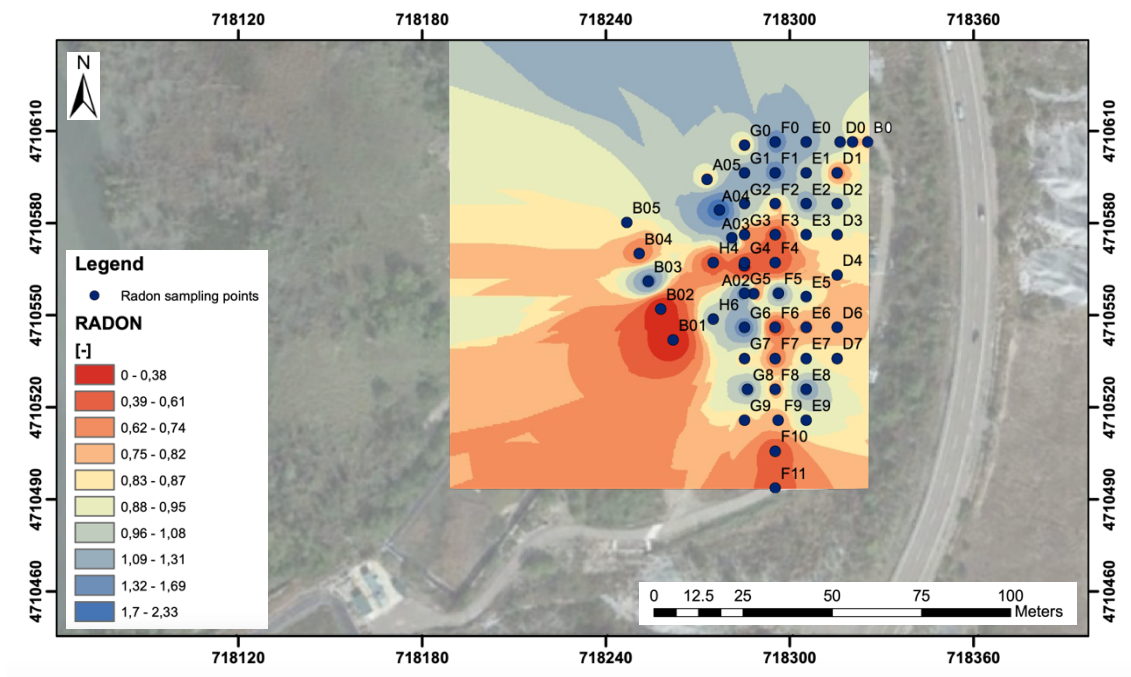
Figure 4.15 - IDW Interpolation of Rn concentration (campaigns 1-4)
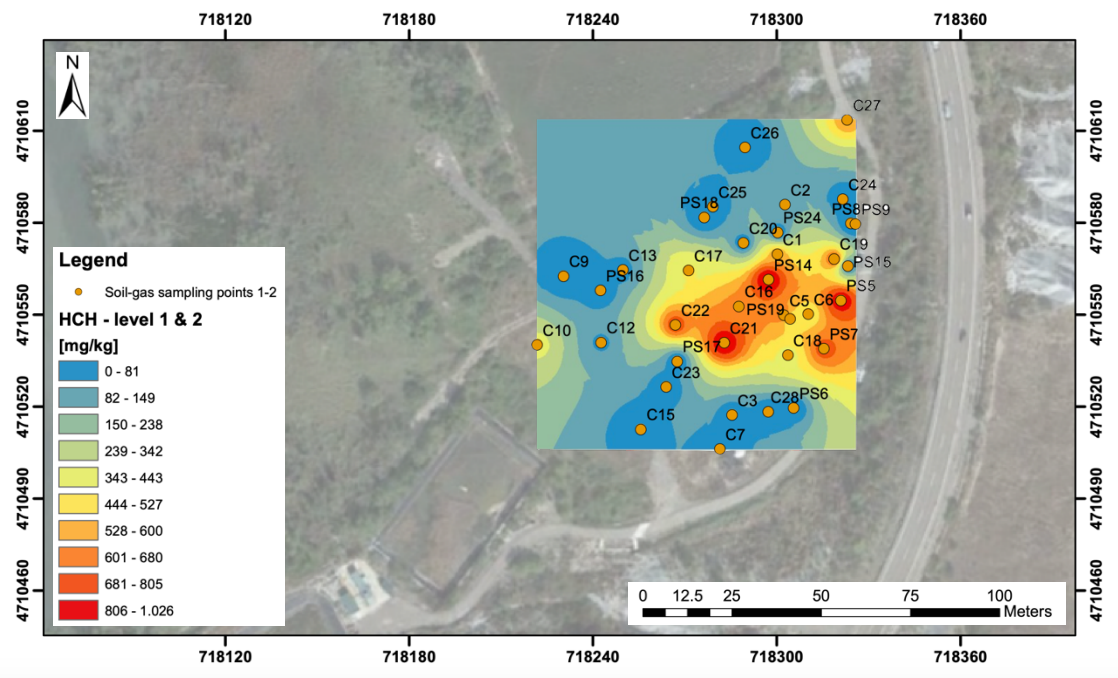
Figure 4.16 - IDW Interpolation of HCHs in soil (level 1 and 2)
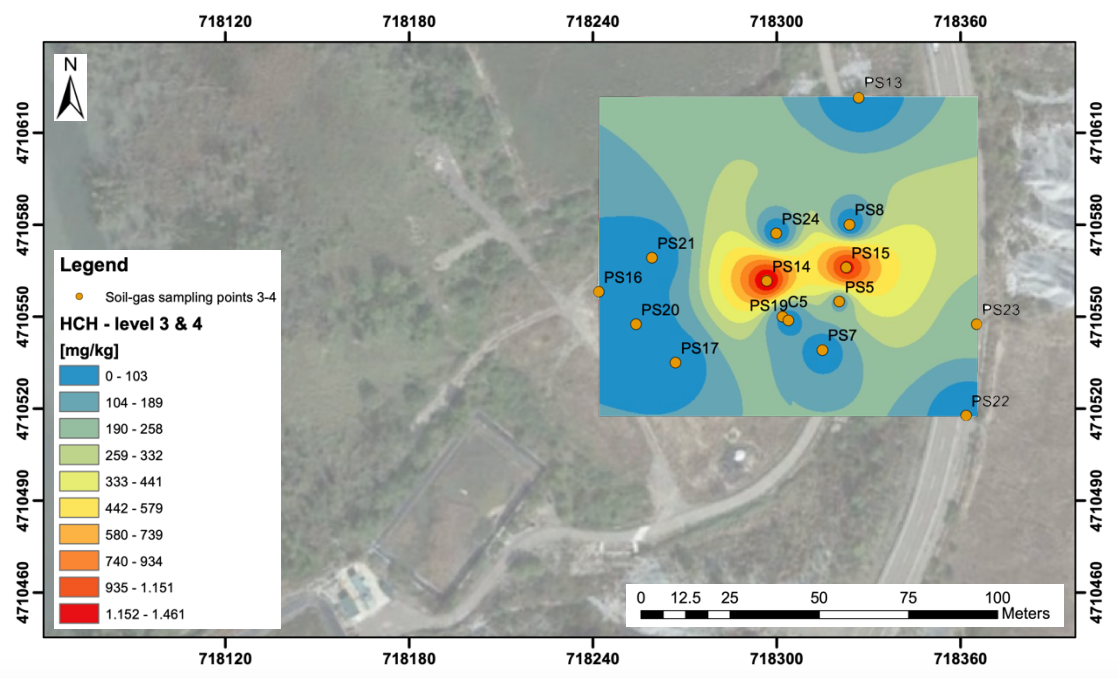
Figure 4.17 - IDW Interpolation of HCHs in soil (level 3 and 4)

As it is possible to see from the spatial location of the interpolation in Figure 4.15 and 4.16 the Rn concentration distribution identifies almost precisely the contamination's hotspots, the correspondence can be seen in Figure 4.18. Radon deficit peaks and HCHs are not exactly overlapped because of some inaccuracy of the method and because the coordinate system conversion to which the gas sampling points were subjected is not

100% precise. Area 1 represent the Radon deficit peaks, and Area 2 the HCHs concentration hotspots for the anthropic and the silt layer gathered.
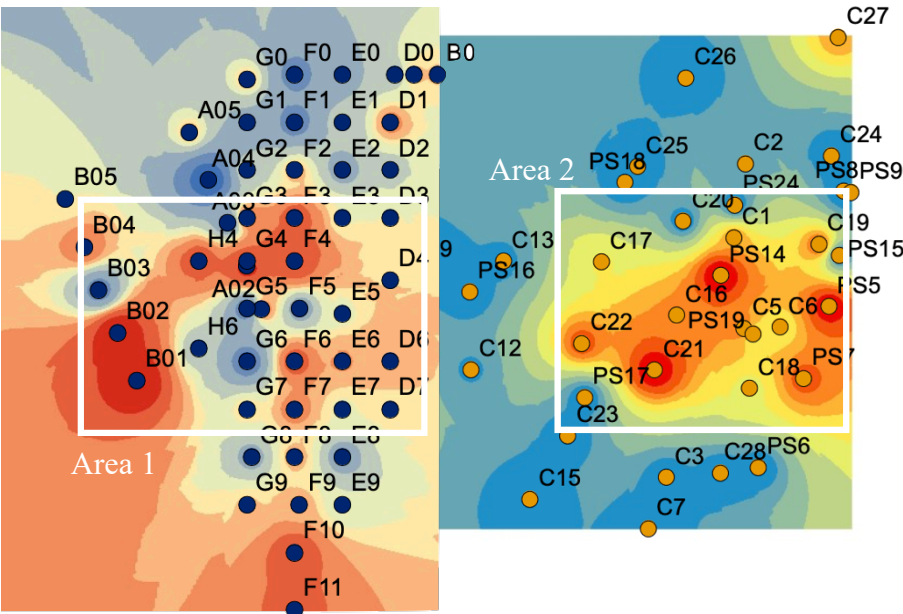
Figure 4.18 - Correspondence between Rn signal (campaigns 1-4) and HCHs (level 1 and 2)

The same result can be represented for campaign 4 individually (Figure 4.19), in which the correspondence between Rn deficit peaks (B02, A02 and A01) and HCHs is very clear.
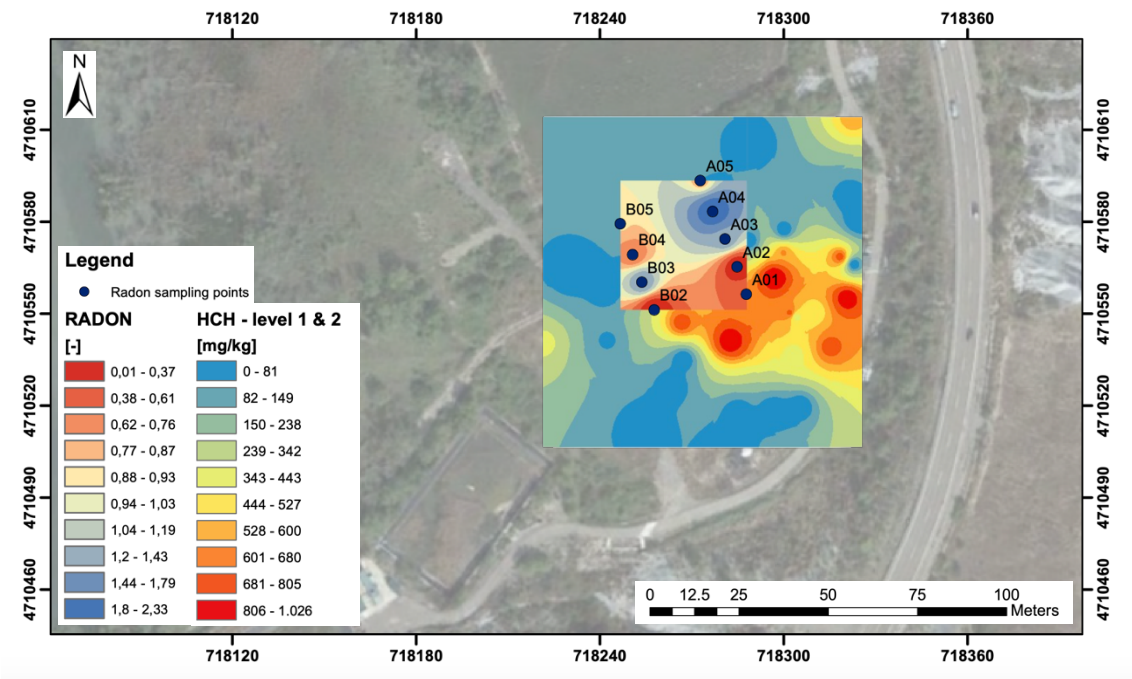
Figure 4.19 - Comparison between Rn concentration (campaign 4) and HCHs (level 1 and 2)

Same as the previous paragraph it can be concluded that the Radon deficit technique allows to detect residual saturation up to the depth of the silt layer. Correlation decreases under the gravel layer.

The qualitative correspondence between the Rn representation in Figure 4.15 and the HCHs of the first two layers, in addition to the results obtained in paragraph 4.4, demonstrate the applicability of this technique, despite the heterogeneity of Sardas site and possible errors that can occur in the development of the procedure.

Chapter 5

5. CONCLUSIONS

This study has tested the applicability of the Radon Deficit Technique to delineate DNAPLs contaminated areas in a macro-site with heterogeneous lithology. To assess the Radon Emanometry in Sardas site, the current work analyzed data from four different campaigns, lasting from 2016 to 2019.

The statistical analysis undertaken in this work has allowed to identify two different Radon's concentration data populations. The results of the ANOVA test have shown that the only atmospheric condition that influence the measurement of Radon is the temperature, in fact, the Rn flow is determined by thermo-diffusive mechanisms. This result also confirmed that the sampling is done at a sufficient depth for which there is no influence of wind speed and atmospheric pressure. Moreover, it explains the temporal variability of the measurements.

IDW interpolation was chosen to carry out spatial representations of Radon's concentration and contaminants. Results have shown that between Rn signal and contaminants in water it is possible to find only a qualitative comparison. The cause could be the inaccuracy of the method and the effect of halo, or that deepest geological layers are contaminated following the water regime, so Radon's deficit peaks are shifted according to the movement of the aquifer.

The most promising results are the correlations of Radon's emanation with concentrations of contaminants in the vadose zone. A significative Pearson correlation between the decrease in the Rn signal and HCHs present in the first two geological layers (anthropic fill and silt) was found. The results showed that with the increasing of depth, correlation decreases. Behavior that can be related with the limited Radon's migration capacity.

Pearson correlation, as the qualitative comparison, allowed to recognize DNAPLs contaminated areas, this result makes the Radon Deficit Technique applicable as a screening technique for the detection of DNAPLs contamination in a heterogeneous site.

The Radon Emanometry presents some important strengths as a non-intrusive method, is a low-cost alternative to detect DNAPLs on the surface and to monitor and control site remediation.

However, on the basis of this work, future studies should take into account that rather than repeating too many measurements for each sampling point, it would be better for these measurements to take place at almost constant temperature, with a single type of equipment, and covering a sufficiently wide area compared to the assumed contamination.

BIBLIOGRAPHY

Anderson, M., Johnson, R., & Pankow, J. (1992). Dissolution of dense chlorinated solvents into groundwater. 3. Modeling contaminant plumes from fingers and pool of solvent. (901-908).

Arco, G. (2017). Assessment of Radon monitoring as a screening methodology for DNAPL's contaminated sites. *Tesi di laurea magistrale - Politecnico di Torino*.

Artalejo Lopez, A., Barrio Parra, F., Biosca Valiente, B., Medina Ferro, R., Caparrini Marin, N., & Diaz-Curiel, J. (2017). Análisis Multivariante De Datos Físico-Químicos De Aguas Subterráneas En Un Emplazamiento Contaminado Por Dnapls Clorados.

Barbosa, E., Galhardi, J., & Bonotto, D. (2014). The use of radon (Rn- 222) and volatile organic compounds in monitoring soil gas to lo- calize NAPL contamination at a gas station in Rio Claro, São Paulo State, Brazil. *66*(1-4).

Barrio Parra, F., De Miguel, E., Izquierdo Diaz, M., Garcia Gonzalez, J., Artalejo Lopez, A., Diaz Curiel, J., Bolonio Martin, D. (2017). Aplicación De La Emanometría De Rn Para La Caracterización De Emplazamientos Afectados Por Contaminantes Densos (Dnapls): Una Antigua Instalación De Producción De Lindano Como Caso De Estudio.

Bear, J. (1972). Dynamics of Fluids in Porous Media. (763).

Bretz, F., Hothorn, T., & Westfall, P. (2011). *Multiple Comparisons Using R.* Chapman & Hall / CRC Taylor & Francis Group.

Casado, I., Mahjoub, H., Lovera, R., Fernandez, J., & Casas, A. (2015). Use of electrical tomography methods to determinate the extension and main migration routes of uncontrolled landfill leachates in fractured areas. *506-507*(546-553).

Crawford, C., & Quinn, B. (2017). The interactions of microplastics and chemical pollutants. In C. B. Crawford, & B. Quinn, *Microplastic Pollutants* (Vol. Pages 131-157).

Crawley, M. (2013). *The R Book.* Imperial College London at Silwood Park, UK: Wiley.

Davis, B., Semprini, L., & Istok, J. (2002). Development of Radon-222 as a Natural Tracer for Monitoring the Remediation of NAPL in the Subsurface.

De Miguel, E., Barrio-Parra, F., Elío, J., Izquierdo-Díaz, M., García-González, J., Mazadiego, L., & Medina, R. (2018). Applicability of radon emanometry in

lithologically discontinuous sites contaminated by organic chemicals. *25*(20255–20263).

De Simone, G., Lucchetti, C., & Pompilj, F. (2017). Soil radon survey to assess NAPL contamination from an ancient spill. Do kerosene va- pors affect radon partition? *171*(138–147).

Di Molfetta, A., & Sethi, R. (2012). *Ingegneria degli Acquiferi.* Springer.

Dirección General de Calidad Ambiental, G. d. (2010). Research survey and detail geotechnical and hydrogeological study for the mitigation of pollution in the affected area of the Sardas landfill, Sabiñánigo (Huesca) in 2009. Alternatives approaches and additional works for a definitive solution.

Etiope, G., & Martinelli, G. (2002). Migration of carrier and trace gases in the geosphere: an overview. *Phys. Earth Planet. Inter. - 129* (185-204).

European Commission, (2004). *Regulation No. 850/2004 of the European Parliament and of the Council of 29 April 2004 on Persistent Organic Pollutants and Amending Directive 79/117/EEC.* Tratto il giorno 10 2019, 10 da https://eur-lex.europa.eu/legal-content/EN/TXT/PDF/?uri=CELEX:02004R0850-20120710&from=EN

Fernandez, J., Cacho, C., & Arjol, M. (2012). Hch Contamination In The Environment Of Sabiñanigo (Spain). *20*(1937-1950).

Fetter, C. (1999). *Contaminant Hydrogeology (2nd ed.).* Upper Saddle River, NJ.: Prentice-Hall.

Galarnyk, M. (2018, September 12). *Towards Data Science.* Tratto il giorno September 28, 2019 da https://towardsdatascience.com/understanding-boxplots-5e2df7bcbd51

Gandhi, R., Hopkins, G., Goltz, M., Gorelick, S., & McCarty, P. (2002). Full-scale demonstration of in situ cometabolic biodegradation of trichloroethylene in groundwater, 2: comprehensive analysis of field data using reactive transport modelling. *38*.

García-González, J., Ortega, M., Chacón, E., Mazadiego, L., & Miguel, E. (2008). Field validation of radon monitoring as a screening methodology for NAPL-contaminated sites. *23*(2753–2758).

Girden, R. (1992). *ANOVA - Repeated Measures.* SAGE Publications.

Goes, B., & Meekes, J. (2004). An Effective Electrode Configuration for the Detection of DNAPLs with Electrical Resistivity Tomography. *9-3*(pp. 127-141).

Harris, R., & Bezdickek, D. (1994). Descriptive aspects of soil quality and health in Doran J. W., D. C. Coleman and B. A. Stewart (eds) Defining Soil Quality for a sustainable development.

Huang, F., Liu, D., Tan, X., Wang, J., Chen, Y., & He, B. (2011). Explorations of the implementation of a parallel IDW interpolation algorithm in a Linux cluster-based parallel GIS. *Computers & Geosciences*, 426-434.

Huling, S., & Weaver, J. (1991). EPA Ground Water Issue - Dense Nonaqueous Phase Liquids.

Jin, M., Delshad, M., Dwarakanath, V., McKinney, D., Pope, G., Sepehrnoori, K., . . . Jackson, R. (1995). Partitioning tracer test for detection, estimation and remediation performance assessment of subsurface nonaqueous phase liquids. . *5*(1201-1211).

Kong, X., Xu, F., He, W., & Qin, H. (2014). Development of Level-IV Fugacity-Based QWASI Model for Dynamic Multimedia Fate and Transport Processes of HCHs in Lake Chaohu, China. In *Developments in Environmental Modelling* (Vol. 26, Pages 35-73).

Kram, M., Keller, A., Rossabi, J., & Everett, G. (2001). DNAPL Characterization Methods and Approaches, Part 1: Performance Comparisons. *Groundwater Week 2019.* NGWA The Groundwater Association .

Lemke, L., & Abriola, L. (2004). Dense nonaqueous phase liquid (DNAPL) source zone characterization: Influence of hydraulic property correlation on predictions of DNAPL infiltration and entrapment. *40*.

Lyman, W., Reehl, W., & Rosenblatt, D. (1982). *Handbook of Chemical Property Estimation Methods.* McGraw-Hill Book Company.

Martinelli, G. (1998). Gas geochemistry and 222Rn migration process. *78*(77–82).

Mazadiego, L. (1994). Desarrollo de una metodologfa para la prospeccion geoqufmica en superficie de combustibles fosiles. .

Mercer, J., & Cohen, R. (1990). A review of immiscible fluids in the subsurface: properties, models, characterization and remediation. *6*(107-163).

Minkin, L. (2002). Is diffusion, thermodiffusion, or advection a primary mechanism of indoor radon entry? *Radiat. Prot. Dosimetry. 102*(153-162).

Morrow, N. (1979). Interplay of Capillary, Viscous and Bouyancy Forces in the Mobilization of Residual Oil. *18*(3, pp. 35-46).

Nelson, N., Oostrom, M., Wietsma, T., & Brusseau, M. (1999). Partitioning tracer method for the in situ measurement of DNAPL saturation: Influence of heterogeneity and sampling method. *22*(4046 - 4053).

Newmark, R., Daily, W., Kyle, K., & Raminez, A. (1998). Monitoring DNAPL pumping using integrated geophysical techniques. *3* (1. 7 - 13).

OGP. (2009). Coordinate Conversions and Transformations including Formulas.

Pankow, J., & Cherry, J. (1996). Dense chlorinated solvents and other DNAPLs in groundwater: history, behavior, and remediation. (1-52).

QGIS Training Manual. (2019, October 28). *Documentation QGIS*. Tratto da https://docs.qgis.org/2.18/en/docs/training_manual/

Santos, A., Fernandez, J., Guadano, J., Lorenzo, D., & Romero, A. (2018). Chlorinated organic compounds in liquid wastes (DNAPL) from lindane production dumped in landfills in Sabinanigo (Spain). *242*(1616-1624).

Semprini, L., & Istok, J. (2006). Radon-222 as a Natural Tracer for Monitoring the Remediation of NAPL Contamination in the Subsurface.

Semprini, L., Broholm, K., & McDonald, M. (1993). Radon-222 deficit method for locating and quantifying NAPL contamination in the subsurface. *74*(43).

Semprini, L., Hopkins, O., & Tasker, B. (1998). Laboratory, Field and Modeling Studies of Radon-222 as a Natural Tracer for Monitoring NAPL Contamination. *33*(223-240).

Semprini, L., Hopkins, O., & Tasker, B. (2000). Laboratory, field and model- ing studies of radon-222 as a natural tracer for monitoring NAPL contamination. *38*(223–240).

Starr, R. (2007). Evaluation of the Rn222 Deficit Technique for Delineating Milford, New Hampshire: Final Report.

Teixell, A., & García-San Segundo, J. (1994). Mapa geológico de España. E. 1:50000. Hoja n° 118: Zuriza. 2° serie MAGNA. ITGE;.

Thomas, D., Cotter, J., & Holford, D. (1992). Experimental-Design for Soil Gas Radon Monitoring. . *J. Radioanal. Nucl. Chem.*, 161, 313–323.

U.S. EPA, (1990). Laboratory Investigation of Residual Liquid Organics from Spills, Leaks, and Disposal of Hazardous Wastes in Groundwater, EPA/600/6-90/004.

USEPA. (2003). The DNAPL remediation challenge: is there a case for source depletion? National Service Center for Environmental Publications (NSCEP). (112).

Vijgen, J., Abhilash, P., Li, Y., Forter, M., Torres, J., Singh, N., Tian, G. (2011). Hexachlorocyclohexane (HCH) as new Stockholm Convention POPsda global perspective on the management of Lindane and its waste isomers. *18 (2)*(152 e 156).

Vijgen, J., De Borst, B., Weber, R., Stobiecki, T., & Forter, M. (2019). HCH and lindane contaminated sites: European and global need for a permanent solution for a long-time neglected issue. *248*(696 e 705).

Walker, K., Vallero, D., & Lewis, R. (1999). Factors influencing the distribution of lindane and other hexachlorocyclohexanes in the environment. *33*(4373–4378).

Wayne, R. (1990). A Physical Explanation of the Lognormality of Pollutant Concentrations. *26* (1378-1383).

Yoon, Y., Koh, D., Lee, K., Cho, X., Yang, J., & Lee, K. (2013). Using 222Rn as a naturally occurring tracer to estimate NAPL contamination in an aquifer. *81*(233-237).

Zutphen, M., van Hetterschijt, R., Valstar, J., & Schuren, C. (2000). First Partitioning Tracer test for DNAPL characterisation in the Netherlands, Groundwater 2000. (141-142).

APPENDIX A

ID	Point	CoordX	CoordY	Date	Time	Campaign	Day	Morning/ Aftern. (T)	Radon (Bq/m3)	Equip.	Depth (m)	Pressure (mbar)	Temp. (ºC)	Wind speed (m/s)	Problem
1	E2	718304,42	4710585,093	27/09/16	13	1	1	M	31500	RM2	0,8	938,11	22,91	0,93	No
2	E3	718304,42	4710575,093	27/09/16	13	1	1	M	25200	RM2	0,8	938,59	22,58	1,87	No
3	E5	718304,42	4710555,093	27/09/16	13	1	1	M	25700	RM2	0,8	938,59	22,58	1,87	No
4	E6	718304,42	4710545,093	27/09/16	13	1	1	M	19000	RM2	0,8	938,59	22,58	1,87	No
5	E7	718304,42	4710535,093	27/09/16	16	1	1	T	25500	RM2	0,8	940,62	21,31	4,01	Si
6	E8	718304,42	4710525,093	27/09/16	16	1	1	T	700	RM2	0,8	940,62	21,31	4,01	Si
7	E9	718304,42	4710515,093	27/09/16	16	1	1	T	27200	RM2	0,8	940,41	21,06	3,86	No
8	D1	718314,42	4710595,093	27/09/16	16	1	1	T	17400	RM2	0,8	940,41	21,06	3,86	Si
9	D2	718314,42	4710585,093	27/09/16	17	1	1	T	29000	RM2	0,8	940,41	21,06	3,86	No
10	D3	718314,42	4710575,093	27/09/16	17	1	1	T	24800	RM2	0,8	940,22	20,96	3,05	No
11	D6	718314,42	4710545,093	27/09/16	17	1	1	T	19300	RM2	0,8	940,22	20,96	3,05	No
12	D7	718314,42	4710535,093	27/09/16	17	1	1	T	24000	RM2	0,8	940,22	20,96	3,05	Si
13	F2	718294,42	4710585,093	27/09/16	13	1	1	M	19500	RM2	0,8	938,11	22,91	0,93	Si
14	F3	718294,42	4710575,093	27/09/16	12	1	1	M	68500	RM2	0,8	937,58	20,53	2,55	No
15	F4	718294,42	4710566,093	27/09/16	13	1	1	M	25600	RM2	0,8	938,11	22,91	0,93	No
16	F5	718295,48	4710556,153	27/09/16	12	1	1	M	35600	RM2	0,8	937,58	20,53	2,55	No
17	F6	718294,42	4710545,093	27/09/16	11	1	1	M	12700	RM2	0,8	937,58	20,53	2,55	No
18	F7	718294,42	4710535,093	27/09/16	11	1	1	M	15100	RM2	0,8	937,62	20,52	1,65	No
19	F8	718294,42	4710525,093	27/09/16	11	1	1	M	22200	RM2	0,8	937,62	20,52	1,65	No
20	F9	718295,42	4710515,093	27/09/16	11	1	1	M	12100	RM2	0,8	937,62	20,52	1,65	No

21	F10	718294,42	4710505,093	27/09/16	11	1	1	M	9000	RM2	0,8	937,53	20,04	1,68	No
22	F11	718294,42	4710493,093	27/09/16	11	1	1	M	9800	RM2	0,8	937,53	20,04	1,68	Si
23	E0	718304,42	4710605,09	28/09/16	12	1	2	M	34500	RM2	0,8	942,53	22,78	3,45	No
24	E1	718304,42	4710595,09	28/09/16	17	1	2	T	28600	RM2	0,8	937,68	20,48	1,94	No
25	E8	718304,42	4710525,09	28/09/16	12	1	2	M	59100	RM2	0,8	942,25	22,34	2,32	No
26	D0	718315,42	4710605,09	28/09/16	12	1	2	M	29700	RM2	0,8	942,25	22,34	2,32	No
27	D4	718314,42	4710562,09	28/09/16	12	1	2	M	23600	RM2	0,8	942,25	22,34	2,32	No
28	C0	718319,42	4710605,09	28/09/16	17	1	2	T	22400	RM2	0,8	939,33	21,00	2,42	Si
29	B0	718324,42	4710605,09	28/09/16	17	1	2	T	23000	RM2	0,8	939,33	21,00	2,42	No
30	F0	718294,42	4710605,09	28/09/16	12	1	2	M	41600	RM2	0,8	942,53	22,78	3,45	No
31	F1	718294,42	4710595,09	28/09/16	13	1	2	M	42700	RM2	0,8	942,51	22,67	2,92	No
32	F10	718294,42	4710505,09	28/09/16	12	1	2	M	13400	RM2	0,8	942,53	22,78	3,45	No
33	F11	718294,42	4710493,09	28/09/16	12	1	2	M	19550	RM2	0,8	942,53	22,78	3,45	Si
34	G0	718284,42	4710604,09	28/09/16	12	1	2	M	22300	RM2	0,8	942,53	22,78	3,45	No
35	G1	718284,42	4710595,09	28/09/16	12	1	2	M	31850	RM2	0,8	942,18	22,27	2,44	No
36	G2	718284,42	4710585,09	28/09/16	12	1	2	M	24300	RM2	0,8	942,18	22,27	2,44	No
37	G3	718284,42	4710575,09	28/09/16	12	1	2	M	34000	RM2	0,8	942,18	22,27	2,44	No
38	G4	718284,42	4710566,09	28/09/16	12	1	2	M	23200	RM2	0,8	942,51	22,67	2,92	No
39	G5	718284,42	4710556,15	28/09/16	12	1	2	M	25100	RM2	0,8	942,51	22,67	2,92	Si
40	G7	718284,42	4710535,09	28/09/16	13	1	2	M	23400	RM2	0,8	942,62	22,91	2,51	No
41	G8	718285,42	4710525,09	28/09/16	13	1	2	M	34100	RM2	0,8	942,62	22,91	2,51	No
42	G9	718284,42	4710515,09	28/09/16	13	1	2	M	20700	RM2	0,8	942,62	22,91	2,51	Si
43	Fondo 1	718189,51	4710784,71	28/09/16	17	1	2	T	14200	RM2	0,8	937,68	20,48	1,94	Si
44	Fondo 2	718189,01	4710785,21	28/09/16	17	1	2	T	14900	RM2	0,8	937,68	20,48	1,94	Si
45	E1	718304,42	4710595,09	29/09/16	12	1	3	M	28900	RM2	0,8	937,54	23,25	1,54	No
46	E2	718304,42	4710585,09	29/09/16	12	1	3	M	38400	RM2	0,8	937,55	23,73	1,37	No

47	E6	718304,42	4710545,09	29/09/16	10	1	3	M	22000	RM2	0,8	938,76	21,39	1,80	Nd
48	E8	718304,42	4710525,09	29/09/16	13	1	3	M	49500	RM2	0,8	938,73	24,83	1,57	No
49	D1	718314,42	4710595,09	29/09/16	12	1	3	M	20500	RM2	0,8	937,62	23,35	1,77	No
50	D2	718314,42	4710585,09	29/09/16	12	1	3	M	28000	RM2	0,8	937,55	23,73	1,37	No
51	D6	718314,42	4710545,09	29/09/16	10	1	3	M	24150	RM2	0,8	938,76	21,39	1,80	Nd
52	F1	718294,42	4710595,09	29/09/16	12	1	3	M	42700	RM2	0,8	937,54	23,25	1,54	No
53	F2	718294,42	4710585,09	29/09/16	13	1	3	M	24400	RM2	0,8	937,55	23,73	1,37	Si
54	F3	718294,42	4710575,09	29/09/16	13	1	3	M	51200	RM2	0,8	937,78	24,07	1,96	No
55	F5	718295,48	4710556,15	29/09/16	10	1	3	M	36600	RM2	0,8	938,76	21,39	1,80	No
56	F6	718294,42	4710545,09	29/09/16	10	1	3	M	18450	RM2	0,8	938,76	21,39	1,80	Si
57	F7	718294,42	4710535,09	29/09/16	10	1	3	M	21100	RM2	0,8	938,82	20,92	1,41	No
58	F9	718295,42	4710515,09	29/09/16	10	1	3	M	32750	RM2	0,8	939,02	19,89	0,21	No
59	F10	718294,42	4710505,09	29/09/16	9	1	3	M	10700	RM2	0,8	939,02	19,89	0,21	No
60	F11	718294,42	4710493,09	29/09/16	9	1	3	M	16000	RM2	0,8	938,99	19,35	0,52	Nd
61	G2	718284,42	4710585,09	29/09/16	13	1	3	M	31500	RM2	0,8	937,55	23,73	1,37	No
62	G6	718284,42	4710545,09	29/09/16	10	1	3	M	18000	RM2	0,8	938,91	20,65	0,42	Si
63	G9	718284,42	4710515,09	29/09/16	10	1	3	M	25600	RM2	0,8	939,02	19,89	0,21	Si
64	Fondo 1	718189,51	4710784,71	29/09/16	15	1	3	T	20800	RM2	0,8	941,79	24,48	1,88	Si
65	Fondo 2	718189,01	4710785,21	29/09/16	15	1	3	T	14100	RM2	0,8	941,79	24,48	1,88	Si
66	G6	718284,42	4710545,09	14/03/17	12	2	1	M	29100	RM3	1,7	936,13	18,19	1,27	No
67	G6	718284,42	4710545,09	14/03/17	13	2	1	M	26700	RM3	1,7	936,18	18,27	2,53	No
68	G6	718284,42	4710545,09	14/03/17	17	2	1	T	50200	RM3	1,7	936,25	18,36	4,75	No
69	G6	718284,42	4710545,09	14/03/17	17	2	1	T	50500	RM1	1,7	936,32	18,45	2,70	No
70	G6	718284,42	4710545,09	14/03/17	18	2	1	T	27300	RM2	1,7	936,39	18,54	2,13	No
71	G6	718284,42	4710545,09	14/03/17	18	2	1	T	29100	RM3	1,7	936,46	18,63	3,56	No
72	G5	718284,42	4710556,15	14/03/17	12	2	1	M	28200	RM3	1,7	936,77	16,41	1,27	No

73	G5	718284,42	4710556,15	14/03/17	13	2	1	M	24300	RM3	1,7	936,74	16,41	2,56	No
74	G5	718284,42	4710556,15	14/03/17	17	2	1	T	50300	RM3	1,7	936,72	16,52	4,75	No
75	G5	718284,42	4710556,15	14/03/17	17	2	1	T	48000	RM1	1,7	936,69	16,64	2,70	No
76	G5	718284,42	4710556,15	14/03/17	18	2	1	T	34900	RM2	1,7	936,67	16,76	2,13	No
77	G5	718284,42	4710556,15	14/03/17	18	2	1	T	32400	RM3	1,7	936,12	17,01	3,56	No
78	G4	718284,42	4710566,09	14/03/17	12	2	1	M	0	RM3	1,7	na	na	na	Si
79	G4	718284,42	4710566,09	14/03/17	13	2	1	M	20500	RM3	1,7	937,07	13,78	2,56	No
80	G4	718284,42	4710566,09	14/03/17	17	2	1	T	3500	RM3	1,7	937,04	13,95	4,67	No
81	G4	718284,42	4710566,09	14/03/17	17	2	1	T	4400	RM1	1,7	937,03	14,10	1,14	No
82	G4	718284,42	4710566,09	14/03/17	18	2	1	T	0	RM2	1,7	na	na	na	Si
83	G4	718284,42	4710566,09	14/03/17	18	2	1	T	0	RM3	1,7	na	na	na	Si
84	G3	718284,42	4710575,09	14/03/17	12	2	1	M	5700	RM3	1,7	936,43	17,05	1,85	Si
85	G3	718284,42	4710575,09	14/03/17	13	2	1	M	10900	RM3	1,7	935,93	17,00	2,70	No
86	G3	718284,42	4710575,09	14/03/17	17	2	1	T	9700	RM3	1,7	934,43	16,19	4,67	No
87	G3	718284,42	4710575,09	14/03/17	17	2	1	T	4300	RM1	1,7	934,43	15,96	1,14	No
88	G3	718284,42	4710575,09	14/03/17	18	2	1	T	0	RM2	1,7	na	na	na	Si
89	G3	718284,42	4710575,09	14/03/17	18	2	1	T	0	RM3	1,7	na	na	na	Si
90	H4	718274,42	4710566,093	14/03/17	12	2	1	M	0	RM3	1,7	na	na	na	Si
91	H4	718274,42	4710566,093	14/03/17	13	2	1	M	6000	RM3	1,7	937,55	18,37	2,56	No
92	H4	718274,42	4710566,093	14/03/17	17	2	1	T	4300	RM3	1,7	936,23	17,78	4,75	No
93	H4	718274,42	4710566,093	14/03/17	17	2	1	T	4300	RM1	1,7	936	17,69	1,14	No
94	H4	718274,42	4710566,093	14/03/17	18	2	1	T	0	RM2	1,7	na	na	na	Si
95	H4	718274,42	4710566,093	14/03/17	18	2	1	T	0	RM3	1,7	na	na	na	Si
96	G6	718284,42	4710545,09	15/03/17	10	2	2	M	48000	RM3	1,7	938,57	18,63	0,00	No
97	G6	718284,42	4710545,09	15/03/17	10	2	2	M	0	RM3	0,8	na	na	na	Si
98	G6	718284,42	4710545,09	15/03/17	11	2	2	M	24400	RM2	1,7	938,61	18,63	0,83	No

99	G6	718284,42	4710545,09	15/03/17	12	2	2	M	23500	RM1	1,7	938,64	18,63	2,04	No
100	G6	718284,42	4710545,09	15/03/17	13	2	2	M	47300	RM3	1,7	938,5	18,64	2,16	No
101	G6	718284,42	4710545,09	15/03/17	16	2	2	T	44500	RM3	1,7	938,36	18,65	3,53	No
102	G6	718284,42	4710545,09	15/03/17	17	2	2	T	34100	RM3	1,7	938,22	18,66	3,20	No
103	G6	718284,42	4710545,09	15/03/17	18	2	2	T	30900	RM3	1,7	938	18,56	0,52	No
104	G5	718284,42	4710556,15	15/03/17	10	2	2	M	34900	RM3	1,7	936,07	17,03	0,15	No
105	G5	718284,42	4710556,15	15/03/17	10	2	2	M	26000	RM3	0,8	936,04	17,11	0,45	No
106	G5	718284,42	4710556,15	15/03/17	11	2	2	M	27200	RM2	1,7	935,97	17,28	1,50	Nd
107	G5	718284,42	4710556,15	15/03/17	12	2	2	M	27400	RM1	1,7	935,98	17,34	2,04	No
108	G5	718284,42	4710556,15	15/03/17	13	2	2	M	37700	RM3	1,7	935,98	17,44	2,26	No
109	G5	718284,42	4710556,15	15/03/17	16	2	2	T	38000	RM3	1,7	936,02	17,97	3,53	No
110	G5	718284,42	4710556,15	15/03/17	17	2	2	T	41000	RM3	1,7	936,03	18,02	2,11	No
111	G5	718284,42	4710556,15	15/03/17	18	2	2	T	37400	RM3	1,7	936,08	18,11	0,52	No
112	G4	718284,42	4710566,09	15/03/17	10	2	2	M	46200	RM3	1,7	936,97	14,88	0,48	No
113	G4	718284,42	4710566,09	15/03/17	10	2	2	M	45500	RM3	0,8	936,95	15,37	0,45	No
114	G4	718284,42	4710566,09	15/03/17	11	2	2	M	200	RM2	1,7	936,94	15,62	1,50	No
115	G4	718284,42	4710566,09	15/03/17	12	2	2	M	18100	RM1	1,7	936,92	15,86	1,54	No
116	G4	718284,42	4710566,09	15/03/17	13	2	2	M	8100	RM3	1,7	936,91	15,94	2,26	No
117	G4	718284,42	4710566,09	15/03/17	17	2	2	T	2700	RM3	1,7	936,82	16,58	2,79	No
118	G4	718284,42	4710566,09	15/03/17	17	2	2	T	3500	RM3	1,7	936,8	16,66	2,11	No
119	G4	718284,42	4710566,09	15/03/17	18	2	2	T	1300	RM3	1,7	936,79	16,54	0,07	No
120	G3	718284,42	4710575,09	15/03/17	10	2	2	M	19400	RM3	1,7	934,39	15,00	0,48	No
121	G3	718284,42	4710575,09	15/03/17	11	2	2	M	16500	RM3	0,8	934,42	14,90	0,37	No
122	G3	718284,42	4710575,09	15/03/17	11	2	2	M	8400	RM2	1,7	937,19	12,77	1,14	No
123	G3	718284,42	4710575,09	15/03/17	12	2	2	M	9000	RM1	1,7	937,18	12,93	1,38	No
124	G3	718284,42	4710575,09	15/03/17	13	2	2	M	14800	RM3	1,7	937,16	13,10	2,73	No
125	G3	718284,42	4710575,09	15/03/17	17	2	2	T	4200	RM3	1,7	937,14	13,27	2,62	No

126	G3	718284,42	4710575,09	15/03/17	17	2	2	T	5500	RM3	1,7	937,12	13,44	0,93	No
127	G3	718284,42	4710575,09	15/03/17	18	2	2	T	1500	RM3	1,7	937,09	13,61	0,08	No
128	H4	718274,42	4710566,093	15/03/17	10	2	2	M	12200	RM3	1,7	935,7	17,57	0,48	No
129	H4	718274,42	4710566,093	15/03/17	11	2	2	M	25100	RM3	0,8	935,4	17,46	0,45	No
130	H4	718274,42	4710566,093	15/03/17	11	2	2	M	3000	RM2	1,7	935,09	17,35	1,14	No
131	H4	718274,42	4710566,093	15/03/17	12	2	2	M	8900	RM1	1,7	934,76	17,21	1,54	No
132	H4	718274,42	4710566,093	15/03/17	13	2	2	M	24700	RM3	1,7	934,42	17,07	2,73	No
133	H4	718274,42	4710566,093	15/03/17	17	2	2	T	3900	RM3	1,7	933,65	16,95	2,79	No
134	H4	718274,42	4710566,093	15/03/17	17	2	2	T	4600	RM3	1,7	932,38	16,21	0,93	No
135	H4	718274,42	4710566,093	15/03/17	18	2	2	T	3200	RM3	1,7	932,33	16,01	0,07	No
136	H6	718274,42	4710545,093	15/03/17	10	2	2	M	18100	RM3	1,7	932,28	15,82	0,15	No
137	H6	718274,42	4710546,093	15/03/17	11	2	2	M	18000	RM2	1,7	932,23	15,62	0,83	No
138	H6	718274,42	4710547,093	15/03/17	12	2	2	M	21300	RM1	1,7	932,17	15,42	2,04	No
139	H6	718274,42	4710548,093	15/03/17	13	2	2	M	25100	RM3	1,7	932,12	15,22	2,16	No
140	H6	718274,42	4710549,093	15/03/17	16	2	2	T	28900	RM3	1,7	932,07	15,03	3,53	No
141	H6	718274,42	4710550,093	15/03/17	17	2	2	T	16400	RM3	1,7	932,07	14,96	3,20	No
142	H6	718274,42	4710551,093	15/03/17	18	2	2	T	15200	RM3	1,7	932,06	14,89	0,52	No
143	F6	718294,42	4710545,093	15/03/17	10	2	2	M	18400	RM3	1,7	941,14	18,21	0,00	No
144	F6	718294,42	4710545,093	15/03/17	10	2	2	M	7400	RM3	0,8	940,9	18,12	0,21	No
145	F6	718294,42	4710545,093	15/03/17	11	2	2	M	5100	RM2	1,7	940,66	18,03	0,83	No
146	F6	718294,42	4710545,093	15/03/17	12	2	2	M	0	RM1	1,7	na	na	2,04	Si
147	F6	718294,42	4710545,093	15/03/17	13	2	2	M	8200	RM3	1,7	940,41	17,94	2,16	No
148	F6	718294,42	4710545,093	15/03/17	16	2	2	T	5700	RM3	1,7	938,65	17,27	3,53	No
149	F6	718294,42	4710545,093	15/03/17	17	2	2	T	11700	RM3	1,7	937,91	17,19	3,20	No
150	F6	718294,42	4710545,093	15/03/17	18	2	2	T	6000	RM3	1,7	937,17	17,12	1,08	No
151	F4	718294,42	4710566,093	15/03/17	10	2	2	M	10100	RM3	1,7	939,41	18,31	0,15	Si
152	F4	718294,42	4710566,093	15/03/17	11	2	2	M	0	RM2	1,7	na	na	1,50	Si

153	F4	718294,42	4710566,093	15/03/17	12	2	2	M	0	RM1	1,7	na	na	1,54	Si
154	F4	718294,42	4710566,093	15/03/17	13	2	2	M	12100	RM3	1,7	939,5	18,37	2,26	No
155	F4	718294,42	4710566,093	15/03/17	16	2	2	T	3000	RM3	1,7	939,64	18,50	2,79	No
156	F4	718294,42	4710566,093	15/03/17	17	2	2	T	7800	RM3	1,7	939,88	18,71	2,11	No
157	F4	718294,42	4710566,093	15/03/17	18	2	2	T	5100	RM3	1,7	941,13	18,21	0,07	No
158	F3	718294,42	4710575,093	15/03/17	10	2	2	M	600	RM3	1,7	939,21	15,52	0,48	No
159	F3	718294,42	4710575,093	15/03/17	11	2	2	M	900	RM2	1,7	939,18	15,67	1,14	No
160	F3	718294,42	4710575,093	15/03/17	12	2	2	M	0	RM1	1,7	na	na	1,38	Si
161	F3	718294,42	4710575,093	15/03/17	13	2	2	M	2600	RM3	1,7	939,12	15,97	2,73	No
162	F3	718294,42	4710575,093	15/03/17	17	2	2	T	0	RM3	1,7	na	na	2,62	Si
163	F3	718294,42	4710575,093	15/03/17	17	2	2	T	0	RM3	1,7	na	na	0,93	Si
164	F3	718294,42	4710575,093	15/03/17	18	2	2	T	4200	RM3	1,7	939,32	18,24	0,07	No
165	G3	718284,42	4710575,09	28/04/17	16	3	2	T	40300	RM3	1,7	928,79	14,95	na	No
166	G3	718284,42	4710575,09	28/04/17	18	3	2	T	40500	RM3	1,7	926,12	12,83	na	No
167	G4	718284,42	4710566,09	28/04/17	16	3	2	T	24300	RM3	1,7	928,79	14,95	na	No
168	G4	718284,42	4710566,09	28/04/17	17	3	2	T	27600	RM3	1,7	928,15	14,66	na	No
169	G4	718284,42	4710566,09	28/04/17	18	3	2	T	36100	RM3	1,7	926,12	12,83	na	No
170	G5	718284,42	4710556,15	28/04/17	16	3	2	T	28800	RM3	1,7	928,79	14,95	na	No
171	G5	718284,42	4710556,15	28/04/17	18	3	2	T	29800	RM3	1,7	926,7	13,34	na	No
172	G6	718284,42	4710545,09	28/04/17	16	3	2	T	27700	RM3	1,7	928,79	14,95	na	No
173	G6	718284,42	4710545,09	28/04/17	18	3	2	T	27800	RM3	1,7	926,7	13,34	na	No
174	H4	718274,42	4710566,093	28/04/17	17	3	2	T	18800	RM3	1,7	928,15	14,66	na	No
175	H4	718274,42	4710566,093	28/04/17	18	3	2	T	7300	RM3	1,7	926,12	12,83	na	No
176	H6	718274,42	4710546,093	28/04/17	16	3	2	T	32600	RM3	1,7	928,65	14,91	na	No
177	F3	718294,42	4710575,093	28/04/17	17	3	2	T	0	RM3	1,7	927,91	14,43	na	Si
178	F4	718294,42	4710566,093	28/04/17	17	3	2	T	0	RM3	1,7	927,91	14,43	na	Si
179	F6	718294,42	4710545,093	28/04/17	17	3	2	T	0	RM3	1,7	928,15	14,66	na	Si

180	F6	718294,42	4710545,093	28/04/17	18	3	2	T	20600	RM3	1,7	926,7	13,34	na	No
181	A01	718287,409	4710556,035	04/06/19	10	4	1	M	19500	RM3	1,7	917,0	24,00	0,00	No
182	A02	718284,409	4710565,035	05/06/19	10	4	1	M	0	RM3	1,7	917,2	24,20	0,00	Si
183	A03	718280,409	4710574,035	06/06/19	10	4	1	M	60300	RM3	1,7	917,4	24,40	0,00	No
184	A04	718276,409	4710583,035	07/06/19	10	4	1	M	87400	RM3	1,7	917,6	24,60	0,00	No
185	A05	718272,409	4710593,035	08/06/19	10	4	1	M	31500	RM3	1,7	917,8	24,80	0,00	No
186	B01	718261,409	4710541,035	09/06/19	10	4	1	M	0	RM3	1,7	918,0	25,00	0,00	Si
187	B02	718257,409	4710551,035	10/06/19	10	4	1	M	500	RM3	1,7	917,8	25,25	0,00	No
188	B03	718253,409	4710560,035	11/06/19	11	4	1	M	57200	RM3	1,7	917,5	25,50	0,00	No
189	B04	718250,409	4710569,035	12/06/19	11	4	1	M	25700	RM3	1,7	917,3	25,75	0,00	No
190	B05	718246,409	4710579,035	13/06/19	11	4	1	M	35900	RM3	1,7	917,0	26,00	0,00	No
191	A01	718287,409	4710556,035	28/06/19	17	4	1	T	28500	RM3	1,7	914,0	32,00	0,00	No
192	A02	718284,409	4710565,035	29/06/19	17	4	1	T	1700	RM3	1,7	913,8	32,00	0,00	No
193	A03	718280,409	4710574,035	30/06/19	17	4	1	T	56100	RM3	1,7	913,6	32,00	0,00	No
194	A04	718276,409	4710583,035	01/07/19	17	4	1	T	112000	RM3	1,7	913,4	32,00	0,00	No
195	A05	718272,409	4710593,035	02/07/19	17	4	1	T	34400	RM3	1,7	913,0	32,00	0,00	No
196	B01	718261,409	4710541,035	03/07/19	17	4	1	T	0	RM3	1,7	913,0	31,00	0,00	Si
197	B02	718257,409	4710551,035	04/07/19	18	4	1	T	0	RM3	1,7	913,3	30,75	0,00	Si
198	B03	718253,409	4710560,035	05/07/19	18	4	1	T	69300	RM3	1,7	913,5	30,50	0,00	No
199	B04	718250,409	4710569,035	06/07/19	18	4	1	T	24800	RM3	1,7	913,8	30,25	0,00	No
200	B05	718246,409	4710579,035	07/07/19	18	4	1	T	38800	RM3	1,7	914,0	30,00	0,00	No

APPENDIX B

Shapiro-Wilk normality test is performed on groups with number of data lower than 50, for higher number of data is performed Kolmogorov-Smirnov.

```
        Shapiro-Wilk normality test

data:  shap1
W = 0.93774, p-value = 0.01959


>
> ks2 <- datos02$Radon
> ks.test(ks2, "pnorm", mean(ks2), sd(ks2))

        One-sample Kolmogorov-Smirnov test

data:  ks2
D = 0.14968, p-value = 0.05305
alternative hypothesis: two-sided


> shap3 <- datos03$Radon
> shapiro.test(shap3)

        Shapiro-Wilk normality test

data:  shap3
W = 0.94283, p-value = 0.4946


>
> shap4 <- datos04$Radon
> shapiro.test(shap4)

        Shapiro-Wilk normality test

data:  shap4
W = 0.94186, p-value = 0.3725
```

APPENDIX C

R-Studio code 1 – Chapter 3 – Statistical analysis

```
setwd("/Users/Elia/Desktop/Dati")
dati <- read.table(file = "Statistic.txt", header = TRUE, sep = "\t",
na.strings = "na", dec = ",")

datos <- dati[dati$Problema =="No", ] #measurements without problem

datos$Campana <- as.factor(datos$Campana)
datos$Profundidad<- as.factor(datos$Profundidad)

datos01 <- datos[datos$Campana == "1", ] #campaign 1
datos08 <- datos[datos$Profundidad == "0.8", ] #depth 0.8
datos0108 <- datos08[datos$Campana == "1", ] #campaign 1 and depth 0.8
datos02 <- datos[datos$Campana == "2", ] #campaign 2
datos0208 <- datos02[datos02$Profundidad == "0.8", ] #campaign 2 and
depth 0.8
datos17 <- datos[datos$Profundidad == "1.7", ] #depth 1.7
datos0217 <- datos17[datos$Campana == "2", ] #campaign 2 and depth 1.7
datos03 <- datos[datos$Campana == "3", ] #campaign 3 (depth only 1.7)
datos04 <- datos[datos$Campana == "4", ] #campaign 4 (depth only 0.8)

#Histogram of data
par(mfrow = c(1,1))
  a <- datos$Radon
  hist (a, main = paste ("Data campaign 1 - 4"), col = "light green",
        xlim = c(0, 120000), ylim = c (0, 80),
        xlab = "Rn [Bq/m3]")
  print (summary(a))

#Histogram of data differenciated on CAMPAIGN
par(mfrow = c(2,2))
for (i in levels(datos$Campana)){
  a <- datos$Radon[datos$Campana == i]
  hist (a,main = paste ("Campaign ", i), col = "light green",
        xlim = c(0, 120000), ylim = c (0, 25),
        xlab = "Rn [Bq/m3]")
  print (summary(a))
}

#Boxplot of data differenciated on CAMPAIGN
par(mfrow = c(2,2))
for (i in levels(datos$Campana)){
  a <- datos$Radon[datos$Campana == i]
  boxplot(a, main = paste ("Boxplot Campaign ", i), col = "orange", ylim
= c(0,120000),
          ylab = "Rn [Bq/m3]")
  print (summary(a))
}

#Histogram of data differenciated on DEPTH
par(mfrow = c(2,1))
```

```
for (i in levels(datos$Profundidad)){
  a <- datos$Radon[datos$Profundidad == i]
  hist (a, main = paste ("Depth ", i, "m"), col = "light green",
        xlim = c(0, 120000), ylim = c (0, 35),
        xlab = "Rn [Bq/m3]")
  print (summary(a))
}


#Boxplot of data differenciated by campaign
par(mfrow = c(1,1))

b <- datos$Radon
plot(datos$Punto, b, col ="light blue", main = "Boxplot campaign 1 - 4",
     xlab = "Point" , ylab = "Rn [Bq/m3]")

par(mfrow = c(2,2))

b <- datos01$Radon
plot(datos01$Punto, b, col ="light blue", main = "Boxplot campaign 1",
     xlab = "Point" , ylab = "Rn [Bq/m3]", ylim = c (0,80000))
b <- datos02$Radon
plot(datos02$Punto, b, col ="light blue", main = "Boxplot campaign 2",
     xlab = "Point" , ylab = "Rn [Bq/m3]", ylim = c (0,80000))
b <- datos03$Radon
plot(datos03$Punto, b, col ="light blue", main = "Boxplot campaign 3",
     xlab = "Point" , ylab = "Rn [Bq/m3]", ylim = c (0,80000))
b <- datos04$Radon
plot(datos04$Punto, b, col ="light blue", main = "Boxplot campaign 4",
     xlab = "Point" , ylab = "Rn [Bq/m3]", ylim = c (0,80000))

#QQ-plot all the dataset
par(mfrow = c(1,1))
b <- datos$Radon
qqnorm(b)
qqline(b, col = "blue")

#QQ-plot differenciated on CAMPAIGN
par(mfrow = c(2,2))
for (i in levels(datos$Campana)){
  b <- datos$Radon[datos$Campana == i]
  qqnorm(b, main = paste ("Q-Q plot campaign ", i),
         xlim = c(-3, 3), ylim = c (0, 120000))
  qqline(b, col = "blue")
  print (summary(b))
}

#QQ-plot of datas differenciated on DEPTH
par(mfrow = c(2,1))
datos$Profundidad <- as.factor(datos$Profundidad)
for (i in levels(datos$Profundidad)){
  b <- datos$Radon[datos$Profundidad == i]
  qqnorm(b, main = paste ("Depth ", i, "m"),
         xlim = c(-3, 3), ylim = c (0, 120000))
  qqline(b, col = "blue")
  print (summary(b))
```

```
}

#QQ-plot of datas differenciated on DEPTH AND CAMPAIGN
par(mfrow = c(2,2))

#QQplot campaign 1 depth 0,8 m
b <- datos0108$Radon
qqnorm(b, main = paste ("Campaign 1", "Depth 0.8 m"),
       xlim = c(-3, 3), ylim = c (0, 120000))
qqline(b, col = "blue")

#QQplot campaign 2 depth 1,7 m
b <- datos0217$Radon
qqnorm(b, main = paste ("Campaign 2", "Depth 1.7 m"),
       xlim = c(-3, 3), ylim = c (0, 120000))
qqline(b, col = "blue")

#QQplot campaign 3 depth 1,7 m
b <- datos03$Radon
qqnorm(b, main = paste ("Campaign 3", "Depth 1.7 m"),
       xlim = c(-3, 3), ylim = c (0, 120000))
qqline(b, col = "blue")

#QQplot campaign 4 depth 0,8 m
b <- datos04$Radon
qqnorm(b, main = paste ("Campaign 4", "Depth 0.8 m"),
       xlim = c(-3, 3), ylim = c (0, 120000))
qqline(b, col = "blue")


#STATISTIC TEST (campaign 1,3 and 4 = Shapiro.test , campaign 2 =
Kolmogorov)
shap1 <- datos01$Radon
shapiro.test(shap1)

ks2 <- datos02$Radon
ks.test(ks2, "pnorm", mean(ks2), sd(ks2))

shap3 <- datos03$Radon
shapiro.test(shap3)

shap4 <- datos04$Radon
shapiro.test(shap4)

#transform data into logdata

datoslog <- log(datos$Radon)

#Histograms (log)
par(mfrow = c(2,2))
for (i in levels(datos$Campana)){
  a <- datoslog[datos$Campana == i]
  hist (a, main = paste ("Campaign ", i), col = "light green",
        xlim = c(0, 20), ylim = c (0, 25),
        xlab = "log (Rn)")
  print (summary(a))
```

```
}

#ANOVA TEST

Radon <- datos$Radon
Campaign <- datos$Campana
Depth <- datos$Profundidad
Pression <- datos$Presion
Temperature <- datos$Temperatura
Windspeed <- datos$Vviento
Point <- datos$Punto

#Tukey test
b <- aov(datoslog ~ Campaign)
par(mfrow = c(1,1))
Tuk <- TukeyHSD(x=b, conf.level=0.95)
plot(Tuk)

#Tukey test (no log)
b <- aov(Radon ~ Campana)
par(mfrow = c(1,1))
Tuk <- TukeyHSD(x=b, conf.level=0.95)
plot(Tuk)


Radon <- datos$Radon[datos$Campana != "5"]

model1 <- lm(Radon ~ Depth + Campaign)
summary(aov(model1))

model2 <- lm(Radon ~ Point + Campaign + Pression + Temperature +
Windspeed)
summary(aov(model2))

model3 <- lm(Radon ~ Point + Pression + Temperature + Windspeed)
summary(aov(model3))

model4 <- lm(Radon ~ Pression + Temperature + Windspeed)
summary(aov(model4))


#linear dependence Rn-Temperature

m1 <- mean(datos$Radon[datos$Campana == "1"])
m2 <- mean(datos$Radon[datos$Campana == "2"])
m3 <- mean(datos$Radon[datos$Campana == "3"])
m4 <- mean(datos$Radon[datos$Campana == "4"])
Var_Radon <- c("mean1"= m1, "mean2"= m2, "mean4"= m4)

t1 <- mean(datos$Temperatura[datos$Campana == "1"])
t2 <- mean(datos$Temperatura[datos$Campana == "2"])
t3 <- mean(datos$Temperatura[datos$Campana == "3"])
t4 <- mean(datos$Temperatura[datos$Campana == "4"])
Var_Temperature <- c("temp1"= t1, "temp2"= t2, "temp4"= t4)

#LM <- lm(Var_Depnd~Var_Independent)
```

```
LM <- lm (Var_Radon~Var_Temperature)
plot(Var_Radon~Var_Temperature)
abline(LM, col="blue")
summary(LM)
plot(LM)
```

R-Studio code 2 – Chapter 4 – Spatial correlation

```
#--------------------- RADON ---------------------#

library(geoR)
library(sp)
library(gstat)
library (raster)
library(tmap)

setwd("//Mac/Home/Desktop/Dati")
dati <- read.table(file = "Statistic2.txt", header = TRUE, sep = "\t",
na.strings = "na", dec = ",")

datos <- dati[dati$Problema =="No", ] #measurements without problem
datos$Campana <- as.factor(datos$Campana)
Campa <- levels (datos$Campana)

#RAPPRESENTATION OF HISTOGRAMS, QQPLOTS AND VARIOGRAM, FOR EACH
CAMPAIGN
#CREATE INTERPOLATION AREA

Xmin <- min (datos$CoordX)-10
Xmax <- max (datos$CoordX)+10
Ymin <- min (datos$CoordY)-10
Ymax <- max (datos$CoordY)+10
XX <- c (Xmin, Xmax)
YY <- c (Ymin, Ymax)
limites <- as.data.frame (cbind (XX, YY))
coordinates (limites) <- ~ XX +YY
grd <- as.data.frame (spsample (limites, "regular", n = 50000))
names(grd)       <- c("X", "Y")
coordinates(grd) <- c("X", "Y")
gridded(grd)     <- TRUE  # Create SpatialPixel object
fullgrid(grd)    <- TRUE  # Create SpatialGrid object

par(mfrow = c(1, 1))

for (i in 1:5)
{
  geodata<-as.geodata(datos[datos$Campana == Campa[i], ], coords.col =
4:5, data.col= 19)
  variog<-variog(geodata)
  env<-variog.mc.env(geodata,obj.var = variog)
```

```r
  hist(geodata$data,freq = F,main = paste ("Campaign #",i, "(m)")
        , col = "red", xlim = c(0, 120000))
  lines(density(geodata$data))
  qqnorm(geodata$data,main = "Q-Q plot")
  qqline(geodata$data)
  plot(variog, envelope = env, main = "Variogram", xlab = "Distance
(m)")

  #SPATIAL RAPPRESENTATION IDW

  Rad <- datos[datos$Campana ==Campa[i],]$Radon_Norm
  #Rad <- datos[datos$Campana ==Campa[i],]$Radon
  X   <- datos[datos$Campana ==Campa[i],]$CoordX
  Y   <- datos[datos$Campana ==Campa[i],]$CoordY
  dat <- as.data.frame(cbind (Rad, X, Y))
  coordinates(dat) <- ~ X + Y
  dat.idw <- gstat::idw(Rad ~ 1, dat, newdata=grd, idp=2.0)
  r       <- raster(dat.idw)
  plot (r, col =topo.colors (19, alpha = 1), main = paste("Radon -
Campaign ", i))
  points(dat,pch =16, col = "red")
}


#--------------------- HCH IN SOIL --------------------#

library(geoR)
library(sp)
library(gstat)
library (raster)
library(tmap)

setwd("//Mac/Home/Desktop/Dati")
dati <- read.table(file = "Suelos3.txt", header = TRUE, sep = "\t",
na.strings = "na", dec = ",")

#AREA OF INTERPOLATION
XX <- c (Xmin, Xmax)
YY <- c (Ymin, Ymax)
limites <- as.data.frame (cbind (XX, YY))
coordinates (limites) <- ~ XX + YY
grd <- as.data.frame (spsample (limites, "regular", n = 50000))
names(grd)       <- c("X", "Y")
coordinates(grd) <- c("X", "Y")
gridded(grd)     <- TRUE  # Create SpatialPixel object
fullgrid(grd)    <- TRUE  # Create SpatialGrid object

par(mfrow = c(1, 1))

dati1 <- dati[dati$nivel == "1", ]
dati2 <- dati[dati$nivel == "2", ]
dati3 <- dati[dati$nivel == "3", ]
dati4 <- dati[dati$nivel == "4", ]
dati5 <- dati[dati$nivel == "5", ]
dati6 <- dati[dati$nivel == "6", ]
```

```
#LEVEL 1

geodata<-as.geodata(dati1, coords.col = 4:5,data.col=8)
variog<-variog(geodata)
env<-variog.mc.env(geodata,obj.var = variog)
hist(geodata$data,freq = F,main = paste ("HCHs"), col = "red")
lines(density(geodata$data))
qqnorm(geodata$data,main = "Q-Q plot")
qqline(geodata$data)
plot(variog, envelope = env, main = "Variogram", xlab = "Distance
(m)")
#IDW
HCH <- dati1$HCH
X   <- dati1$X
Y   <- dati1$Y
dat <- as.data.frame(cbind (HCH, X, Y))
coordinates(dat) <- ~ X + Y
dat.idw <- gstat::idw(HCH ~ 1, dat, newdata=grd, idp=2.0)
hch1       <- raster(dat.idw)
plot (hch1, col =topo.colors (8, alpha = 1), main = paste ("HCHs -
LEVEL 1"))
points(dat,pch =16, col = "red")


#LEVEL 2

geodata<-as.geodata(dati2, coords.col = 4:5,data.col=8)
variog<-variog(geodata)
env<-variog.mc.env(geodata,obj.var = variog)
hist(geodata$data,freq = F,main = paste ("HCHs"), col = "red")
lines(density(geodata$data))
qqnorm(geodata$data,main = "Q-Q plot")
qqline(geodata$data)
plot(variog, envelope = env, main = "Variogram", xlab = "Distance
(m)")
#IDW
HCH <- dati2$HCH
X   <- dati2$X
Y   <- dati2$Y
dat <- as.data.frame(cbind (HCH, X, Y))
coordinates(dat) <- ~ X + Y
dat.idw <- gstat::idw(HCH ~ 1, dat, newdata=grd, idp=2.0)
hch2       <- raster(dat.idw)
plot (hch2, col =topo.colors (8, alpha = 1), main = paste ("HCHs -
LEVEL 2"))
points(dat,pch =16, col = "red")


#LEVEL 3

geodata<-as.geodata(dati3, coords.col = 4:5,data.col=8)
variog<-variog(geodata)
env<-variog.mc.env(geodata,obj.var = variog)
```

```r
hist(geodata$data,freq = F,main = paste ("HCHs"), col = "red")
lines(density(geodata$data))
qqnorm(geodata$data,main = "Q-Q plot")
qqline(geodata$data)
plot(variog, envelope = env, main = "Variogram", xlab = "Distance
(m)")
#IDW
HCH <- dati3$HCH
X   <- dati3$X
Y   <- dati3$Y
dat <- as.data.frame(cbind (HCH, X, Y))
coordinates(dat) <- ~ X + Y
dat.idw <- gstat::idw(HCH ~ 1, dat, newdata=grd, idp=2.0)
hch3      <- raster(dat.idw)
plot (hch3, col =topo.colors (8, alpha = 1), main = paste ("HCHs -
LEVEL 3"))
points(dat,pch =16, col = "red")


#LEVEL 4

geodata<-as.geodata(dati4, coords.col = 4:5,data.col=8)
variog<-variog(geodata)
env<-variog.mc.env(geodata,obj.var = variog)
hist(geodata$data,freq = F,main = paste ("HCHs"), col = "red")
lines(density(geodata$data))
qqnorm(geodata$data,main = "Q-Q plot")
qqline(geodata$data)
plot(variog, envelope = env, main = "Variogram", xlab = "Distance
(m)")
#IDW
HCH <- dati4$HCH
X   <- dati4$X
Y   <- dati4$Y
dat <- as.data.frame(cbind (HCH, X, Y))
coordinates(dat) <- ~ X + Y
dat.idw <- gstat::idw(HCH ~ 1, dat, newdata=grd, idp=2.0)
hch4      <- raster(dat.idw)
plot (hch4, col =topo.colors (8, alpha = 1), main = paste ("HCHs -
LEVEL 4"))
points(dat,pch =16, col = "red")


#LEVEL 1 AND 2

geodata<-as.geodata(dati5, coords.col = 4:5,data.col=8)
variog<-variog(geodata)
env<-variog.mc.env(geodata,obj.var = variog)
hist(geodata$data,freq = F,main = paste ("HCHs"), col = "red")
lines(density(geodata$data))
qqnorm(geodata$data,main = "Q-Q plot")
qqline(geodata$data)
plot(variog, envelope = env, main = "Variogram", xlab = "Distance
(m)")
#IDW
```

```r
HCH <- dati5$HCH
X   <- dati5$X
Y   <- dati5$Y
dat <- as.data.frame(cbind (HCH, X, Y))
coordinates(dat) <- ~ X + Y
dat.idw <- gstat::idw(HCH ~ 1, dat, newdata=grd, idp=2.0)
hch5       <- raster(dat.idw)
plot (hch5, col =topo.colors (8, alpha = 1), main = paste ("HCHs -
LEVEL 1 AND 2"))
points(dat,pch =16, col = "red")


#LEVEL 3 AND 4

geodata<-as.geodata(dati6, coords.col = 4:5,data.col=8)
variog<-variog(geodata)
env<-variog.mc.env(geodata,obj.var = variog)
hist(geodata$data,freq = F,main = paste ("HCHs"), col = "red")
lines(density(geodata$data))
qqnorm(geodata$data,main = "Q-Q plot")
qqline(geodata$data)
plot(variog, envelope = env, main = "Variogram", xlab = "Distance
(m)")
#IDW
HCH <- dati6$HCH
X   <- dati6$X
Y   <- dati6$Y
dat <- as.data.frame(cbind (HCH, X, Y))
coordinates(dat) <- ~ X + Y
dat.idw <- gstat::idw(HCH ~ 1, dat, newdata=grd, idp=2.0)
hch6       <- raster(dat.idw)
plot (hch6, col =topo.colors (8, alpha = 1), main = paste ("HCHs -
LEVEL 3 AND 4"))
points(dat,pch =16, col = "red")


#--------------------- PEARSON CORRELATION ---------------------#


library (raster)
library(rgdal)

colores= colorRampPalette(c("red", "yellow", "blue"))(255)
plot(r, col= colores)

#PEARSON CORRELATION

for (i in 1:5)
{
  par(mfrow=c(2,2))
  geodata<-as.geodata(datos[datos$Campana == Campa[i], ], coords.col =
4:5, data.col= 19)
  variog<-variog(geodata)
  env<-variog.mc.env(geodata,obj.var = variog)
  hist(geodata$data,freq = F,main = paste ("Campaign #",i, "(m)")
```

```
      , col = "red", xlim = c(0, 70000))
  lines(density(geodata$data))
  qqnorm(geodata$data,main = "Q-Q plot")
  qqline(geodata$data)
  plot(variog, envelope = env, main = "Variogram", xlab = "Distance
(m)")

  #IDW

  Rad <- datos[datos$Campana ==Campa[i],]$Radon_Norm
  X   <- datos[datos$Campana ==Campa[i],]$CoordX
  Y   <- datos[datos$Campana ==Campa[i],]$CoordY
  dat <- as.data.frame(cbind (Rad, X, Y))
  coordinates(dat) <- ~ X + Y
  dat.idw <- gstat::idw(Rad ~ 1, dat, newdata=grd, idp=2.0)
  r       <- raster(dat.idw)
  plot (r, col =topo.colors (19, alpha = 1), main = paste ("IDW
Campaign #", i))
  points(dat,pch =16, col = "red")

  par(mfrow=c(1,1))

  a <- corLocal(x=r,y=hch1, method = "pearson",ngb=5, test= T)
  plot(a, col =colores)
  xm <- mask(a[[1]], a[[2]] < 0.1, maskvalue=FALSE) # solo celdas
significativas
  plot(xm, main = "HCHs and Radon Correlation - Level 1", col
=heat.colors(5), zlim=c(-1,1))

  a <- corLocal(x=r,y=hch2, method = "pearson",ngb=5, test= T)
  plot(a, col =colores)
  xm <- mask(a[[1]], a[[2]] < 0.1, maskvalue=FALSE) # solo celdas
significativas
  plot(xm, main = "HCHs and Radon Correlation - Level 2", col
=heat.colors(5), zlim=c(-1,1))

  a <- corLocal(x=r,y=hch3, method = "pearson",ngb=5, test= T)
  plot(a, col =colores)
  xm <- mask(a[[1]], a[[2]] < 0.1, maskvalue=FALSE) # solo celdas
significativas
  plot(xm, main = "HCHs and Radon Correlation - Level 3", col
=heat.colors(5), zlim=c(-1,1))

  a <- corLocal(x=r,y=hch4, method = "pearson",ngb=5, test= T)
  plot(a, col =colores)
  xm <- mask(a[[1]], a[[2]] < 0.1, maskvalue=FALSE) # solo celdas
significativas
  plot(xm, main = "HCHs and Radon Correlation - Level 4", col
=heat.colors(5), zlim=c(-1,1))

  a <- corLocal(x=r,y=hch5, method = "pearson",ngb=5, test= T)
  plot(a, col =colores)
  xm <- mask(a[[1]], a[[2]] < 0.1, maskvalue=FALSE) # solo celdas
significativas
  plot(xm, main = "HCHs and Radon Correlation - Level 1 and 2", col
```

```
=heat.colors(5), zlim=c(-1,1))

  a <- corLocal(x=r,y=hch6, method = "pearson",ngb=5, test= T)
  plot(a, col =colores)
  xm <- mask(a[[1]], a[[2]] < 0.1, maskvalue=FALSE) # solo celdas
significativas
  plot(xm, main = "HCHs and Radon Correlation - Level 3 and 4", col
=heat.colors(5), zlim=c(-1,1))

}


#--------------------- CONTAMINANTS IN WATER --------------------#


setwd("//Mac/Home/Desktop/Dati")
dati <- read.table(file = "DatosAgua.txt", header = TRUE, sep = "\t",
na.strings = "na", dec = ",")

#AREA
XX <- c (Xmin, Xmax)
YY <- c (Ymin, Ymax)
limites <- as.data.frame (cbind (XX, YY))
coordinates (limites) <- ~ XX + YY
grd <- as.data.frame (spsample (limites, "regular", n = 50000))
names(grd)       <- c("X", "Y")
coordinates(grd) <- c("X", "Y")
gridded(grd)     <- TRUE  # Create SpatialPixel object
fullgrid(grd)    <- TRUE  # Create SpatialGrid object

par(mfrow = c(1, 1))

#BTEX -b1

geodata<-as.geodata(dati, coords.col = 3:4,data.col=7)
variog<-variog(geodata)
env<-variog.mc.env(geodata,obj.var = variog)
hist(geodata$data,freq = F,main = paste ("BTEX"), col = "red")
lines(density(geodata$data))
qqnorm(geodata$data,main = "Q-Q plot")
qqline(geodata$data)
plot(variog, envelope = env, main = "Variogram", xlab = "Distance
(m)")
#IDW
BTEX <- dati$BETEX
X   <- dati$X
Y   <- dati$Y
dat <- as.data.frame(cbind (BTEX, X, Y))
coordinates(dat) <- ~ X + Y
dat.idw <- gstat::idw(BTEX ~ 1, dat, newdata=grd, idp=2.0)
b1       <- raster(dat.idw)
plot (b1, col =topo.colors (7, alpha = 1), main = paste ("BTEX"))
points(dat,pch =16, col = "red")
```

```
#CLOROBENCENOS - Cb

geodata<-as.geodata(dati, coords.col = 3:4,data.col=8)
variog<-variog(geodata)
env<-variog.mc.env(geodata,obj.var = variog)
hist(geodata$data,freq = F,main = paste ("CHLOROBENZENES"), col =
"red")
lines(density(geodata$data))
qqnorm(geodata$data,main = "Q-Q plot")
qqline(geodata$data)
plot(variog, envelope = env, main = "Variogram", xlab = "Distance
(m)")
#IDW
CLOROBEN <- dati$Clorobencenos
X    <- dati$X
Y    <- dati$Y
dat <- as.data.frame(cbind (CLOROBEN, X, Y))
coordinates(dat) <- ~ X + Y
dat.idw <- gstat::idw(CLOROBEN ~ 1, dat, newdata=grd, idp=2.0)
Cb        <- raster(dat.idw)
plot (Cb, col =topo.colors (8, alpha = 1), main = paste
("CHLOROBENZENES"))
points(dat,pch =16, col = "red")


#HCH - Hc

geodata<-as.geodata(dati, coords.col = 3:4,data.col=9)
variog<-variog(geodata)
env<-variog.mc.env(geodata,obj.var = variog)
hist(geodata$data,freq = F,main = paste ("HCHs"), col = "red")
lines(density(geodata$data))
qqnorm(geodata$data,main = "Q-Q plot")
qqline(geodata$data)
plot(variog, envelope = env, main = "Variogram", xlab = "Distance
(m)")
#IDW
HCH <- dati$HCH
X    <- dati$X
Y    <- dati$Y
dat <- as.data.frame(cbind (HCH, X, Y))
coordinates(dat) <- ~ X + Y
dat.idw <- gstat::idw(HCH ~ 1, dat, newdata=grd, idp=2.0)
Hc        <- raster(dat.idw)
plot (Hc, col =topo.colors (9, alpha = 1), main = paste ("HCHs"))
points(dat,pch =16, col = "red")


#---------------------- PEARSON CORRELATION ---------------------#

for (i in 1:5)
{
  par(mfrow=c(2,2))
  geodata<-as.geodata(datos[datos$Campana == Campa[i], ], coords.col =
4:5, data.col= 12)
```

```r
  variog<-variog(geodata)
  env<-variog.mc.env(geodata,obj.var = variog)
  hist(geodata$data,freq = F,main = paste ("Campaign #",i, "(m)")
       , col = "red", xlim = c(0, 70000))
  lines(density(geodata$data))
  qqnorm(geodata$data,main = "Q-Q plot")
  qqline(geodata$data)
  plot(variog, envelope = env, main = "Variogram", xlab = "Distance
(m)")

  #IDW
  Rad <- datos[datos$Campana ==Campa[i],]$Radon_Norm
  X   <- datos[datos$Campana ==Campa[i],]$CoordX
  Y   <- datos[datos$Campana ==Campa[i],]$CoordY
  dat <- as.data.frame(cbind (Rad, X, Y))
  coordinates(dat) <- ~ X + Y
  dat.idw <- gstat::idw(Rad ~ 1, dat, newdata=grd, idp=2.0)
  r       <- raster(dat.idw)
  plot (r, col =topo.colors (19, alpha = 1), main = paste ("IDW
Campaign #", i))
  points(dat,pch =16, col = "red")

  par(mfrow=c(1,1))
  #mapa de correlacione entre BTEX y Radon
  a <- corLocal(x=r,y=b1, method = "pearson",ngb=5, test= T)
  plot(a, col =colores)
  xm <- mask(a[[1]], a[[2]] < 0.1, maskvalue=FALSE) # solo celdas
significativas
  plot(xm, main = "Radon and BTEX Correlation", col =heat.colors(5),
zlim=c(-1,1))

  #mapa de correlacione entre Clorobencenos y Radon
  a <- corLocal(x=r,y=Cb, method = "pearson",ngb=5, test = T)
  #plot(a, col =colores, main = "Correlaci?n entre Clorobenceno y Rad?
n")
  xm <- mask(a[[1]], a[[2]] < 0.1, maskvalue=FALSE) # solo celdas
significativas
  plot(xm, main = "Radon and Chlorobenzenes Correlation", col
=heat.colors(5), zlim=c(-1,1))

  #mapa de correlacione entre HCHs y Radon
  a <- corLocal(x=r,y=Hc, method = "pearson",ngb=5, test = T)
  #plot(a, col =colores, main = "Correlaci?n entre HCHs y Rad?n")
  xm <- mask(a[[1]], a[[2]] < 0.1, maskvalue=FALSE) # solo celdas
significativas
  plot(xm, main = "Radon and HCHs Correlation",col =
heat.colors(5),zlim=c(-1,1))

}
```

Ringraziamenti

Uno arriva alla fine di questo percorso e vorrebbe solo scrivere "F I N A L M E N T E!", ma poi in realtà ci pensi bene e ti viene anche un po' il magone.

Un sincero grazie ai professori Fernando Barrio Parra e Tiziana Tosco, per l'opportunità di questo lavoro e la paziente supervisione, a Madrid, e a Torino.

A Lucia, per aver percorso questa strada insieme, pensavamo che questa volta saremmo stati ospiti uno alla laurea dell'altro, e invece, squadra che vince, non si cambia!

A chi ha reso questi anni uno spasso. Alle risate sfrenate e ai bagni al mare, alle foto brutte e le prese in giro. A chi sa che per divertirsi basta poco, a chi c'è per una bevuta improvvisata. A chi è stato, o sarà, un compagno di viaggio. Agli Smartissimi e a agli amici di sempre, a voi, che siete indispensabili.

Ad Antonio, per l'insopportabile divertimento, per i regali, quelli più piccoli, e per l'idea, di qualcosa di grande.

A Pietro, perché il bene ognuno se lo dimostra a modo suo, preparato lo zaino?

A Cinzia e Lauro. Per avermi fatto suonare il pianoforte, per esservi buttati con me e Pietro con il paracadute, per l'idea dell'alba in mezzo al mare. Un giorno, voglio essere anche io così pieno di risorse.
Per essermi stati vicini con consigli e discussioni, ma senza porre limiti alla mia creatività. L'università non è facile questo si sa, e arrivare alla fine dà soddisfazione, ma arrivare alla fine senza perdersi è magico. Questo traguardo ve lo dedico con tutto il cuore.

E grazie a quelli che sono qui oggi, anche solo con il pensiero.
Un abbraccio a tutti quanti, vi voglio bene!

Elia

"...E non ho altro da dire su questa faccenda."